UNIVERSIDAD DE CÓRDOBA

Programa de Doctorado Dinámica de flujos biogeoquímicos y su aplicación

TESIS DOCTORAL

Influencia de la evolución de la humedad del suelo en los procesos formadores.

Influence of the evolution of the moisture profile on the soil forming processes

Autor

Vanesa García Gamero

Dirigida por

Dr. Juan Vicente Giráldez Cervera

Dr. Adolfo Peña Acevedo

Octubre 2021

TITULO: *Influence of the evolution of the moisture profile on the soil forming processes*

AUTOR: *Vanesa García Gamero*

Campus de Rabanales
Ctra. Nacional IV, Km. 396 A
14071 Córdoba

https://www.uco.es/ucopress/index.php/es/
ucopress@uco.es

TÍTULO DE LA TESIS: Influence of the evolution of the moisture profile on the soil forming processes

DOCTORANDA: Vanesa García Gamero

INFORME RAZONADO DE LOS DIRECTOR/ES DE LA TESIS

(se hará mención a la evolución y desarrollo de la tesis, así como a trabajos y publicaciones derivados de la misma).

La doctoranda ha abordado un tema de gran interés puesto que, ante la magnitud de la degradación del suelo tanto por la extensión como por la intensidad, es necesario analizar y estimular los procesos formadores del mismo. Ha escogido una zona privilegiada, los terrenos graníticos de Sierra Morena en los que, en algunas partes, la meteorización del granito es muy intensa, que tiene, además, la ventaja de estar dentro del ecosistema de la dehesa mediterránea.

Partiendo de unos objetivos muy sencillos ha planteado un sistema de adquisición de datos muy completa que van desde la humedad y temperatura del suelo, pasando por la temperatura y profundidad de la capa freática, hasta el índice diferencial normalizado de vegetación para explorar los procesos hidrológicos y formadores en una cuenca.

Los resultados recogen muy bien la influencia de los factores ambientales como radiación neta, temperatura del aire y precipitación sobre la evolución de los suelos y de su humedad, cumpliendo así con los objetivos planteados.

Entre el material publicado, además de comunicaciones a congresos y reuniones especializadas, está un artículo recién salido con el título Factors controlling the asymmetry of soil moisture and vegetation dynamics in a hilly Mediterranean catchment, (J. Hydrol. 598, 2021, 126207) y otro con aceptación preliminar con el título Modelling the effect of catena position and hydrology on soil chemical weathering (Soil, 2021).

Por todo ello, se autoriza la presentación de la tesis doctoral.

Córdoba, 22 de octubre de 2021

Firma de los directores

GIRALDEZ CERVERA JUAN VICENTE - 31165788Y
Firmado digitalmente por GIRALDEZ CERVERA JUAN VICENTE - 31165788Y
Fecha: 2021.10.22 16:17:17 +02'00'

Fdo.: Juan Vicente Giráldez Cervera

PEÑA ACEVEDO ADOLFO - 30531374R
Firmado digitalmente por PEÑA ACEVEDO ADOLFO - 30531374R
Fecha: 2021.10.22 13:37:59 +02'00'

Fdo.: Adolfo Peña Acevedo

This thesis has been carried out within Hidrología e Hidráulica Agrícola research group (AGR-127), at University of Córdoba, by the project AGL2015-65036-C3-2-R (MINECO/FEDER, UE).

Vanesa García Gamero was funded by:

- FPU scholarship, Spanish program for professional training of university lecturers (Programa de Formación del Profesorado Universitario-FPU), with reference FPU15/05279 from the Spanish Ministry of Education, Culture and Sport.
- Research stay granted by Universidad de Córdoba "CONVOCATORIA DE AYUDAS PARA LA REALIZACIÓN DE ESTANCIAS PARA LA OBTENCIÓN DE LA MENCIÓN INTERNACIONAL EN EL TÍTULO DE DOCTOR" at Ghent University, Deparment of Environment, Belgium, 3 months.

Agradecimientos

En primer lugar, deseo expresar mi agradecimiento a los directores de esta tesis doctoral, al profesor Juan Vicente Giráldez y al profesor Adolfo Peña, por el inestimable apoyo que han brindado a este trabajo a través de sus conocimientos y experiencia, su dedicación, esfuerzo, enriquecedores comentarios y valiosos consejos. Sin su labor como tutores esta tesis no hubiese sido posible.

Asimismo, al profesor Tom Vanwalleghem por el tiempo dedicado a este trabajo, incalculable ayuda, orientación y atención a mis consultas, confianza y respeto a mis sugerencias y a la profesora Ana Laguna por su disponibilidad, apoyo constante y sus convenientes observaciones que han contribuido a la mejora de este trabajo.

Al profesor Peter. A. Finke por haberme recibido durante mi estancia en la Universidad de Gante, por su guía, su tiempo y el entusiasmo transmitido con su forma de trabajar.

A mis compañeros del grupo de investigación, por su ayuda tanto en el trabajo de campo como en el de laboratorio.

Al investigador Karl Vanderlinden, del Instituto de Investigación y Formación Agraria y Pesquera (IFAPA), por su implicación, valiosos comentarios y mostrarse constantemente dispuesto a colaborar para mejorar este trabajo.

Al grupo de la investigadora Mª Pat González en el IFAPA por la accesibilidad de los datos meteorológicos de la zona de estudio. Al propietario y trabajadores de la finca Santa Clotilde por facilitar el acceso y trabajo en ella. A los ingenieros Juan Carlos Cuerva, Manuel Morón, Mario Ramos, Cristian Cuesta y Abraham Castillo que colaboraron en la puesta a punto de la instalación y su mantenimiento.

Agradezco al Programa Estatal de Investigación, Desarrollo e Innovación orientada a los retos de la sociedad 81/150 para el cuatrienio 2016-2020 que financió el proyecto de investigación "Estableciendo un Observatorio de la Zona Crítica para la Hidropedología y Agricultura Sostenible en el Mediterráneo" (AGL2015-65036-C3-2-R) dentro del que se desarrolló esta tesis.

Agradezco al Ministerio de Educación, Cultura y Deporte la concesión de un contrato predoctoral FPU, que ha posibilitado que me dedique completamente a la elaboración de este trabajo.

A todos aquellos que han colaborado para que esta tesis sea una realidad. Muchas gracias.

.

Resumen

Los cinco factores formadores del suelo descritos por Jenny en 1941: clima, relieve, actividad biológica, litología y tiempo, dependen del agua. Su degradación, especialmente debida a la pérdida por erosión, es uno de los graves problemas a los que se enfrenta la humanidad para su subsistencia en el planeta. Por ello, no solo hay que conservar el suelo, sino que es necesario conocerlo más bien para mejorarlo, y, en particular, para estimular los procesos formadores, y de ahí el papel relevante del agua. En esta tesis se analiza la evolución de la humedad del suelo durante un cierto periodo de tiempo en una zona en la que se ha detectado una meteorización intensas de rocas de granito en la Sierra Morena.

Se han estudiado los procesos hidrológicos de una cuenca formada sobre material granítico situada en el término municipal de Cardeña (Córdoba, España), que vierte al arroyo Martín Gonzalo afluente del Río Guadalquivir en su margen derecha. Se instaló una red sensores en campo, con sistema de transferencia de datos GPRS para la determinación de la dinámica de humedad y la temperatura del suelo, en unas laderas que convergen en el cauce del arroyo mencionado, una orientada hacia el norte y otra hacia al sur, para discernir el efecto de la distinta insolación sobre ellas. Se ha medido, también, la variación de la profundidad de la capa freática que hay en la ladera orientada hacia el norte. Finalmente, se ha explorado la formación de suelo con un modelo unidimensional en el se combinan procesos físicos y químicos de meteorización.

La humedad del suelo sigue trayectorias muy similares entre ambas laderas tanto ella como la vegetación estimada por el índice de vegetación diferencial normalizado (NDVI) muestran diferencias notables. La vegetación absorbe agua de distintas zonas tanto del suelo como del resto de la franja de la zona vadosa, lo que algunos llaman la 'humedad de la roca'. La temperatura puede indicar la variación de la humedad del suelo. El nivel piezométrico del acuífero somero responde de forma rápida a la recarga generada por los diversos chubascos. Por último, la simulación de la formación del suelo a través del índice CDF, usando el modelo SoilGen, muestra una buena correspondencia entre valores medidos y simulados, R^2=0.47. La variabilidad del índice depende en mayor medida de la hidrología que de la topografía.

Abstract

The five soil-forming factors described by Jenny in 1941: climate, relief, biological activity, lithology, and time, depend on the water. Soil degradation, especially due to erosion, is one of the most serious problems facing humanity for its subsistence on this planet. Therefore, we should not only conserve the soil but also enhance their forming processes, where the relevance of the water comes from. This dissertation analyzes the evolution of soil moisture for a four years period in an area where an intense weathering of granite rocks has been detected.

The research area is a watershed forming on granitic terrane located near the village of Cardeña (Córdoba province in southern Spain), which flows into the Martín Gonzalo Creek, a tributary of the Guadalquivir River, on its right margin. A soil moisture and temperature sensors network coupled to a GPRS data transfer system was installed on two opposite hillslope that converge in the course of the creek, one north-facing, and the other south-facing, in order to assess the effect of the different insolation on them. The water table depth on the north-facing slope was also measured on several piezometers. Soil formation processes were simulated with a one-dimensional model combining physical and chemical weathering processes.

Soil moisture followed similar trends in the two hillslopes, although both soil moisture and vegetation, as estimated by the Normalized Difference Vegetation Index (NDVI), showed notable differences between them. Vegetation uptook water from different water pools, soil as well as the rest of the vadose zone, what is also known as rock moisture. Temperature can trace field soil moisture changes. The piezometric level of the shallow aquifer responds fast to the recharge induced by the rain pulses. Finally, the simulation of soil formation through the Chemical Depletion Fraction (CDF), using the SoilGen model, shows a good correspondence between simulated and measured values, R2=0.47. The variability of the index is better explained by hydrological variables than by the position along the catena. The model sensitivity evaluated with a precipitation gradient (200-1,200 mm yr-1) showed a maximum CDF for intermediate precipitation values of 800 mm yr-1.

Table of contents

List of figures

List of tables

Chapter 1

General Introduction and Objectives

1.1. General background

The five soil-forming factors described by Jenny (1941): climate, living organisms, relief, parent material, and time are water dependent (Kirkby, 2016). Soil is essential storage in the water cycle not for the volume it represents, but because of its continuous renovation which allows easy access for humans, fauna, and flora. Soil water content, or soil moisture, in the vadose zone, defined as the unsaturated porous space overlying the zone of saturation (Meinzer, 1923), plays a major role in food security, human health, ecosystems organization and biodiversity, and weather predictions (McColl et al., 2017).

In recent years, and, in particular, in the summer season of 2021, devastating wildfires and floods hit Europe. The recent heatwave has caused an increase in temperature to almost the highest recorded in Europe, 48°C (Greece, July, 10,1977), and wildfires in Turkey, Greece, and other countries have already calcined thousands of hectares causing grave losses without unprecedented proportions. However, while different parts of South Europe are affected by heatwaves, heavy rains have caused flooding in Central Europe: Germany, Belgium, or the Netherlands even in northern Turkey after wildfires ravaged the south of the country. Based on floods that occurred last years, Blöschl et al., (2015) explored changes in the flood magnitudes and frequency that have occurred in the past decades in a European overview. They pointed out that differences in the observational window would therefore introduce uncertainty in the analysis, with increasing or decreasing trends depend on the period selected. Regarding future predictions of floods, they proposed to focus on changes in the drivers triggering the floods in the three compartments: atmosphere, catchment, and rivers.

The key role of soil moisture in the hydrological behaviour of the catchment determinant of flood and wildfire risk and the severity of soil degradation point out that there is an urgent need for improving the understanding of soil-water-plant interaction (Kirkby, 2016). In a

recent paper, Krueger et al. (2021) pointed out the important role of soil moisture-based decision tools, from an agronomic perspective, to estimate grassland biomass production using soil moisture measurements taken on the state of Oklahoma (USA) from 1997 to 2017.

1.2. Water in the Critical Zone

Soil moisture which, among other effects, controls the partitioning of water and energy fluxes at the land surface (Vereecken et al., 2008), has been studied at many different time and spatial scales, and monitoring, mostly indirectly, using different techniques: neutron, impedance or capacitance probes, time-domain reflectometry (TDR) and remote sensing methods (Ochsner et al., 2013). In situ and remote measurements of soil moisture are employed as predictors of floods, landslides, or wildfires. Sungmin et al. (2020) carried out a global analysis based on 18-year fire and soil moisture data (2001-2018) in similar climate regions: in arid regions, fires are preceded by wet soil moisture anomalies while in contrast in humid regions fires are preceded by dry soil moisture anomalies. In this way modelling and fire predicting may be improved with the role of soil moisture as predictors. Furthermore, Massari et al. (2014) pointed out the potential of soil moisture improving modelling runoff and flooding generation.

Although Ashley (1998) first coined the term Critical Zone (CZ) as “Surface to Bedrock-the Critical Zone. The upper few meters, are crucial for life” more than two decades ago, it remains still new. The CZ is defined as the Earth near-surface layer from the top of the vegetation to the bottom of the groundwater where rock, soil, water, air, and living organisms interact and regulate the natural habitat and determine the availability of life-sustaining resources (National Research Council (NRC), 2001). In 2006, The National Science Foundation (NSF), USA, starts a network of nine Critical Zone Observatories (CZO) to study in an interdisciplinary way the physical, biological and chemical processes that

shape the Earths' surface in a wide range of geological, climatic and land use environments. Following the success of the CZO program, whose funding concludes in 2021, a new project will focus on studying nine CZ networks clusters instead of a single observatory. The CZOs have been replicated around the World ever since. Different works have studied CZ architecture. Rempe & Dietrich (2014) proposed a model to predict the CZ thickness along a hillslope, pointing out years later the importance of the thickness of the weathered zone because of the water stored there or what they defined as *rock moisture* a hidden component of the water cycle, a particularly important component in supporting vegetation in a climate with a dry period, such as the Mediterranean climate. The coupled study of complex interactions between plants and soil and subsurface hydrology is still poorly developed but necessary to understand the importance of the weathered zone to support vegetation (Fan et al., 2019) and the interplay on the determination of depth and structure of the CZ. Water percolation in the unsaturated zone has a strong effect on soil's thermal regime because of the convective heat transfer and induces soil temperature differences (Nassar & Horton, 1992). Heat transport in the soil may be used as a hydrogeological tracer in phreatic aquifers (Constantz et al., 2003). To explore the hydrological processes and the CZ structure direct field observations and drilling were made within the study site, Santa Clotilde CZO in a granitic watershed of the Sierra Morena, close to Cardeña (Córdoba, Spain). Chapter 2 introduces the site and the methods used.

The study of the CZ structure (Fig.1.1) using hillslope as instrumentation and modelling scale, is crucial to understand how hydrological processes are driven (Rempe & Dietrich, 2018). In hillslopes and watersheds, every point is influenced by upslope areas and each of them has unique behavior (Kirkby, 2016). Lateral drainage and aspect determine the difference in hillslope CZ structure (Fan et al., 2019).

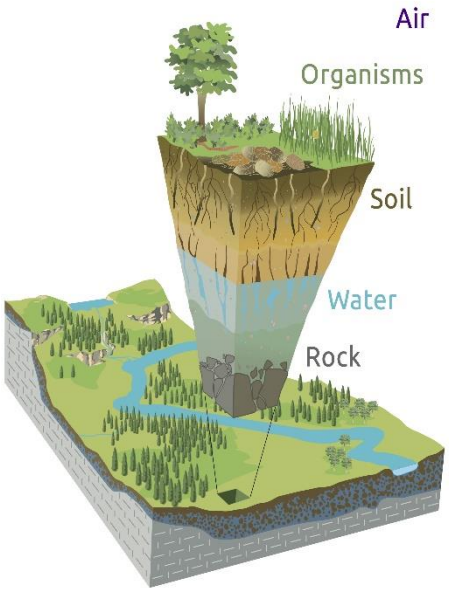

Figure 1.1. The Critical Zone. Modified from Chorover, J., R. Kretzschmar, F. Garcia-Pichel, and D. L. Sparks. 2007. Soil biogeochemical processes in the critical zone. Elements 3, 321-326. (Artwork by R. Kindlimann).

The amount of data was integrated, because of the water flow critical importance in soil-forming processes, in the SoilGen mechanistic model developed by Finke & Hutson (2008). Although lateral drainage is not included soil toposequences are studied with this model because it includes water flow, according to Opolot et al.(2015) it is often missing in soil development models.

1.3. Focus of this thesis

The research contained in this dissertation was part of the coordinated project "Optimizing vegetation use in concentrated flow areas of cultivated fields for minimizing soil erosion and offsite contamination and enhancing landscape values and biodiversity (OPTVAGUADA)". The general objective of this project was "to understand the ecohydrology of spatially concentrated use of vegetation (particularly riparian buffer strips) in olive and dehesa farmland using a combination of field studies including high resolution soil moisture data and model analysis". To accomplish this objective the Project encompassed three subprojects, the PhD research presented here focused on subproject 3: "*Estableciendo un*

Observatorio de la Zona Crítica para la Hidropedología y Agricultura sostenible en el Mediterráneo" (AGL2015-65036-C3-2R) whose overall objective was to study the hydrological, biological and edaphic processes that form the CZ. The main and specific objectives and organization of this PhD research are discussed in the subsequent sections.

1.4. Objectives

The main **objective** of this study is the overall characterization of soil moisture over a granitic Mediterranean catchment and its interaction with soil formation processes**.**

The **specific objectives** addressed in this study include:

1. To analyze soil moisture evolution patterns in a hilly Mediterranean catchment in granitic soils identifying the influence of vegetation, the presence of unweathered bedrock, and the relief. (Chapter 2,4,5; García-Gamero et al., 2021).
2. To explore the interaction between soil moisture and soil-forming processes in a hilly Mediterranean catchment in granitic soils. (Chapter 3;García-Gamero et al., 2021[in review]) .
3. To estimate aquifer recharge and explore water table evolution in a hilly Mediterranean catchment in granitic soils. (Chapter 6).
4. To explore the interaction between soil moisture and soil temperature in a hilly Mediterranean catchment in granitic soils. (Chapter 7).

1.5. Thesis Outline

This thesis has been divided in eight (8) chapters:

Chapter 1: A general introduction to this thesis.

Chapter 2: On two opposing hillslopes of a semi-arid, Mediterranean catchment in southern Spain, the study of the interaction between hydrology, terrain and vegetation have been performed through soil moisture, vegetation, and water table dynamics measurement, to

quantify the aspect influence on ecohydrological dynamics of an oak-woodland savanna or "*dehesa*".

Chapter 3: Chemical weathering is modelled and compared to topographical position and hydrological parameters through the chemical depletion fraction (CDF) (Riebe et al., 2003) defined as the ratio of total denudation corresponding to chemical weathering. Such a model may be used to evaluate global change and address decisions.

Chapter 4: To complete Chapter 2 a temporal stability analysis of soil moisture and a Principal Component Analysis was performed to evaluate the spatio-temporal variability of soil moisture on two opposing hillslopes of a semi-arid, Mediterranean catchment in southern Spain.

Chapter 5: The purpose is to illustrate the aspect effects on the early stages of recharge and discharge processes on soils located on two opposing hillslopes of a semi-arid, Mediterranean catchment in southern Spain, one oriented towards the south, or toward the Equator in global terms, and another one oriented towards the north, or toward the Poles.

Chapter 6: To document the water flow through the unsaturated zone and groundwater recharge, the piezometric levels of a hillslope aquifer on a granitic formation have been measured during experimental research on the hydrological, rock weathering, and soil-forming processes, in the Cordobesian part of Sierra Morena in southern Spain. The estimation of the Master Recession Curve using the water table fluctuation method allows an estimation of the aquifer recharge pulses and the specific yield.

Chapter 7: The use of heat as a hydrogeological tracer in phreatic aquifers has been applied to the analysis of the soil water recharge from the study of the temporal variation of the temperature measured at several depths along a large period.

Chapter 8: Gives general conclusions and areas for future research.

1.6. References

Ashley, G. M. (1998). Where are we headed? “Soft” rock research into the new millennium. *Geological Society of America Abstract/Program*, *30*(A-148).

Blöschl, G., Gaál, L., Hall, J., Kiss, A., Komma, J., Nester, T., Parajka, J., Perdigão, R. A. P., Plavcová, L., Rogger, M., Salinas, J. L., & Viglione, A. (2015). Increasing river floods: fiction or reality? *WIREs Water*, *2*(4), 329–344. https://doi.org/10.1002/wat2.1079

Constantz, J., Tyler, S. W., & Kwicklis, E. (2003). Temperature-Profile Methods for Estimating Percolation Rates in Arid Environments. *Vadose Zone Journal*, *2*(1), 12–24. https://doi.org/10.2136/vzj2003.1200

Fan, Y., Clark, M., Lawrence, D. M., Swenson, S., Band, L. E., & Brantley, S. L. (2019). Hillslope Hydrology in Global Change Research and Earth System Modeling Water Resources Research. *Water Resources Research*, *55*, 1737–1772. https://doi.org/10.1029/2018WR023903

Finke, P. A., & Hutson, J. L. (2008). Modelling soil genesis in calcareous loess. *Geoderma*, *145*, 462–479. https://doi.org/10.1016/j.geoderma.2008.01.017

García-Gamero, V., Peña, A., Laguna, A. M., Giráldez, J. V., & Vanwalleghem, T. (2021). Factors controlling the asymmetry of soil moisture and vegetation dynamics in a hilly Mediterranean catchment. *Journal of Hydrology*, *598*, 126207. https://doi.org/10.1016/j.jhydrol.2021.126207

García-Gamero, V., Vanwalleghem, T., Peña, A., Román-sánchez, A., & Finke, P. A. (2021). Modelling the effect of catena position and hydrology on soil chemical weathering. *SOIL Discuss*, *August*, 1–26. https://doi.org/https://doi.org/10.5194/soil-2021-78

Jenny, H. (1941). *Factors of soil formation: A System of Quantitative Pedology*. McGraw-Hill Book Company Inc.

Kirkby, M. J. (2016). Water in the critical zone : soil , water and life from profile to planet.

Soil, *2*(4), 631–645. https://doi.org/10.5194/soil-2-631-2016

Krueger, E. S., Ochsner, T. E., Levi, M. R., Basara, J. B., Snitker, G. J., & Wyatt, B. M. (2021). Grassland productivity estimates informed by soil moisture measurements: Statistical and mechanistic approaches. *Agronomy Journal*, *113*(4), 3498–3517. https://doi.org/10.1002/agj2.20709

Massari, C., Brocca, L., Moramarco, T., Tramblay, Y., & Lescot, J. D. (2014). Advances in Water Resources Potential of soil moisture observations in flood modelling : Estimating initial conditions and correcting rainfall. *Advances in Water Resources*, *74*, 44–53. https://doi.org/10.1016/j.advwatres.2014.08.004

McColl, K. A., Wang, W., Peng, B., Akbar, R., Short Gianotti, D. J., Lu, H., Pan, M., & Entekhabi, D. (2017). Global characterization of surface soil moisture drydowns. *Geophysical Research Letters*, *44*(8), 3682–3690. https://doi.org/10.1002/2017GL072819

Meinzer, O. E. (1923). Outline of Ground-Water Hydrology. In *US Geologycal Survey Water Supply paper* (Vol. 494). U.S Government Printing Office.

Nassar, I. N., & Horton, R. (1992). Simultaneous Transfer of Heat, Water, and Solute in Porous Media: I. Theoretical Development. *Soil Science Society America Journal*, *56*, 1350–1356.

National Research Council (NRC). (2001). *Basic Research Opportunities in Earth Science*. The National Academies Press. https://doi.org/10.17226/9981

Ochsner, T. E., Cosh, M. H., Cuenca, R. H., Dorigo, W. A., Draper, C. S., Hagimoto, Y., Kerr, Y. H., Larson, K. M., Njoku, E. G., Small, E. E., & Zreda, M. (2013). State of the Art in Large-Scale Soil Moisture Monitoring. *Soil Science Society of America Journal*. https://doi.org/10.2136/sssaj2013.03.0093

Opolot, E., Yu, Y. Y., & Finke, P. A. (2015). Modeling soil genesis at pedon and landscape scales: Achievements and problems. *Quaternary International*, *376*, 34–46. https://doi.org/10.1016/j.quaint.2014.02.017

Rempe, D. M., & Dietrich, W. E. (2014). A bottom-up control on fresh-bedrock topography under landscapes. *Proceedings of the National Academy of Sciences*, *111*(18), 6576–6581. https://doi.org/10.1073/pnas.1404763111

Rempe, D. M., & Dietrich, W. E. (2018). Direct observations of rock moisture, a hidden component of the hydrologic cycle. *Proceedings of the National Academy of Sciences*, *115*(11), 2664–2669. https://doi.org/10.1073/pnas.1800141115

Riebe, C. S., Kirchner, J. W., & Finkel, R. C. (2003). Long-term rates of chemical weathering and physical erosion from cosmogenic nuclides and geochemical mass balance. *Geochimica et Cosmochimica Acta*, *67*(22), 4411–4427. https://doi.org/10.1016/S0016-7037(03)00382-X

Sungmin, O., Hou, X., & Orth, R. (2020). Observational evidence of wildfire - promoting soil moisture anomalies. *Scientific Reports*, 1–8. https://doi.org/10.1038/s41598-020-67530-4

Vereecken, H., Huisman, J. A., Bogena, H., Vanderborght, J., Vrugt, J. A., & Hopmans, J. W. (2008). On the value of soil moisture measurements in vadose zone hydrology : A review. *Water Resources Research*, *44*, 1–21. https://doi.org/10.1029/2008WR006829

Chapter 2

Factors controlling the asymmetry of soil moisture and vegetation dynamics in a hilly Mediterranean catchment

FACTORS CONTROLLING THE ASYMMETRY OF SOIL MOISTURE AND VEGETATION DYNAMICS IN A HILLY MEDITERRANEAN CATCHMENT

Published as: García -Gamero, V., Peña, A., Laguna, A. M., Giráldez, J. V., y Vanwalleghem, T. 2021. Factors controlling the asymmetry of soil moisture and vegetation dynamics in a hilly Mediterranean catchment. Journal of Hydrology, 598, 126207. https://doi.org/10.1016/j.jhydrol.2021.126207

Journal of Hydrology 598 (2021) 126207

Contents lists available at ScienceDirect

Journal of Hydrology

journal homepage: www.elsevier.com/locate/jhydrol

Research papers

Factors controlling the asymmetry of soil moisture and vegetation dynamics in a hilly Mediterranean catchment

V. García-Gamero [a,*], A. Peña [b], A.M. Laguna [c], J.V. Giráldez [a,d], T. Vanwalleghem [a]

[a] Depto. de Agronomía, Universidad de Córdoba, Edif. Da Vinci, Ctra. Madrid km 396, 14071 Córdoba Spain
[b] Depto. de Ingeniería Rural, Universidad de Córdoba, Edif. Da Vinci, Ctra. Madrid km 396, 14071 Córdoba Spain
[c] Depto. de Física Aplicada, Universidad de Córdoba, Edif. C2, Ctra. Madrid km 396, 14071 Córdoba Spain
[d] Depto. de Agronomía, Instituto de Agricultura Sostenible, CSIC, Avda. Menéndez Pidal s/n. 14004 Córdoba Spain

ARTICLE INFO

This manuscript was handled by Corrado Corradini, Editor-in-Chief, with the assistance of Renato Morbidelli, Associate Editor

Keywords:
Soil moisture
Slope aspect
Mediterranean environments
Shallow aquifer recharge

ABSTRACT

The interaction between hydrology, terrain, and vegetation, is an essential element in understanding complex landscapes, and in forecasting their evolution under climate change. In Mediterranean Europe, few studies have been performed on the interrelation between them. In this study, soil moisture, vegetation, and water table dynamics were measured on opposing hillslopes of a semi-arid, Mediterranean catchment in southern Spain, to quantify the aspect influence on ecohydrological dynamics of an oak-woodland savanna or "*dehesa*".

Observations of a network of 32 soil moisture sensors on two opposing hillslopes, a north-facing slope (NFS), and a south-facing one (SFS), detected a similar moisture dynamics, although the influence of the vegetation induces a lagged response where the NFS dries out earlier compared to the SFS. Analysis of successive soil water profiles after storm events suggests that the water moves downwards as an unsaturated preferential flow along the walls of the fractured granite material, with residence times between 16.3 and 36.7 days. Our results show that there is a direct coupling between the hillslope hydrology, the depth of the weathered bedrock, much higher on the NFS, and the vegetation dynamics. Vegetation is much denser on NFS, as LIDAR-derived biomass estimates were 29% higher than on the SFS. The evolution of the normalized difference vegetation index (NDVI), obtained from the Sentinel-2 time series, also shows completely opposing trends with a minimum value at the end of winter for the NFS, whereas the SFS reaches minimum values in summer. A significant correlation between NDVI and soil moisture was found for the SFS (Pearson's R of 0.81). However, this correlation is very poor on the NFS, but a good correlation with water table was found (R = 0.46). This shows how the deep weathering on the NFS allows for an additional water source, contained in the rock moisture and saturated zone, that represents an important source for the vegetation, whereas on the SFS only soil moisture supports the vegetation. These vegetation differences in turn directly impact surface soil moisture, leading to the observed, relatively similar trends on both hillslopes.

ABSTRACT

The interaction between hydrology, terrain, and vegetation, is an essential element in understanding complex landscapes, and in forecasting their evolution under climate change. In Mediterranean Europe, few studies have been performed on the interrelation between them. In this study, soil moisture, vegetation, and water table dynamics were measured on opposing hillslopes of a semi-arid, Mediterranean catchment in southern Spain, to quantify the aspect influence on ecohydrological dynamics of an oak-woodland savanna or "*dehesa*".

Observations of a network of 32 soil moisture sensors on two opposing hillslopes, a north-facing slope (NFS), and a south-facing one (SFS), detected a similar moisture dynamics, although the influence of the vegetation induces a lagged response where the NFS dries out earlier compared to the SFS. Analysis of successive soil water profiles after storm events suggests that the water moves downwards as an unsaturated preferential

flow along the walls of the fractured granite material, with residence times between 16.3 and 36.7 days. Our results show that there is a direct coupling between the hillslope hydrology, the depth of the weathered bedrock, much higher on the NFS, and the vegetation dynamics. Vegetation is much denser on NFS, as LIDAR-derived biomass estimates were 29% higher than on the SFS. The evolution of the normalized difference vegetation index (NDVI), obtained from the Sentinel-2 time series, also shows completely opposing trends with a minimum value at the end of winter for the NFS, whereas the SFS reaches minimum values in summer. A significant correlation between NDVI and soil moisture was found for the SFS (Pearson's R of 0.81). However, this correlation is very poor on the NFS, but a good correlation with water table was found (R=0.46). This shows how the deep weathering on the NFS allows for an additional water source, contained in the rock moisture and saturated zone, that represents an important source for the vegetation, whereas on the SFS only soil moisture supports the vegetation. These vegetation differences in turn directly impact surface soil moisture, leading to the observed, relatively similar trends on both hillslopes.

Keywords: Soil moisture; Slope aspect; Mediterranean environments; Shallow aquifer recharge.

2.1. Introduction

Soil moisture, plants, and their inter-relations are the base of ecohydrological studies (Eagleson, 2002), especially in water-limited arid and semi-arid systems (D'Odorico et al., 2010). Different works have shown the impact of topography, soil properties, radiation (e.g., Bennie et al., 2008), and vegetation cover, on the spatial and temporal variability of soil moisture in dry environments (Cantón et al., 2004) and in wetter, colder landscapes (Kim, 2009). Solar radiation also exerts a significant control over the spatial organization of ecohydrological processes, such as: rainfall interception, evapotranspiration, root uptake, runoff generation, and vegetation canopy dynamics (Yetemen et al., 2015).

Different studies have addressed the effect of aspect on ecohydrological dynamics. Gutiérrez-Jurado et al. (2013) observed that the energy input was more important than the vegetation in the control of the surface water transfer processes, in the Sevilleta National Wildlife Refuge in New Mexico (USA) as being a major cause of the valleys' slope asymmetry. In this area, the north-facing slopes (NFS) were wetter and colder than the analogous south-facing slopes (SFS). In a similar study, in the Jemez watershed in northern New Mexico, Zapata-Rios et al. (2016) detected a reduction in the incoming radiation by NFS which resulted in a smaller vegetation cover than the analogous east-facing slopes (EFS). Consequently, these authors found that the water partitioning between vaporization and soil wetting in the watershed, whose ratio is defined as the Horton index, was lesser in the NFS than in the EFS.

It is well known that slope aspect is also related to asymmetry in hillslope geomorphology (Istanbulluoglu et al., 2008), but only recently, critical zone research has linked aspect to even deeper changes, in soil properties and the architecture of the critical zone. Geroy et al. (2011) found that the NFS soils formed on the Idaho batholith not far from Boise (USA), have a greater porosity, more organic matter, and a higher silt content than those on the

SFS. They did not explicitly study vegetation differences, and while there is clearly a higher vegetation cover on NFS compared to SFS in their study site, they attribute these differences in soil properties to complex interactions between microclimate, vegetation, lithology, material resource source and erosion. In view of such complex interactions, Poulos et al. (2012) proposed a hillslope asymmetry index, HA, to homogenize the asymmetry comparison caused by different drivers: tectonic, climate, and hydrological. In any case, the observations of Geroy et al. (2011) agree with the measurements of soil hydraulic conductivity in asymmetric slopes in Gabilan Mesa, in California (USA), made by Richardson et al. (2020), which were greater in NFS than in SFS, concluding that surface runoff was the main reason for that asymmetry.

A recent review of Pelletier et al. (2018) summarized most of the research done on slope aspect controls on Critical Zone processes and reviews the causes for the hillslope asymmetry that is observed at different latitudes. They introduced a model separating the water-limited and temperature-limited soil mantle cases and distinguishing a temperature threshold in both Earth hemispheres. They also proposed the terminology pole- and equator-facing hillslopes, instead of NFS and SFS, to generalize in both Earth hemispheres. Otherwise, the results of the studies would be only valid for the corresponding hemisphere in which the study area is located, as is the case with the aforementioned works whose results are valid only for the Northern hemisphere. Kumari et al. (2020), adopting this pole and equatorial-facing slopes terminology, highlight the importance of seasonal variations in the aspect effects of the valley asymmetry.

A relatively unknown component of the hydrological cycle whose importance was recently brought to light is rock moisture, which is the water stored in the vadose zone of the fractured bedrock. It is well known that vegetation in areas with thin soils extracts water from fractured bedrock, exploiting either groundwater or rock moisture (Lubczynski et al., 2009). Eliades et al. (2018) measured with sap flow sensors that this contributed over 70%

of the transpiration of Mediterranean pine trees in Cyprus. However, Rempe and Dietrich (2018) were among the first to specifically quantify the contribution of rock moisture as a significant source of water, containing up to 27% of the annual rainfall in their study site in the Northern California Coast ranges, USA. Schmidt and Rempe (2020) were the first to quantify water dynamics of rock moisture by nuclear magnetic resonance. Hahm et al. (2020) corroborated the importance of rock moisture for vegetation dynamics. With isotope tracers, they showed how oak transpiration during the summer dry season in California was drawn from the fractured bedrock. They found that the depth of dynamic storage reaches up to 9 m and claim that this would reflect the depth of root water uptake, which will need to be confirmed by further studies. Hahm et al. (2019) found that regional plant composition along the Northern California Coastal ranges was controlled by the thickness of the subsurface critical zone, and therefore by the size of this rock moisture reservoir, i.e., the moisture content within the vadose zone that is not properly soil (e.g., Meinzer,1923). Hahm et al. (2019) analyzed vegetation differences between seven catchments from the Northern California coast range. They found important differences in plant productivity and mortality and relate these differences to the size of the rock moisture storage capacity. Counterintuitively, they conclude that catchments with a low subsurface water storage capacity would be less sensitive to rainfall variations.

It is clear that the coupling between vegetation dynamics on the one hand, and soil and subsurface water dynamics, on the other remains poorly understood. The impact of aspect on the interaction of these factors has not yet been analyzed. If the conclusion of Hahm et al. (2019) hold, differences between plant productivity could also be expected as a function of topography, as critical zone architecture and soil properties differ as function of aspect.

Also, while some studies have analyzed the effect of aspect or topographic position on soil moisture, or the effect of aspect on vegetation dynamics, very few studies have examinated the interrelations between them. In any case, it is also not clear what happens in other

regions and landscapes and this requires further study. In Mediterranean Europe, few studies have been performed on the interrelation between landscape position, soil moisture and vegetation (e.g., Nadal-Romero et al.,2014) and no studies on rock moisture have been done. In this region, there is a common semi-natural land use system called *dehesa* or *montado* (in Spain and Portugal, respectively) which is ideally suited for such further study. This land management system is also called a Mediterranean savanna (Eagleson and Segarra, 1985; Scholes and Archer, 1997), as it consists of a homogeneous grassland with woody plants. On the local scale, the influence of tree canopies (mainly *Quercus ilex L*, *Quercus suber L*, and *Quercus Pyrenaica Willd*.) is detected by the increase in actual evapotranspiration and the reduction in the water yield in the analogical processes occurring in the open space between trees as evaluated by Joffre and Rambal (1993).

The main objective of this work is to explore the valley asymmetry characteristics of a dehesa system by considering the soil moisture evolution and its controlling factors. The specific objectives are: (i) to analyze soil moisture dynamics in different landscape positions, (ii) to determine the specific aspect influence on the soil moisture dynamics and hillslope hydrology, (iii) to quantify vegetation response through the normalized difference vegetation index (NDVI) on two opposite slopes in a dehesa watershed, and analyze its relation to soil moisture and water table evolution.

2.2. Material and methods

2.2.1. *Study area*

This study was conducted in a semi-natural area of oak-woodland savanna or *dehesa*, located in Sierra Morena in the north of the region of Córdoba (Fig. 2.1a), southern Spain (38.2° N; 4.17° W, 700 m a.m.s.l.). The Sierra Morena ecosystem is included in the Natura 2000 network, protected by the Habitat Directive 92/43/EEC.

The zone has a continental Mediterranean climate (BSk) in the Köppen-Geiger diagram

(Peel et al., 2007), with an average annual rainfall of 878 mm (from 1981 to 2010), cold winters and dry, long summers. The mean annual air temperature is 15.3 °C, with the coldest month being January, with a mean monthly temperature of 7°C, and the hottest July, with a mean monthly temperature of 25.4°C (Carpintero et al., 2020).

The study site (Fig. 2.1c) is within the so-called Santa Clotilde Critical Zone Observatory (CZO) and is named after the privately-owned Santa Clotilde farm, where it is located. This CZO is situated within the 48.3 km^2 catchment draining into the Martin Gonzalo reservoir. There is a vegetation difference, which could be attributed to the aspect. With the purpose of exploring this potential asymmetry, opposing north and south-facing slopes were selected to install soil moisture monitoring equipment. To simplify the analysis, we will henceforth refer to these as respectively, NFS and SFS. In this study area, vegetation composition in the NFS is dominated by a closed canopy of evergreen oaks (Quercus spp), 95% of trees and bushes cover, in association with 5% of annual grasses cover while the SFS is a wooded grassland with sparse oaks, 60% of trees and bushes cover, 20% of annual grasses and 20% bare soil.

Soils in the catchment are derived from Los Pedroches batholith parent material, composed of a main granodioritic unit, several granite plutons, and an important acid- to- basic dyke complex (Carracedo et al., 2009). These soils belong to the orders Regosols, Leptosols, and Cambisols under the FAO-Unesco World Reference Base (IUSS Working Group WRB, 2015). Their texture class is mainly sandy to sandy loam, with a depth generally ranging between 0.5 m along the south aspect part of the transect and 1.0 m along the northern part of the transect (Román-Sánchez et al., 2018).

The climatic seasonality, comprising a long dry summer, and the low fertility of the soil make agriculture unsustainable in this area all year round. As Joffre et al. (1999) explained, the old transhumance system was abandoned and sheep were replaced locally, and almost all over this environment, by beef cattle and the Iberian pig, the largest direct product of

this *dehesa.* The cattle graze equally throughout the area though avoiding steep parts, with a diet based on natural grasses and other supplementary feeding. The Iberian pig is fed on acorns and grass from October to January.

The livestock contributes to the dispersion of the natural pasture seeds and their fertility. Vegetation in a *dehesa* consists of, as anticipated at the beginning of this subsection, sparse trees: holm (*Quercus Ilex* L.), cork oaks (*Quercus suber*), Portuguese oak or Valencian oak (*Quercus faginea*), and other species with no or a scant capacity for natural regeneration, and a tree senescence of 150 years for *Quercus suber* and 250-300 years for other species (Olea & San Miguel-Ayanz, 2006). Bushes, retama (*Retama sphaerocarpa L.*), and annual grasses such as *Lolium sp.*, *Bromus sp.*, and *Trifolium sp.*, with a maximum production in spring and a non-vegetative period in summer are common in the watershed.

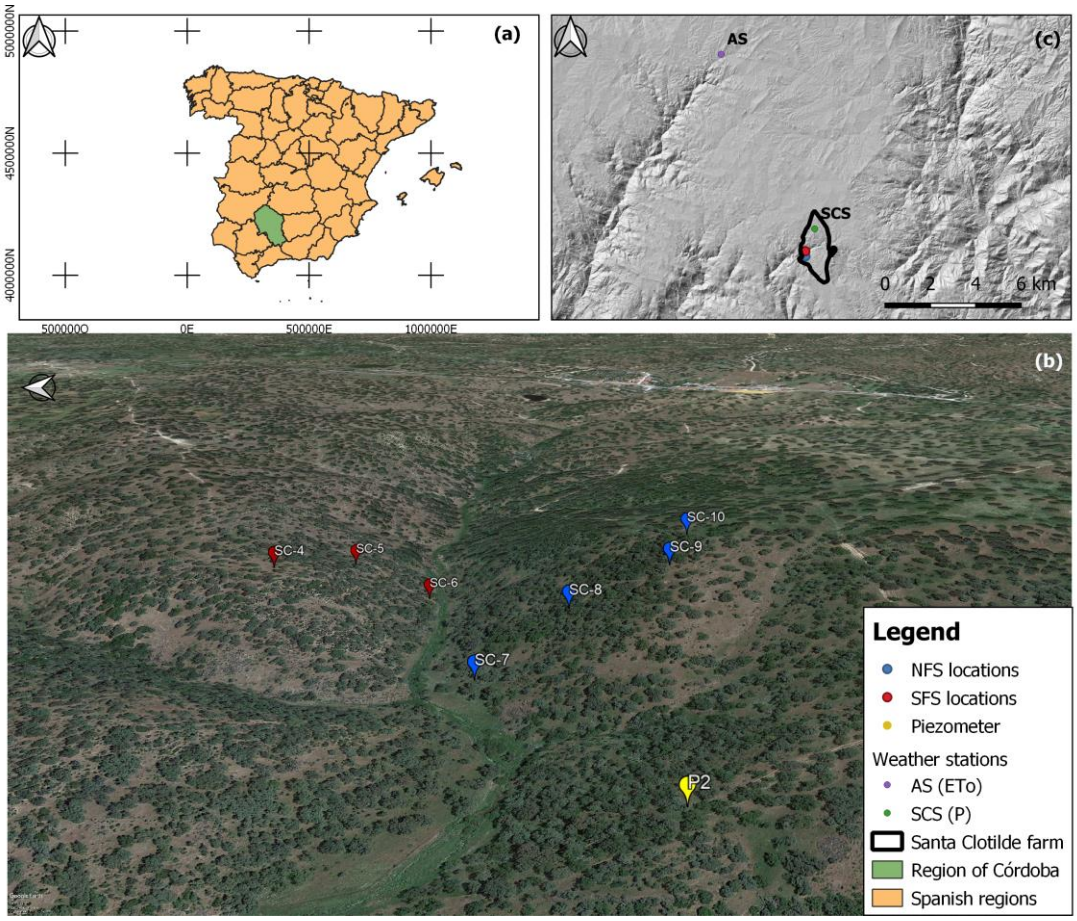

Figure 2.1. (a) General Location of the study zone in the north of the region of Córdoba, southern Spain. (b)Detailed overview of the two studied opposing slopes, with the distribution of 7 soil moisture monitoring sites that cover two opposing slopes and a piezometric well (yellow dot). Red

dots show south-facing slope (SFS) monitoring sites and blue dots show the north-facing slope (NFS) monitoring sites. (c) Location of Santa Clotilde farm (black line) and the rainfall, P, (SCS) (green dot) and reference evapotranspiration, ET_0, (AS) (purple dot) stations. Red and blue dot show the location of the soil moisture monitoring sites on the SFS and NFS, respectively.

2.2.2. *Experimental set up*

A total of seven soil moisture monitoring sites were chosen (Fig. 2.1b and Fig. 2.2), along a toposequence, including two opposite hillslopes, to install soil moisture monitoring stations. The NFS ranges in height from 655 to 725 m a.m.s.l and the SFS, from 655 to 705 m a.m.s.l. (Fig. 2.2). Four monitoring sites (SC10-SC7) were set up along the NFS and three monitoring sites (SC4-SC6) along the SFS, to record soil volumetric moisture content, bulk electrical conductivity, and temperature. The sensors were set out along different landscape positions on each of the opposing slopes, including hilltop, slope and valley bottom, as shown in Table 2.1. The exact positions were determined by the accessibility of the excavator due to the difficult terrain conditions with high slopes, trees and rocks. The difficult accessibility of the area also determined that the line of monitoring sites on the NFS was not perfectly convergent with that on the SFS (Fig. 2.1b). Each monitoring site consisted of five soil moisture sensors (Campbell Scientific, CS655), at depths of 0.05, 0.15, 0.25, 0.35, and 0.45 m, except SC4 and SC5, in which the two deepest and the deepest sensor, respectively, could not be installed because of the shallower depth to bedrock. On the SFS it was observed that hard bedrock directly underlying the soil profile while on the NFS we observed the presence of highly weathered saprolite as the excavator could easily dig through this material and it could be broken manually. After the sensor installation, the profile pits were covered with soil again. Five dataloggersCR200 (Campbell Sci., Inc), one CR800, and one CR1000 (Campbell Sci., Inc) were used to monitor all the sensors located along the north-south transect. The clocks on the dataloggers were synchronized and periodically checked to ensure that the measurement timing throughout the site was always consistent. Measurements were recorded at half-hourly intervals from

November 2016 to early January 2018, and at 10 min intervals from January 2018 to November 2019, providing a precise timing of the arrival of the wetting front with the depth. The system is powered by solar cells with a maximum power of 15 W and 12 V that supply the necessary energy for data maintenance and storage to the dataloggers.

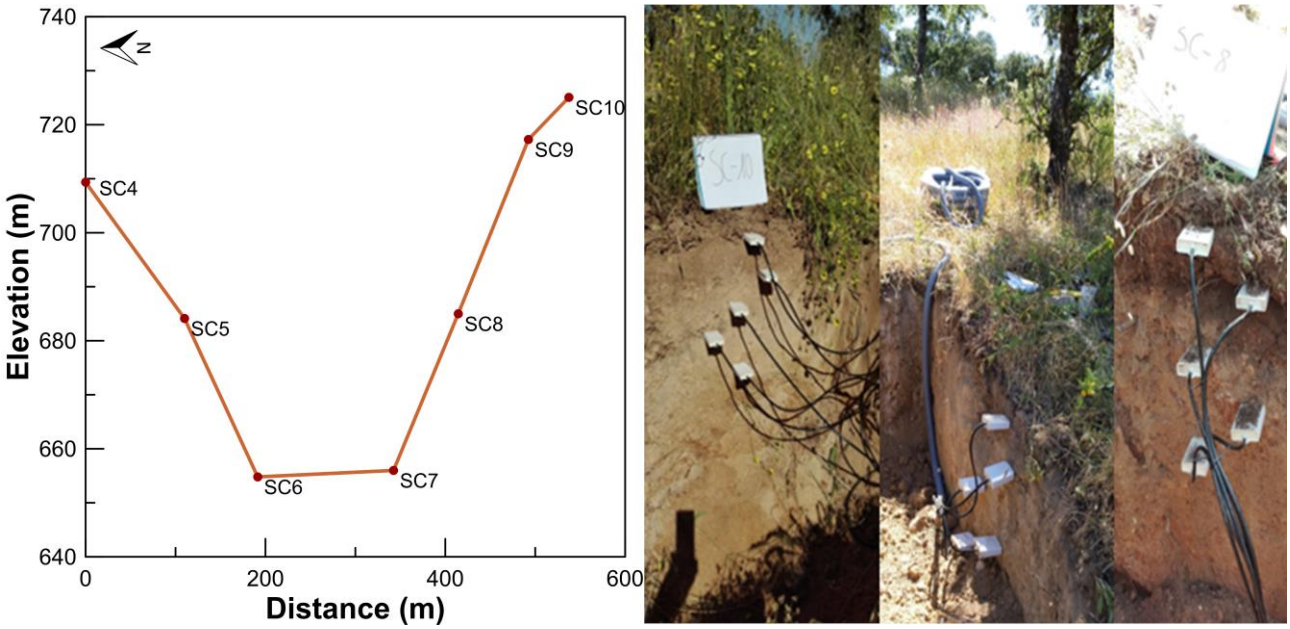

Figure 2.2. Profile showing soil moisture monitoring sites on NFS and SFS and depth distribution of sensors at different locations. Note that the profile pits were covered with soil after the sensor installation.

Topographic factors and soil properties at each of the measuring locations are shown in Table 2.1. On average, the sand fraction dominated the particle size distribution (~74.3%). The average proportion of coarse gravel was high, i.e., ~32%. Table 2.1 also shows that the organic matter content (OM) was scant (~1.06%), which is consistent with the Mediterranean climate and topographic conditions. The annual global solar radiation and the topographic wetness index (TWI) were calculated using the spatial analysis tools in ArcGIS software from a digital elevation model (DEM) with a spatial resolution of 5 m (ETRS89 UTM Zone 30). The TWI was derived according to the following relation (Beven and Kirkby, 1979):

$$\mathrm{TWI} = \ln\left(\frac{\mathrm{UCA}}{\tan \mathrm{Slope}}\right) \tag{2.1}$$

Where UCA is the Upstream contributing area and tan Slope is the tangent of the slope angle in Equation 2.1.

Table 2.1. Topographic factors and soil properties, weighted mean for 0-0.50 m, at the measuring locations.S, local slope gradient, RAD $_{annual}$, Annual global solar radiation, TWI, Topographic Wetness Index, OM, Organic matter, ρb, Bulk density, Z, Soil depth, ks, Saturated hydraulic conductivity determined by the Phili-Dunne method (Philip,1993) at different locations on NFS and SFS.

Aspect	Location	Landform types	S (°)	RAD_{annual} ($kWhm^{-2}$)	TWI	Sand	Silt	Clay	Stone %	OM %	ρ_b (Mgm^{-3})	Z (m)	k_s (cms^{-1})
						Without coarse fraction,%							
SFS	SC4	Hilltop	4	1,393	4.50	73.5	20.1	6.4	25.9	1.16	1.47	0.44	
	SC5	Mid Slope	20	1,395	3.63	83.1	12.0	4.9	44. 1	0.54	1.54	0.60	$2.33 \cdot 10^{-3}$
	SC6	Valley bottom	14	1,391	6.55	69.5	22.4	8.1	32.0	1.21	1.47	0.55	$4.43 \cdot 10^{-2}$
NFS	SC7	Valley bottom	4	1,210	6.24	76.1	15.6	8.3	25.7	1.02	1.66	0.97	
	SC8	Mid Slope	27	1,153	3.88	61.3	29.0	9.7	26.7	1.09	1.41	0.47	$1.75 \cdot 10^{-2}$
	SC9	Upper Slope	19	1,327	4.12	75.2	19.4	5.4	46.3	1.16	1.52	0.57	
	SC10	Hilltop	2	1,324	4.17	81.5	14.3	4.2	23.0	1.27	1.73	0.50	$1.62 \cdot 10^{-3}$

Regarding climate data, rainfall was measured with a tipping bucket rain gauge. Measurements were recorded at half-hourly intervals by a nearby automated weather station Installed by the Andalusian Institute of Agricultural Research and Training (IFAPA) (IFAPA, 2020) in the zone (Fig. 2.1c). Also, reference evapotranspiration, computed with the Penman-Monteith equation (Allen et al., 1998), was obtained by a weather station installed by the Regional Ministry of Agriculture, Fishing, and Environment (Consejería de

Agricultura, Pesca y Medio Ambiente, 2020), close to the study area (Fig.2.1c).

2.2.3. *Soil moisture analysis*

Soil moisture content, θ, was determined by converting the dielectric permittivity measurement into volumetric moisture content using the Topp equation (Topp et al., 1980), which has shown itself to be accurate within a few percent for a wide variety of soils (Dalton, 1992; Skierucha et al., 2012), and has eliminated the necessity of soil-specific calibrations for most routine applications (Ghezzehei, 2008; Persico et al., 2019). The third-degree polynomial Topp equation (Equation 2.2) described the relationship between dielectric permittivity and volumetric moisture content in mineral soils. Sensors measure electromagnetic wave propagation time, by knowing the length of the probe waveguides. The velocity of wave propagation is dependent on the dielectric permittivity of the surrounding media (Kirkham, 2014), including both the fine soil and the stones.

The equation presented by Topp et al. (1980) was:

$$\theta_v = -5.3 \times 10^{-2} + 2.92 \times 10^{-2} K_a - 5.5 \times 10^{-4} K_a^2 + 4.3 \times 10^{-6} K_a^3 \quad (2.2)$$

Being θ_v the volumetric moisture content and K_a the bulk dielectric permittivity of the soil.

θ of the complete 0-0.50 m profile was calculated by averaging the soil moisture of all the depths and was normalized as an effective saturation ratio (*e.g.,* Brutsaert, 2005).

$$s = \frac{\theta - \theta_{min}}{\theta_{max} - \theta_{min}} \quad (2.3)$$

where θ_{min} and θ_{max} are the minimum and maximum θ measured, respectively. Thereafter, we refer to the effective saturation ratio as soil moisture (s) according to Equation 2.3.

2.2.3.1. Evolution of depth-averaged soil moisture

In order to obtain a simple measurement of overall synchrony between the different locations along the toposequence, profile-average soil moisture was calculated for each soil profile and a pairwise correlation was assessed through the Pearson correlation coefficient

(Pearson's R). The statistical analysis and data management were performed with the RStudio software (R Core Team, 2018) and the Hmisc package (v4.3-0; Harrell, 2019). To avoid spurious correlations due to underlying trends in the dataset, the Pearson correlation coefficient is reported for daily soil moisture increments or first differences, i.e., $s' = s(t) - s(t-1)$, with $s(t)$ being the normalized value at time t. Note that s' represents the daily change of storage in the soil, due to the evaporation, infiltration and percolation flow.

2.2.3.2. Soil moisture probabilistic description

After evaluating the overall correlations of s' between the different sites, its general behaviour was described by means of the analysis of the probability density function (pdf). To further inspect the influence of seasonality on soil moisture, two different Weibull pdf's were fitted, one for the dry state, and another one for the wet state. For the dry period, data were gathered from April 16 to November 15 and for the wet one from November 16 to April 15. Dry state data corresponded to the long periods between rain events while wet state data were collected in the rainy periods. Nevertheless, to avoid spurious data, due to sudden warm days between rain events, a threshold value of soil moisture was selected for the wet state, $s = 0.2$. No limit value was established for the dry state. Fittings were made with the maximum likelihood estimation method (e.g., Bury, 1999 §17.12).

The pdf of a Weibull random variable is (Bury, 1999 §17.1):

$$f(x;\kappa,\lambda) = \frac{\kappa}{\lambda}\left(\frac{x}{\lambda}\right)^{\kappa-1} exp\left[-\left(\frac{x}{\lambda}\right)^{\kappa}\right] \quad x \geq 0 \quad \kappa,\lambda > 0 \tag{2.4}$$

x being s, κ the shape parameter and λ the scale parameter.

2.2.3.3. Evaluating the aspect influence

In order to assess the influence of aspect on soil moisture, the dynamics of two sensor sites located on opposing hillslopes, in a similar landscape position on the mid slope, were evaluated in detail, SC5 and SC8. These sites were selected because they are expected to

best represent the effect of aspect on SFS and NFS, respectively (fig. 2.1b). The Wilcoxon signed-rank test was performed with a significance level of $\alpha = 0.05$, every two months, to compare the two independent groups of samples. Then, we evaluated the underlying causes of the differences observed between soil moisture patterns on NFS and SFS. Thus, we compared the difference in daily soil moisture storage changes between SFS and NFS, concerning rainfall (P) and reference evapotranspiration (ET_0). Differences were calculated as that between the daily soil moisture storage change on SFS and that of the NFS, i.e. $\Delta s_{SFS} - \Delta s_{NFS} = (s_{i+1} - s_i)_{SFS} \cdot (s_{i+1} - s_i)_{NFS}$ with s_i being the normalized value at time i.

2.2.3.4. Residence time

The water-transmitting properties of the soil were estimated with the time scales of the surface soil moisture depletion method after a rain pulse of Kurc and Small (2004), and adapted as well by Gutiérrez-Jurado et al. (2013) in the Sevilleta watershed field study, τ, based on a linear relationship (Equation 2.5) between the moisture loss and the moisture content, normalized with the initial value, θ_1, the final of the drydown, θ_f, and the time, t, similar to the T model of Alley (1984), as

$$\theta = \theta_f + (\theta_1 - \theta_f)\, e^{-t/\tau} \quad (2.5)$$

τ was calculated following the guidelines of the above authors. A rain event >8 mm and the surface θ, in the first 10 cm, during the days following the rainfall, until the next rain >2 mm was considered. Then, we made an exponential fit to data and obtained the exponential time constants.

2.2.4. *Water table monitoring*

The water table fluctuations could only be observed on the NFS because no water table was detected on the SFS, whose shallow soil is directly underlain by hard bedrock. A piezometric well was drilled and tubed with PVC pipes on the NFS in 2016, in the mid slope position, with a diameter of 0.076 m and 9.50 m in depth. A pressure transducer (HOBO

U20L-02, Water level (30.6 m) Data Logger) was installed in the well for the monitoring of the water table level at 15-min intervals from November 2016 to November 2019.

2.2.5. *Vegetation dynamics*

The vegetation indices most used resort to the information contained in the red and near-infrared (NIR) canopy reflectances. Different studies have employed the NDVI, derived from remote sensing data, to couple vegetation changes with hydrology (Zapata-Rios et al., 2016). NDVI is equal to NIR minus visible radiation divided by NIR plus visible radiation. This index defines values ranging from -1.0 to 1.0.

The Google Earth Engine has been employed to obtain the NDVI from images from the Copernicus Sentinel-2, a European wide-swath, high-resolution, multi-spectral mission (SENTINEL-2, 2020), with 10-m of spatial resolution. NDVI is one of the best known and most used vegetation indices for quantifying the greenness of vegetation, which was measured in an area with a 21 m radius, covering a grid of approximately 3 x 3 pixels with 10-m of spatial resolution, around the SC8 and SC5 location, from November 2016 to November 2019.

In addition, LiDAR data were used to estimate the biomass. These data originate from the Spanish National Plan for Aerial Orthophotography -LiDAR project starting in 2009, whose objective was to cover the whole Spanish national territory with point clouds with X, Y, Z coordinates, and other attributes, obtained by airborne LiDAR sensors; the study area being covered between March and May 2014. The point density is 0.5 points·m^{-2} and they were geo-referenced in the European Terrestrial Reference System 1989 (ETRS89). The altimetric accuracy and precision have a Root Mean Square Error (RMSEz) ≤ 0.2 m. The ellipsoidal heights obtained were transformed into orthogonal elevations. We work with two common products derived from LiDAR, the Digital Terrain Model (DTM) and the Digital Surface Model (DSM) available at the Download Center of the Spanish National Geographic Institute (CNIG,2020). The DTM product represents the elevation of the ground and DSM

represents the tallest point at that location (ground, vegetation and buildings). Filtering algorithms were used by CNIG (2020) to create both layers. The difference between the DSM and DTM, operation in ArcGIS, gives us the height of the biomass. Then, we estimated the volume of biomass considering the 2 m of raster resolution. To get rid of 0 values, we set a strict limit of height difference at 1 m.

2.2.6. *Correlation analysis between NDVI, soil moisture and water table level*

A correlation analysis by means of the Pearson correlation coefficient was used to assess the relationship between the NDVI values, the profile-average soil moisture, and the groundwater level at NFS and SFS. In the latter, the correlation analysis does not include groundwater level due to its absence in SFS.

2.3. Results and discussion

2.3.1. Soil moisture dynamics

2.3.1.1. Evolution of depth-averaged soil moisture

Soil moisture content responds to the rainfall pulses and the more prolonged spring-summer increasing period of reference evapotranspiration as observed by other works (e.g., Or et al., 2013) in the study period from November 2016 to November 2019 as shown in Figure 2.3. In general, the soil dries quite fast to minimum values after the rain pulses.

The seasonal influence on soil moisture patterns is evident in the data of Figure 2.3. Soils are generally wetter during winter and drier during summer, as can be expected in a Mediterranean climate.

Figure 2.3 also depicts the high variability of daily rainfall. The annual precipitation was much smaller in 2017 and 2019, respectively, 477.5 mm and 286.6 mm (until 2019-10-31), compared to 902.3 mm in 2018. Moreover, three rainfall events of over 40 mm occurred in March 2018.

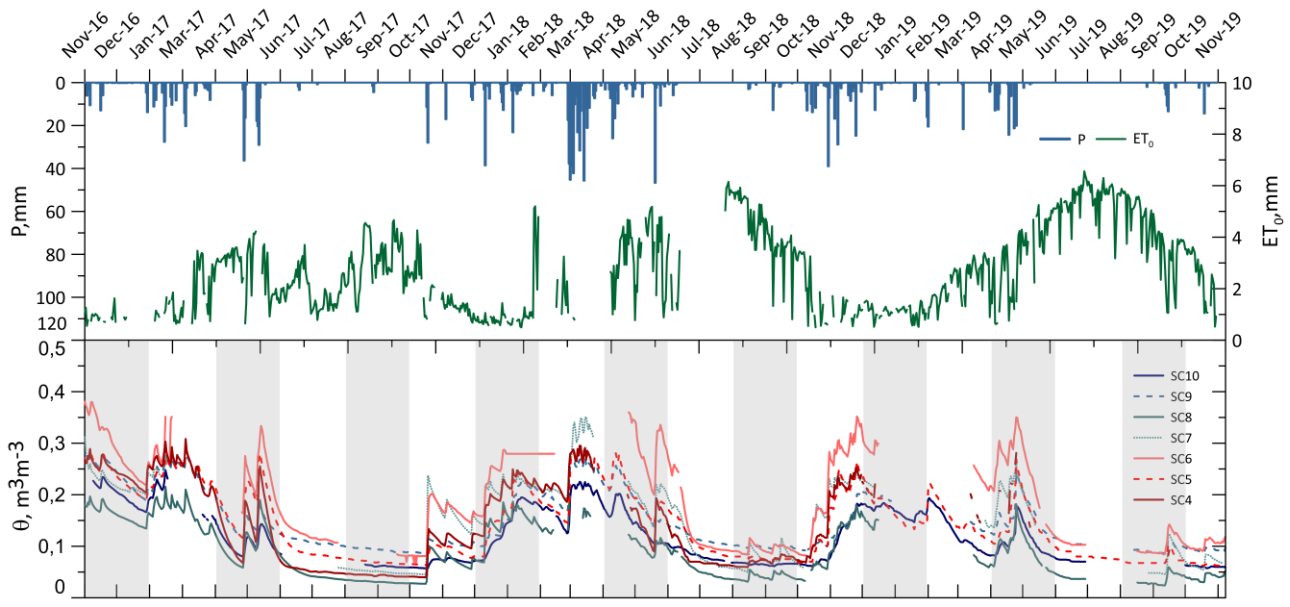

Figure 2.3. Evolution of daily profile-averaged soil moisture content,θ, for the different locations during the study period. Daily precipitation, P, and reference evapotranspiration, ET0, are shown at the top.

The correlation between the soil moisture content of the different sites for the whole measuring period is summarized in Table 2.2. Values shown in bold represent a high positive correlation with Pearson's R values of over 0.60. On the NFS, the moisture content of each sample point is well correlated with that of the closest location. This points out that the locations are wetting and drying out in a similar way. However, there are very important disconnections especially between SC10 and SC7 locations. This suggests lateral redistribution of soil moisture from hilltop to valley bottom (Fan et al., 2019), e.g., rainfall event of May 20, 2018 (Figure 2.3). On the contrary on the SFS, there is a strong correlation between SC4 and SC6 locations, which seems to indicate that lateral redistribution is not important on this slope because of the shallow soil. The correlation between the SC5 and SC6 locations is moderate, just below the subjective limit that we define as high correlation, set a 0.60, possibly due to the greater clay content at SC6 location than that of the SC5.

The soil moisture content of site SC10, the profile at the top of the NFS, is not well correlated with that of site SC4, despite SC4 being in a very similar landscape position at

the top of the opposing SFS. Probably due to the differences mentioned above, with presence of highly weathered saprolite on the NFS and hard bedrock directly underlying the soil profile on the SFS, while on the NFS the water can move to and from the underground aquifer, on the SFS the water cannot percolate from the soil profile. However, the mid-slope profile on the NFS (SC8) has a high correlation with the mid-slope profile on the SFS (SC5) and the valley bottom profile just below on the NFS (SC7) has a high correlation with the corresponding position on the SFS. The presence of coarse particles and the different structure patterns caused by the partial weathering of the granitic rock induced an appreciable variability in the results.

Table 2.2. Pearson correlation coefficient relating soil moisture trends between different locations. Soil moisture series were detrended by calculating s' = s(t) - s(t-1), see text for detailed explanation. Values shown in bold represent a high correlation with values greater than 0.60[a]. Values shown in grey represent the Pearson correlation coefficient between locations on opposite slopes.

Aspect	Landform types	Location	SC10	SC9	SC8	SC7	SC6	SC5	SC4
	Hilltop	SC10	1						
NFS	Upper Slope	SC9	**0.78**	1					
	Mid Slope	SC8	0.56	**0.80**	1				
	Valley bottom	SC7	0.29	0.51	**0.80**	1			
	Valley bottom	SC6	0.45	0.59	**0.72**	**0.73**	1		
SFS	Mid Slope	SC5	**0.81**	**0.80**	**0.72**	0.48	0.58	1	
	Hilltop	SC4	0.51	**0.74**	**0.88**	**0.78**	**0.76**	**0.74**	1

[a] All correlations were significantly correlated with a p-value < 0.05, which is lower than the significance level α= 0.05.

2.3.1.2. Soil moisture probabilistic description

The amount of data of effective saturation ratio, s, allows the estimation of a pdf at each depth and at the depth-averaged profile (Rodriguez-Iturbe et al., 1999). The adjusted pdf showed a bimodal shape with distinct dry and wet states, due to the high seasonality of the Mediterranean climate (D'Odorico et al., 2000; Espejo et al., 2016). Two different Weibull pdf's (Equation 2.4) were fitted, one for the dry state, and another one for the wet state, and are illustrated in Figure 4 for the NFS hilltop site, SC10.

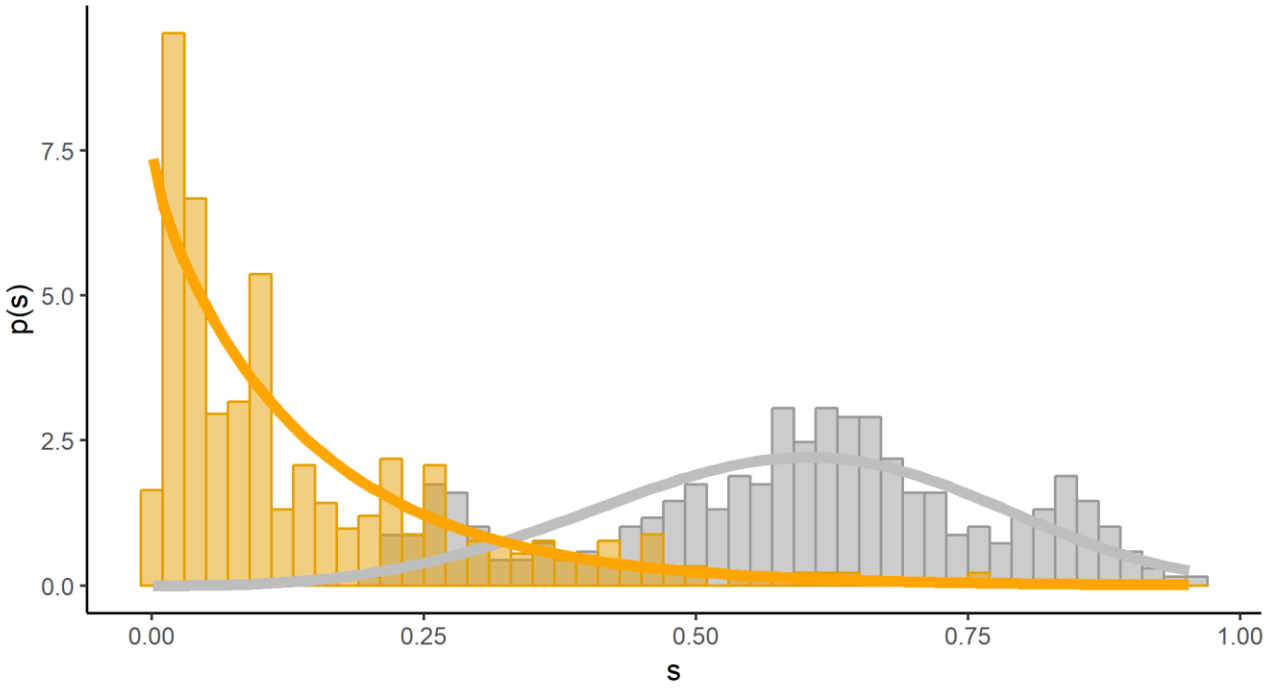

Figure 2.4.Observed (bars) and fitted (lines) effective saturation ratio pdf for the dry (yellow) and wet state (grey) for the NFS hilltop site, SC10. Dry and wet state parameters λ (scale) = 0.14 and κ (shape) = 0.992 and λ = 0.6533 and κ = 3.781, respectively.

The parameters of the fitted pdf's for all monitoring sites are presented in Table 2.3. For detailed information of the goodness of the fits and the relationship between mean and standard deviation of soil moisture at each location at dry and wet states see the supplementary figure S1 and S2, respectively.

Table 2.3. Parameters of the probability density functions (pdfs) fitted to the dry and wet soil moisture states, κ, shape parameter, λ, scale parameter, <s>, mean computed value, σ, standard deviation computed value, CV, coefficient of variation and modea, for the different monitoring locations.

	Dry state: Weibull pdf						Wet state: Weibull pdf					
Location	κ	λ	<s>	σ	CV	mode	κ	λ	<s>	σ	CV	mode
SC4	0.9971	0.1638	0.164	0.165	1.003		4.394	0.7140	0.651	0.168	0.258	0.673
SC5	0.9446	0.1617	0.166	0.176	1.059		.232	0.6857	0.614	0.209	0.340	0.611
SC6	1.242	0.2356	0.220	0.178	0.810	0.063	4.365	0.6914	0.630	0.163	0.259	0.651
SC7	0.8229	0.1862	0.207	0.253	1.223		3.992	0.6324	0.573	0.161	0.281	0.588
SC8	1.12	0.1859	0.178	0.160	0.894	0.025	4.047	0.6856	0.622	0.173	0.278	0.639
SC9	1.097	0.1502	0.145	0.132	0.913	0.016	3.518	0.7093	0.638	0.201	0.315	0.645
SC10	0.9919	0.1439	0.144	0.146	1.008		3.781	0.6533	0.590	0.174	0.295	0.602

[a]If κ is < 1, the mode cannot be calculated (Bury, 1999 Equation 17.10).

For a deeper understanding of the factors affecting the soil moisture, we correlated the fitted pdf means for all sites (SC10·SC4) for the wet and dry states, with environmental covariates (shown in Table 2.1). The Pearson correlation coefficients are in Table 2.4, where the highest values have been highlighted.

Table 2.4. Pearson correlation coefficient (Pearson's R) relating mean of the fitted pdf of the dry and wet state and soil properties and topographic factors. Values shown in bold represent a high correlation with values of over 0.60[a]. ρb, Bulk density, Z, Soil depth, S, Local slope gradient, RAD_{annual}, Annual global solar radiation, TWI, Topographic Wetness Index.

Soil Property and	Dry State		Wet State	
Topographic factor	Pearson's R	p-value	Pearson's R	p-value
ρ_b	-0.21	0.648	**-0.79**	**0.033**
Z	0.48	0.278	-0.72	0.069
S	0.00	0.996	0.36	0.425
RAD_{annual}	-0.16	0.736	0.46	0.304
TWI	**0.85**	**0.014**	-0.26	0.579

[a] All correlations were non-significant with a p-value > 0.05, except for TWI for Dry State and ρb for Wet State.

For dry conditions, the only significant correlation was found with TWI. This correlation, with a coefficient of 0.85, might indicate the predominance of the topography, the gravity component of the water flow equation, on the spatial distribution of soil moisture content, in absence of other factors like the rainfall, as observed in the many Mediterranean landscapes under dry conditions. The importance of TWIs confirms observations by other authors, which are widely used to approximate soil moisture patterns (e.g., Beven and Kirby, 1979). Nyberg (1996) identified macro-topography as being the cause of a large part of the variability in soil moisture by finding that there was a correlation between soil moisture content and TWI. Although Penna et al. (2009) reported that the terrain indices were poor predictors of soil moisture spatial variability, the TWIs, with a positive Pearson correlation coefficient with soil moisture, together with the slope, were found to be the best predictors of soil moisture, explaining up to 42% of its time-averaged spatial variability from data collected at 3 depths on different measurement points over 3 experimental hillslopes in the central eastern Italian Alps. In a review study, Buchanan et al. (2014)

observed widely differing correlation strengths, with R^2 values ranging between 0 and 0.89. Under wet conditions, the correlation with TWI was not significant. However, a significant correlation was found between soil moisture content and bulk density, with a Pearson coefficient of -0.79. Under wet conditions, an increase in soil moisture was correlated with decreasing bulk density, and, consequently with the increase of porosity. This relationship coincides with that observed in samples of weathered granitic rocks obtained in San Bernardino and San Jacinto Mountains (California, USA) by Jones and Graham (1993).

2.3.2. *Aspect influences on soil moisture profiles, recharge and residence time*

Examining the daily moisture profiles of both SC8 location, with a local slope of 27°, and SC5 location, with a local slope of 20°, after the first autumn-winter rain pulses (Figure 2.5) a clear distinction appears between them. On the SFS, profile water accumulates at the bottom, while on the NFS, the moisture content at the bottom remains roughly constant. The small change observed in the moisture content at the bottom of the profile SC8, suggests that the water moves downward as an unsaturated preferential flow. Nimmo (2012) demonstrated that preferential flow in soil fissures, cracks or macropores does not need saturated conditions. In their studies in coastal Mendocino County, in northern California, Salve et al. (2012) and Rempe and Dietrich (2018) detected aquifer recharge without a perceptible moisture change in the unsaturated weathered zone.

The soil moisture residence times of the soil computed as Kurc and Small (2004) indicated, are displayed in Table 2.5. The residence time for the soil moisture in the first 10 cm of the SC8 is about 16 days. Smaller than in the analogous SC5 profile, about 37 days, possibly due to the faster transit of water both upwards and downwards in the SC8 profile as compared to the upward flow only in the SC5. The values are greater than those reported by Gutiérrez-Jurado et al. (2013), possibly due to the smaller evapotranspiration rate estimated in the Santa Clotilde site in autumn and spring.

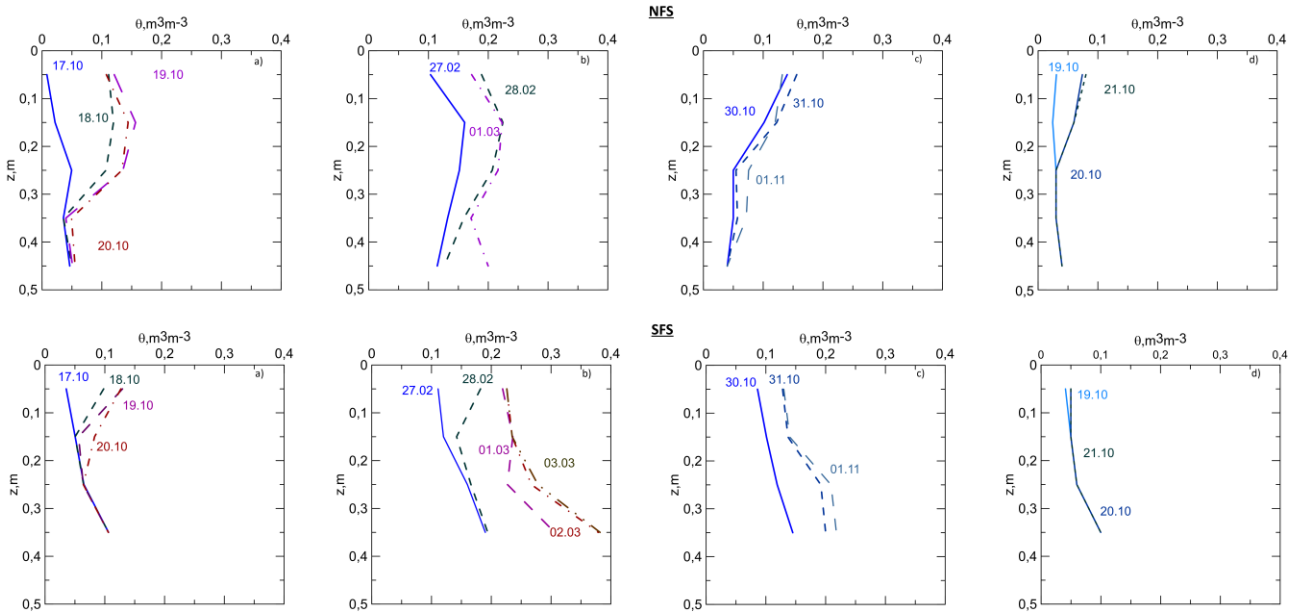

Figure 2.5. Daily soil moisture content profiles of both NFS (SC8) and SFS (SC5) a) from 10.17.2017 to 10.20.2017, b) from 02.27.2018 to 03.0.2018, c) from 10.30.2018 to 11.01.2018 and d) from 10.19.2019 to 10.21.2019. The numbers in each profile indicate date (day followed by month). Note problems in the measuring instruments on 03.02.2018 and 03.03.2018 on the NFS.

Table 2.5. Shallow soil moisture residence time in both SC5 (SFS) and SC8 (NFS). θ1, Initial soil moisture, n, data number, τ, Exponential time constant, R^2, Coefficient of determination.

First Day	Rainfall (mm)	SC5				SC8			
		θ_1, (m^3m^{-3})	n	τ, (d)	R^2	θ_1, (m^3m^{-3})	n	τ, (d)	R^2
10.19.17	28.0	0.130	5	33.9	0.9833	0.120	5	13.2	0.9821
05.26.18	10.8	0.140	11	43.9	0.9314	0.120	11	26.4	0.9602
10.31.18	39.0					0.156	4	12.1	0.8918
04.08.19	12.6	0.120	6	32.3	0.9277	0.180	9	13.4	0.9930
Mean				36.7				16.3	

2.3.3. *Relation between soil moisture, water table and vegetation dynamics*

In order to analyze the influence of aspect on the interaction between hydrology and vegetation of the opposing north and south-facing hillslopes, soil moisture, water table and vegetation dynamics were treated jointly in figure 2.6. Soil moisture content measurements from sites SC5 and SC8 were used. Figure 2.6a shows the precipitation, Figure 2.6b the

vegetation greenness. Figures 2.6 c, d and e give information on the soil moisture status on both opposing hillslopes. Figure 2.6e shows *s*, for the SFS and the NFS during the study period, and the daily difference between both ($\Delta s = s_{SFS} - s_{NFS}$) in Figure 2.6c. The Wilcoxon signed-rank test performed, every two months (Fig. 2.6d) allowed us to detect the periods in which the differences between NFS and SFS were significant (green bar), or not (red bar) (Fig. 2.6d). Data gaps indicate a period with problems in the measuring instruments. The water table evolution on the NFS is shown in Figure 2.6f. It shows a clear link between the maximum values measured in both the water table and in the soil moisture (Fig.2.6e and f). Similar results were obtained on an NFS and SFS of Gordon Gulch, Colorado (USA) by Langston et al. (2015). They reported a soil moisture series of 2 years and attributed this to infiltration events due to snowmelt. Our case without snow, but with a high saturation of the root-zone soil moisture after heavy rainfall events, corresponds well with the recharge of the water table. The depletion period of the aquifer goes on beyond the summer season. Indeed, minimum water levels are not reached in summer but, rather, during winter (Fig.6f). The baseflow draining the aquifer is very slow, and the recharge of small rainfall events is inappreciable. Only when long rainfall events occur, is a recharge observed, for example in February 2018.

The differences between soil moisture on the SFS and the NFS revealed an appreciable seasonal pattern, with an average of 0.003 and a standard deviation of 0.094. The smallest $|\Delta s|$ occurred during summer, as both locations dried out to their minimum value. The maximum $|\Delta s|$ was observed during transition periods, illustrating a different or lagged response, with one hillslope drying faster than the other one. Positive differences were found in the drying phases of 2017 and 2018 when the soil on the NFS started drying earlier with respect to that on the SFS. Only two drying periods were found to not be significantly different, spring-summer (from May 29 to July 29) 2017 and spring (from March 29 to May 29) 2019. Both were similar in that, the profiles on both NFS and SFS

were rewetted after a late rain event in May and April, respectively. Those dried out very fast due to the high reference evapotranspiration rates during this period (Figure 2.3). Negative differences were found during rewetting phases by the first autumn rains. The NFS slope captures more efficiently the rainwater than the SFS, increasing their soil moisture content as it can be appreciated in the case of the autumn-winter of 2017 (Fig.2.6e). This pattern is not observed the other two years, due to the abundance of rain events which recharged the soils of both slopes similarly.

Therefore, both NFS and SFS follow a similar seasonal trend, although small, significant differences between NFS and SFS do exist, due to a time lag in their drying response caused by the distinct composition of the vegetation cover. The NFS, in spite of receiving lower radiation, starts to dry earlier due to a denser tree cover, causing a higher transpirative demand. This attenuation of the differences between NFS and SFS contrasts strongly with the results of Gutiérrez-Jurado et al. (2013), whose differences on opposing slopes of a semiarid catchment in central New Mexico, USA were remarkable. They concluded that the water balance on NFS and SFS followed opposing trajectories and that evapotranspirative demands were met from distinct soil water pools. In the present case, soil moisture does not show any opposing trend. The difference between both studies could be attributed to a combination of factors, such as the annual rainfall, the soil texture, but most importantly, to the different vegetation cover. Gutiérrez-Jurado et al. (2013) report a vegetation cover between 27.4 and 41% on SFS and NFS, respectively. Under these circumstances, it is clear that vegetation has a more limited effect with respect to radiation on soil water balance. In this study, however, vegetation cover is between 80 and 100%, with a significantly higher tree density on the NFS, as will be analyzed below.

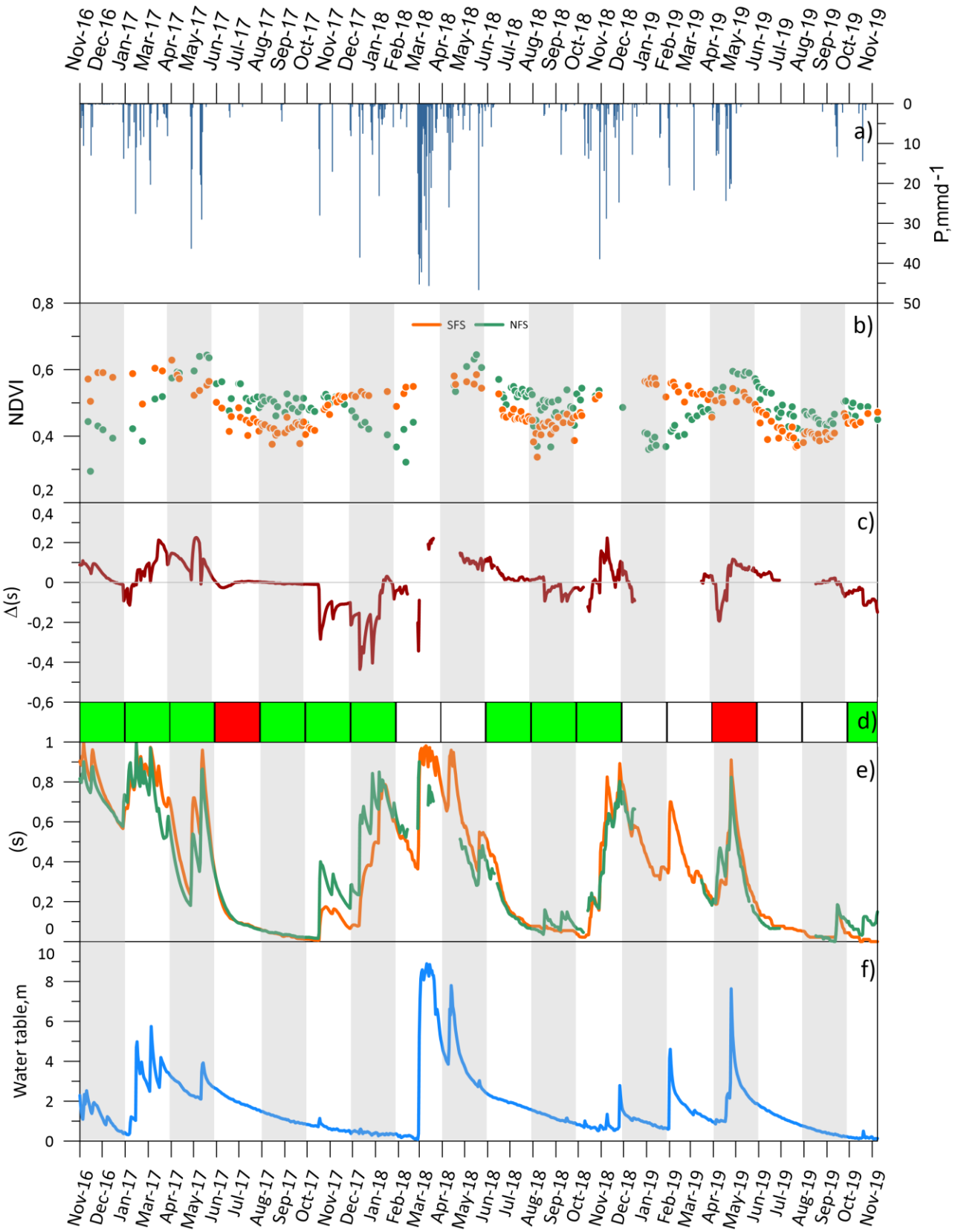

Figure 2.6. The top panel (a) indicates the daily rainfall; the second panel (b) shows the variation in NDVI on SFS (orange dots) and NFS (green dots) during the study period; the third panel (c) shows the difference between both soil moisture at SFS and NFS, Δ(s) (red line). Significant differences between SFS and NFS are indicated in the fourth panel (d) for each 2-month period.

Red indicates no significant differences, while green indicates significant differences (at p=0.05, according to Wilcoxon signed-rank test). The fifth panel (e) shows the evolution of soil moisture on SFS (orange line) and NFS (green line); the sixth panel (f) shows water table evolution during the study period.

To understand better the underlying reasons for these differences, we compared daily soil moisture storage change differences (Δs_{SFS} - Δs_{NFS}) to rainfall in wetting periods and to reference evapotranspiration in drying periods. The result is shown in Figures 2.7a and b. Positive values indicated that soil moisture increased more on SFS in wetting periods and decreased less on SFS in drying periods. The results show a higher number of negative values (Fig. 2.7a). Negative differences indicate a higher infiltration on NFS, which can be attributed to higher infiltration rates. A comparison could be established between the saturated hydraulic conductivity (k_s) values measured on the Mid Slope positions (SC8 and SC5) of both opposing hillslopes (Table 1). The value of k_s is higher on the NFS ($1.75 \cdot 10^{-2}$ cms^{-1}) compared to that on the SFS ($2.33 \cdot 10^{-3}$ cms^{-1}). This was similarly observed by Richardson et al. (2020), who found significantly higher infiltration rates on a NFS in New Mexico, due to its deeper soils and higher organic matter content. This is also the case here, with the OM content on the NFS being double that on the SFS, because of the denser vegetation cover. The soil depths are similar but, on the SFS, the profile overlies hard bedrock, whereas on the NFS there is a deeply weathered saprolite. This is counterintuitive, we would expect positive values due to the interception of denser vegetation on the NFS. However, we only observe positive values for high daily rainfall values of over 30 mm, when it is very unlikely that vegetation interception will play a significant role, indicating that a greater fraction of the rainfall infiltrates and remains in the profile on SFS compared to on NFS. These increments follow 3 dry-down sequences, in February and October 2018 (Figure 2.5b and c, respectively), and April 2017.

The relationship between daily soil moisture storage change differences (Δs_{SFS} - Δs_{NFS}) and ET_0 for drying periods is shown in Figure 2.7b. No clear relation exists between the difference in the drying of the opposing hillslopes with ET_0. The differences were not

significant, except for $ET_0 \leq 1$ mm, where positive values indicated faster NFS drying, due to water uptake by a denser vegetation cover. For higher values of ET_0, no clear trend exists. This means that, as soon as both hillslopes start to dry, the drying rates are similar, as observed in Figure 2.6e, as both NFS and SFS have a similar slope during the drying phases so that no differences between NFS and SFS are found here. The differences between the two soil moisture time series in Figure 2.6e are principally due to a short time lag between both opposing hillslopes, with the NFS slopes starting to dry out earlier. The time lag was calculated for different drying events, resulting in an average value of 4 days. This is consistent with Ng and Miller (1980) who attributed the lower soil moisture on the NFS to greater vegetation cover and greater transpiration losses, in their study in Southern California Chaparral.

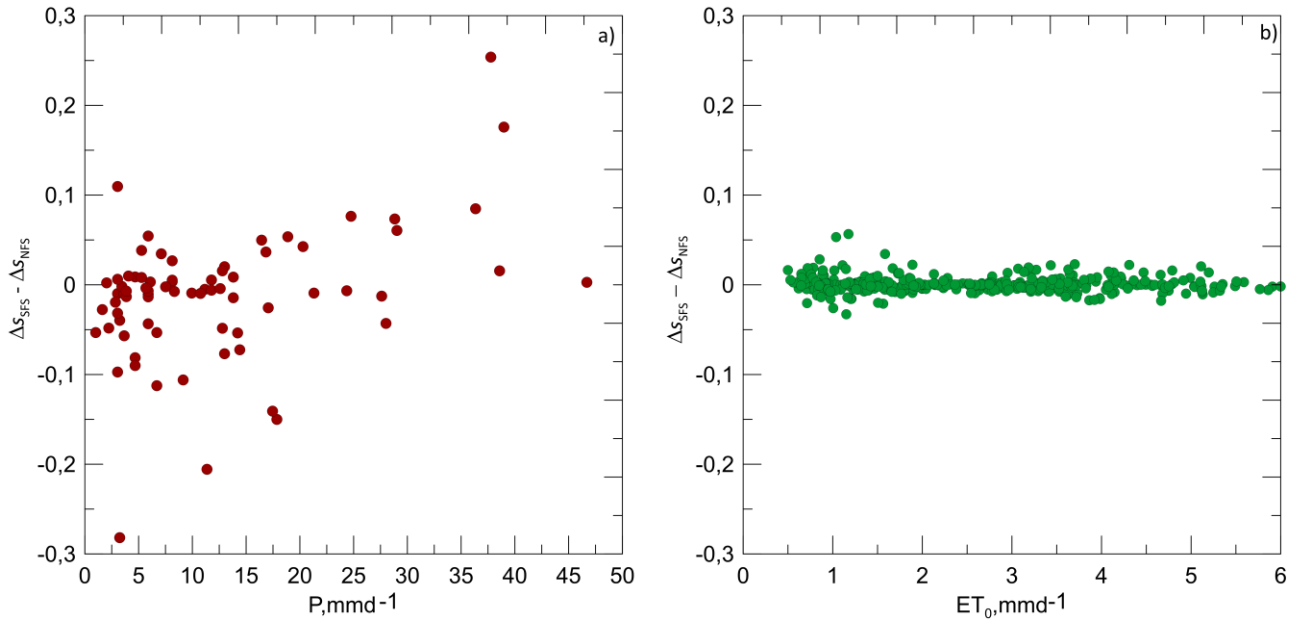

Figure 2.7.Relation of the difference between daily soil moisture storage change on SFS and NFS, $\Delta s_{SFS} - \Delta s_{NFS}$, and (a) daily precipitation, P, and b) reference evapotranspiration, ET_0.

However, very opposing trends between SFS and NFS can be observed in NDVI (Figure 2.6b). In the three-years the same pattern is repeated, from June to October, the value of NDVI on both hillslopes has the same shape, being higher in NFS. The NDVI values on the NFS slope showed a clear decline at the end of the summer followed by recovery after the end of the year. In the SFS, the NDVI decreased from the end of the spring with a slow

recovery initiated at the last part of the summer. The average value of NDVI for the study period was 0.49 on the NFS with a standard deviation of 0.062 while on the SFS it was 0.47 with a standard deviation of 0.061.

This difference can be explained by the density of trees, which is higher on the NFS, aforementioned, whereas the SFS has a greater grass cover. Significant differences have been observed in vegetation cover, based on LiDAR-derived vegetation volumes between the opposite hillslopes (Figure 2.8). The average vegetation volume on the NFS is 6.7 m^3/m^2 with a standard deviation of 2.1, whereas on the SFS it is 5.2 m^3/m^2 with a standard deviation of 1.8. So, it appears that NFS can maintain denser and greener vegetation compared to SFS.

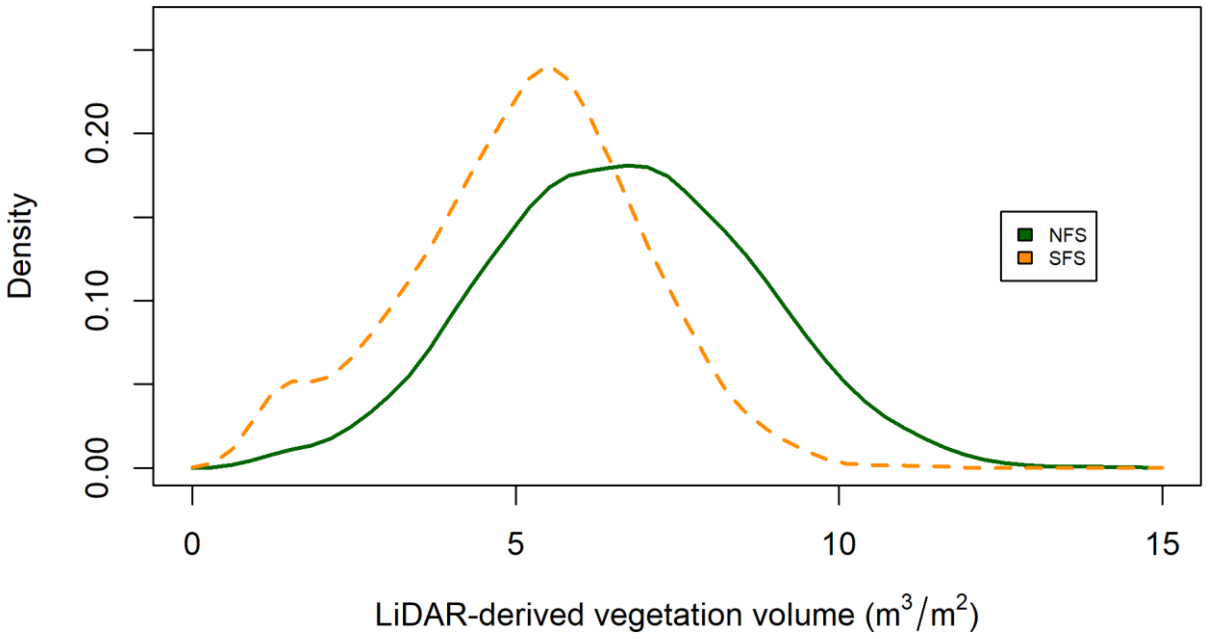

Figure 2.8.LiDAR-derived vegetation density function volumes on NFS and SFS.

These trends are similar to those reported by Liu et al. (2017), in a Mediterranean-type oak-grass savanna in California. However, as NDVI values remain high during the dry season on

the NFS, this indicates that the vegetation must be supported by water coming from a different pool than that of the soil pores, as the latter was depleted (Figure 2.6d). The water that percolates from the soil moves along the complex networks of fractures and cracks in the underlying fractured saprolite. During this movement, the water can be retained in some of these fractures, accessible to the tree roots, before reaching the saturated zone. This water pool was denominated rock moisture by Rempe and Dietrich (2018) to distinguish it from soil moisture. The relevance of this water pool for the survival of trees, oak trees, of many semiarid areas has been discussed by David et al. (2004) in a montado system in Portugal not far from the study site; Balugani et al. (2017) in western Spain in another dehesa ecosystem; and Hahm et al. (2019) in the northern California Coastal range.

In our case, this additional water pool occurs only on the NFS, where, below the soil profile, a deep layer of up to 9.50 m of weathered, fractured saprolite lies. This is not the situation on the SFS, where hard bedrock, hardly weathered and without any appreciable fractures, directly underlies the soil profile.

To explore the relation between NDVI and soil moisture and water table level in more detail, they were correlated directly in Figure 2.9. A significant correlation of NDVI and soil moisture for the SFS was found, with a coefficient of 0.81 (Figure 2.9a), with a parabolic relationship with indicates that as the soil moisture content increases, the NDVI increases as well. This suggests that the soil water pool is the sole source of water for the vegetation. However, the analog correlation analysis on the NFS slope is very poor, which confirms that vegetation here is not supported by soil moisture but rather by a different water pool (Figure 2.9b). Figure 2.9c shows a significant connection of the water table with the NDVI. As was discussed earlier, our data suggests that the rock moisture or non soil vadose zone water pool is key for the sustenance of the vegetation. The water table itself is probably too deep to provide a significant water source for the trees, as no roots were observed below 3

m during the fieldwork. While some authors have reported roots up to 16 m (Hahm et al., 2019) in similar environments, according to Fan et al. (2017), the importance of such accidental deep roots is probably low as the mean rooting depth for Quercus spp. is 5.23 m (Fan et al., 2017). We propose that the good correlation between NDVI and water table depth is rather due to a good correlation of water table and rock moisture content. Although we have no direct measurements of rock moisture, recharge and depletion of groundwater are related to this pool, throughout a complex interrelation as described by Salve et al. (2012).

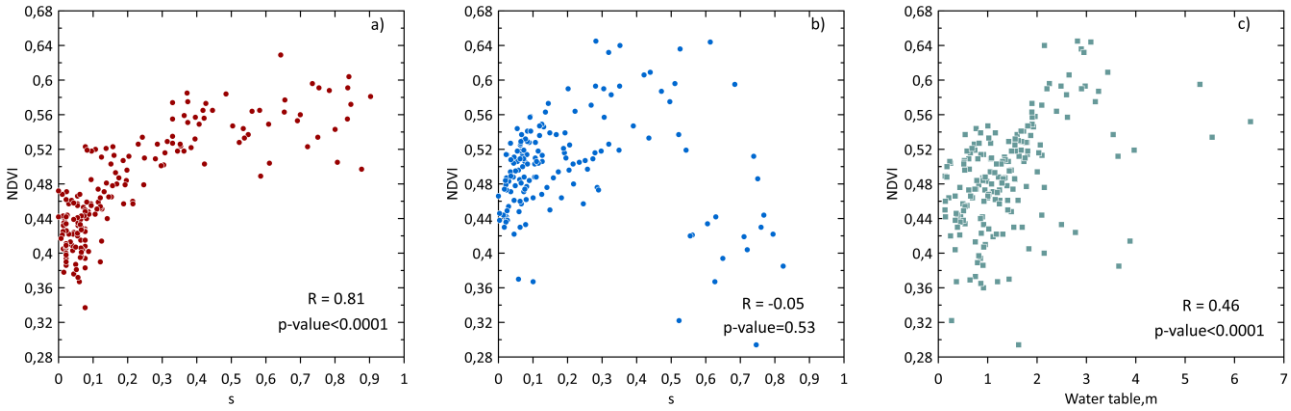

Figure 2.9. Scatter plots for the soil moisture monitoring period data (from November 2016 to November 2019). (a) NDVI vs Soil moisture ('s', unitless) at the SFS, (b) NDVI vs Soil moisture ('s', unitless) at the NFS and (c) NDVI vs Water table, m. Pearson's R and p-value are displayed in the three plots.

The conceptual model of Figure 2.10 illustrates the Santa Clotilde CZO representing the north-south aspect gradient and summarizes the interplay between the subsurface structure of the critical zone, the vegetation, and the hydrological processes. Along the toposequence, the difference in soil moisture content depends on the vegetation and the critical zone structure. The thickness of the critical zone varies from the SFS where the unweathered bedrock is just below the soil profile, i.e., 0.60 m depth, to the NFS where a deep layer of highly weathered bedrock lies between the soil and the underlying intact bedrock, with a total depth of 9.50 m at the mid-slope location. Field observations have shown that the thickness of this unweathered bedrock layer increases towards the top of the transect. Therefore, while on the SFS the vegetation composition is a wooded grassland, on

the NFS the subsurface critical zone structure sustains a closed canopy of evergreen oaks, and roots were observed to 3-m depth during fieldwork. On the NFS, the rainfall flows vertically through the soil and the thick highly weathered bedrock vadose zone, replenishing the rock moisture reservoir. The existence of layers with high hydraulic conductivity in a direction parallel to the slope enhances the lateral subsurface movement of vadose zone water. Simultaneously, through fractures in the weathered bedrock vadose zone, rainwater can flow deeper recharging the underlying aquifer, which was only detected on this slope. The presence of underlying unweathered bedrock, with low conductivity, allows seasonal groundwater development and lateral downslope redistribution of groundwater. Especially at the bottom part of the NFS, runoff may be generated through subsurface flow of vadose zone water and/or groundwater (seep or exfiltration), which may flow back across the land surface. Conversely, on the SFS hard bedrock directly underlying the soil causing the hydrological processes are dominated by vertical infiltration of rainwater. Here, the shallow thickness of the soil profile hampers lateral hydrological connectivity. Guang-Rong et al. (2020) also pointed out in their study in the Qinghai Lake Basin alpine CZO that the thickness of the critical zone on the NFS is larger than on the SFS, being their main findings that the hydrological processes on the SFS are dominated by surface flow and strong vertical infiltration process, while on the NFS are dominated by the subsurface flow.

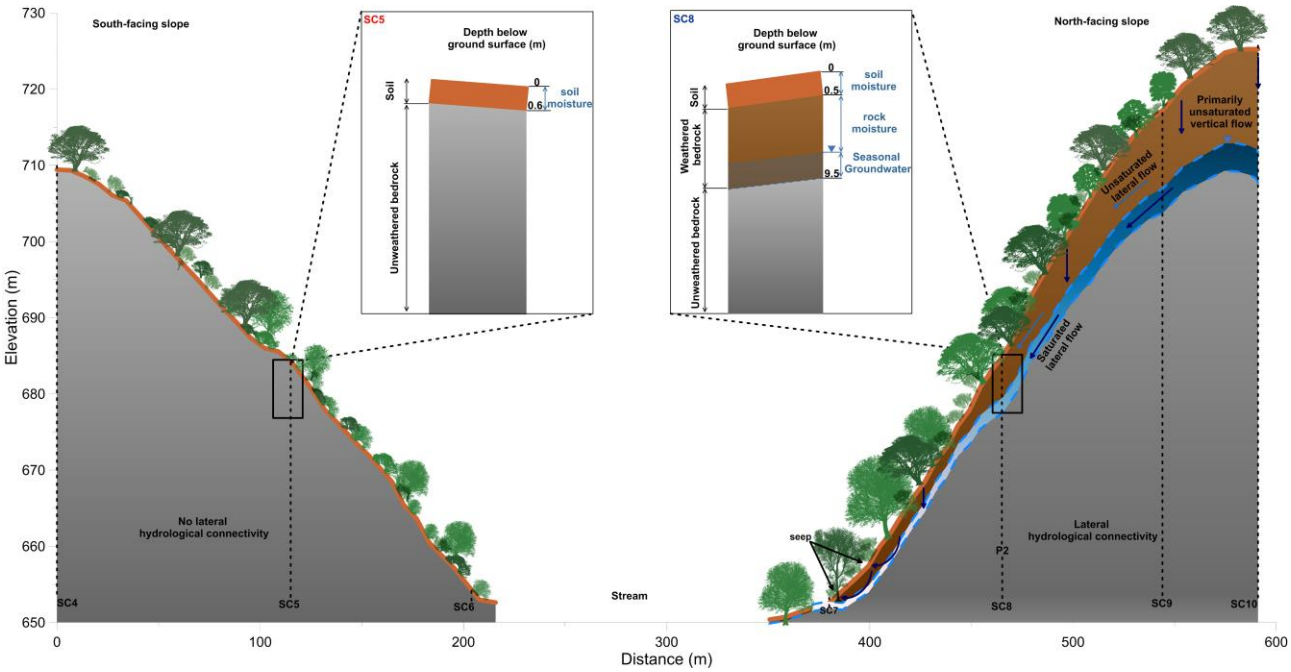

Figure 2.10.Conceptual model illustrating the Santa Clotilde Critical Zone Observatory (CZO) representing the north-south aspect gradient and summarizing the interplay between the subsurface CZ structure, the vegetation and the hydrological processes. Zooming soil profiles in SC5 and SC8 locations, subsurface delineations of the CZ are highlighted on the left side of each panel. On the SC8 location, we also distinguish between soil moisture, rock moisture which resides in the weathered bedrock vadose zone, and the seasonal groundwater (water table depicted with an inverted triangle), which saturates the weathered bedrock, on the right side of the panel. Seep points are located at the valley bottom of the NFS. Conversely, on the SC5 due to the subsurface structure of the CZ, we only distinguish soil moisture.

2.4. Conclusions

In a Mediterranean oak-woodland savanna o dehesa, of southern Spain, soil moisture evolution reflects the influence of the strong seasonality, characterized by two different Weibull probability distribution functions, one for the wet season with a mode at a degree of saturation of about 0.63, and another one with no evident mode as a consequence of the Weibull pdf equation, when the shape parameter, κ is close to unity, in the dry state. The factors that determine the average soil moisture in dry conditions are topographical features such as TWI, while in wet conditions, it is soil bulk density. This indicates the predominance of the topography on the spatial distribution of soil moisture content during dry periods, and soil properties during wet ones.

A detailed analysis of the soil moisture profiles shows a fast response of the water table to the intense rain pulses. This, as well as the shape of the soil water profiles suggests the existence of unsaturated preferential moisture flow in the vadose zone.

Hillslope aspect exerts a hydrological control through the vegetation and the structure of the critical zone. Soil profiles on the SFS are shallow, while on the NFS slope, the soils are underlain by a 9.50 m deep layer of highly weathered bedrock. This expands the water holding capacity on NFS, that can hold soil moisture, rock moisture and a seasonal water table. This allows a greater vegetation density on the NFS slope compared to the SFS, that is highly water-limited even though SFS receives more solar radiation. The estimation of biomass volumes on both opposing hillslopes confirms the more favourable growth conditions of the NFS than those of the SFS.

The relation between soil moisture, water table and NDVI pattern clearly illustrate these feedback effects between vegetation, bedrock weathering and hillslope hydrology. In contrast with other studies that found clear differences between opposing slopes, here, the soil moisture trends between NFS and SFS are very similar, albeit slightly lagged, with the NFS drying out earlier due to the denser vegetation. However, both hillslopes exhibit clearly opposing NDVI trends, with a minimum value in winter to NFS and in summer for SFS. NDVI was well related to soil moisture on SFS, but not on NFS. However, a good correlation was found between water table level and NDVI on the NFS. This allows us to conclude that there is a different water pool on NFS, which corresponds to the rock moisture and the saturated zone.

2.5. References

Allen, R.G., Pereira, L.S., Raes, D., Smith, M. (1998). *Crop evapotranspiration guidelines for computing crop water requirements* FAO Irrigation and drainage paper 56, FAO, Rome, Italy.

Alley, W.M. (1984). On the treatment of evapotranspiration, soil moisture accounting, and aquifer recharge in monthly water balance models. Water Resources Research 20: 1137-1149. https://doi.org/10.1029/WR020i008p01137

Balugani, E., Lubczynski, M.W., Reyes-Acosta, L., van der Tol, C., Francés, A.P., Metselaar, K. (2017). Groundwater and unsaturated zone evaporation and transpiration in a semi-arid open woodland. Journal of Hydrology,547,54-66. https://doi.org/10.1016/j.jhydrol.2017.01.042

Bennie, J., Huntley, B., Wiltshire, A., Hill, M.O., Baxter, R. (2008). Slope, aspect and climate: Spatially explicit and implicit models of topographic microclimate in chalk grasslands. Ecological Modelling 216, 47-59. https://doi.org/10.1016/j.ecolmodel.2008.04.010

Beven, K., & Kirkby, M. (1979). A physically based, variable contributing area model of basin hydrology. Hydrological Sciences Bulletin, 24, 43-69. https://doi.org/10.1080/02626667909491834

Brutsaert, W.H. (2005), *Hydrology: An Introduction*. Cambridge: Cambridge University Press. Cambridge, U.K. doi:10.1017/CBO9780511808470

Buchanan, B.P., Fleming, M., Schneider, R.L., Richards, B.K., Archibald, J., Qiu, Z., & Walter, M.T. (2014). Evaluating topographic wetness indices across central New York agricultural landscapes. Hydrol. Earth Syst. Sci., 18, 3279-3299. https://doi.org/10.5194/hess-18-3279-2014, 2014.

Bury, K., (1999), *Statistical distributions in Engineering*. Cambridge: Cambridge University Press. New York. doi:10.1017/CBO9781139175081

Cantón, Y., Solé-Benet, A., & Domingo, F. (2004). Temporal and spatial patterns of soil moisture in semiarid badlands of SE Spain. Journal of Hydrology, 285(, 199-214. https://doi.org/10.1016/j.jhydrol.2003.08.018

Carpintero, E., Andreu, A., Gómez-Giráldez, P.J., Blázquez, A., González-Dugo, M.P. (2020).

Remote-sensing-based water balance for monitoring of evapotranspiration and water stress of a Mediterranean oak–grass savanna. Water 12, 1418; doi:10.3390/w12051418

Carracedo, M., Paquette, J.L., Alonso Olazabal, A., Santos Zalduegui, J.F., García de Madinabeitia, S., Tiepolo, M., & Gil Ibarguchi, J.I. (2009). U-Pb dating of granodiorite and granite units of the Los Pedroches batholith. Implications for geodynamic models of the southern Central Iberian Zone (Iberian Massif). International Journal of Earth Sciences, 98, 1609-1624. https://doi.org/10.1007/s00531-008-0317-0

CNIG. (2020). Centro de Descargas del Instituto Geográfico Nacional. Retrieved 13 July 2020, from http://centrodedescargas.cnig.es/CentroDescargas/locale?request_locale=en

Consejería de Agricultura, Pesca y Medio ambiente. Dirección General de la Producción Agrícola y Ganadera. (2020). Retrieved 26 August 2020, from http://www.juntadeandalucia.es/agriculturaypesca/fitEmaWeb/faces/pages/infoEstacion.xhtml?id=98

Dalton, F. N. (1992), Development of time-domain reflectometry for measuring soil water content and bulk soil electrical conductivity, in *Advances in measurement of soil physical properties: Bringing theory into practice*, SSSA Spec. Pub. 30, edited by G. C. Topp, W. D. Reynolds, and R. E. Green, pp. 143–167, Soil Sci. Soc. Am., Madison, Wisc. https://doi.org/10.2136/sssaspecpub30.c8

David, T.S., Ferreira, M.I., Cohen, S., Pereira, J.S. David, J.S. (2004). Constraints on transpiration from an evergreen oak tree in southern Portugal. Agricultural and Forest Meteorology, 122,193-205. https://doi.org/10.1016/j.agrformet.2003.09.014

D'Odorico, P., Ridolfi, L., Porporato, A., & Rodriguez-Iturbe, I. (2000). Preferential states of

seasonal soil moisture: the impact of climate fluctuations. Water Resources Research, 36, 2209-2219. https://doi.org/10.1029/2000WR900103

D'Odorico, P., Laio, F., Porporato, A., Ridolfi, L., Rinaldo, A., Rodriguez-Iturbe, I. (2010). Ecohydrology of terrestrial ecosystems. BioScience, 60, 898–907. https://doi.org/10.1525/bio.2010.60.11.6

Eagleson, P.S., & Segarra, R.I. (1985), Water-limited equilibrium of savanna vegetation systems. Water Resources Research 21: 1483-1493. https://doi.org/10.1029/WR021i010p01483

Eagleson, P. S. (2002), *Ecohydrology: Darwinian expression of vegetation form and function*. Cambridge: Cambridge University Press. New York. doi:10.1017/CBO9780511535680.

Eliades, M., Bruggeman, A., Lubczynski, M.W., Christou, A., Camera, C., Djuma, H. (2018). The water balance components of Mediterranean pine trees on a steep mountain slope during two hydrologically contrasting years. Journal of Hydrology, 562, 712-724. https://doi.org/10.1016/j.jhydrol.2018.05.048

Espejo, A.J., Brocca, L., Moramarco, T., Giráldez, J.V., Triantafilis, J., & Vanderlinden, K. (2016). Analysis of soil moisture dynamics beneath olive trees. Hydrological Processes, 30, 4339-4352. https://doi.org/10.1002/hyp.10907

Fan, Y., Miguez-Macho, G., Jobbágy, E.G., Jackson, R.B., Otero-Casal, C. (2017). Hydrologic regulation of plant rooting depth. Proceedings of the National Academy of Sciences of the United States of America, 114, 10572-10577. https://doi.org/10.1073/pnas.1712381114

Fan, Y., Clark, M., Lawrence, D. M., Swenson, S., Band, L. E., Brantley, S. L., et al. (2019). Hillslope hydrology in global change research and Earth system modeling. Water Resources Research, 55, 1737–1772. https://doi.org/10.1029/2018WR023903

Geroy, I.J., Gribb, M.M., Marshall, H.P., Chandler, D.G., Benner, S.G., & McNamara, J.P. (2011). Aspect influences on soil water retention and storage. Hydrological Processes, 25, 3836-3842. https://doi.org/10.1002/hyp.8281

Ghezzehei, T. (2008). Errors in determination of soil water content using time domain reflectometry caused by soil compaction around waveguides. Water Resources Research, vol. 44, doi:10.1029/ /2007WR006502.

Guang-Rong, H., Xiao-Yan, L., Xiao-Fan, Y. (2020). The impact of micro-topography on the interplay of critical zone architecture and hydrological processes at the hillslope scale: Integrated geophysical and hydrological experiments on the Qinghai-Tibet Plateau. Journal of Hydrology,583. 124618, https://doi.org/10.1016/j.jhydrol.2020.124618

Gutiérrez-Jurado, H.A., Vivoni, E.R., Cikoski, C., Harrison, J.B.J, Bras, R.L., Istanbulluoglu, E. (2013). On the observed ecohydrologic dynamics of a semiarid basin with aspect-delimited ecosystems. Water Resources Research,. 49, 8263-8284, doi:10.1002/2013WR014364

Hahm, W. J., Rempe, D. M., Dralle, D. N., Dawson, T. E., Lovill, S. M., Bryk, A. B., et al. (2019). Lithologically controlled subsurface critical zone thickness and water storage capacity determine regional plant community composition. Water Resources Research, 55,3028–3055. https://doi.org/10.1029/2018WR023760

Hahm, W. J., Rempe, D. M., Dralle, D. N., Dawson, T. E., & Dietrich, W. E. (2020). Oak transpiration drawn from the weathered bedrock vadose zone in the summer dry season. Water Resources Research, 56, e2020WR027419. https:// doi.org/10.1029/2020WR027419

Harrell, F. E. (2019). Hmisc: Harrell mscellaneous.R package version 4.3-0. https://CRAN.R -project.org/package=Hmisc

IFAPA. (2020). Retrieved 26 August 2020, from https://www.juntadeandalucia.es/agriculturaypesca/ifapa/web/

Istanbulluoglu, E., Yetemen, O., Vivoni, E.R., Gutiérrez-Jurado, H.A., & Bras, R.L. (2008). Eco-geomorphic implications of hillslope aspect: Inferences from analysis of landscape morphology in central New Mexico. Geophysical Research Letters, vol.35, doi:10.1029/2008GL034477.

IUSS Working Group WRB. (2015). *World reference base for soil resources 2014, update 2015*. World Soil Resources Reports No. 106. FAO, Rome.

Joffre, R., & Rambal, S. (1993). How tree cover influences the water balance of Mediterranean rangelands. Ecology 74, 570-582. https://doi.org/10.2307/1939317

Joffre, R., Rambal, S., Ratte, J.P. (1999). The dehesa system of southern Spain and Portugal as a natural ecosystem mimic. Agroforestry 45, 57-79. https://doi.org/10.1023/A:1006259402496

Jones, D.P., & Graham R.C. (1993). Water-. Soil Science Society of America Journal, 57:256-261. https://doi.org/10.2136/sssaj1993.03615995005700010044x

Kim, S. (2009). Characterization of soil moisture responses on a hillslope to sequential rainfall events during late autumn and spring. Water Resources Research, vol. 45 doi:10.1029/2008WR007239.

Kirkham, M.B. (2014). Chapter 8-Time Domain Reflectometry. In M.B. Kirkham (Ed.), *Principles of soil and plant water relations* (Second Edition) (pp.103-122). https://doi.org/10.1016/B978-0-12-420022-7.00008-2.

Kumari, N., Saco, P.M., Rodríguez, J.F., Johnstone, S.A., Srivastava, A., Chun, K.P., Yetemen, O. (2020). The grass is not always greener on the other side: Seasonal reversal of vegetation greenness in aspect-driven semiarid ecosystems. Geophysical Research Letters, 47, e2020GL088918. https://doi. org/10.1029/2020GL088918

Kurc, S.A., Small, E.E. (2004) Dynamics of evapotranspiration in semiarid grassland and

shrubland ecosystems during the summer monsoon season, central New Mexico. Water Resources Research 40, W09305, doi:10.1029/2004WR003068.

Langston, A., Tucker, G., Anderson, R., & Anderson, S. (2015). Evidence for climatic and hillslope-aspect controls on vadose zone hydrology and implications for saprolite weathering. Earth Surface Processes and Landforms,40, 1254-1269. https://doi.org/10.1002/esp.3718

Liu, Y., Hill, M.J., Zhang, X., Wang, Z., Richardson, A.D., Hufkens, K., Filippa, G., Baldocchi, D.D., Ma, S., Verfaillie, J. & Schaaf, C.B. (2017). Using data from Landsat, MODIS, VIIRS and PhenoCams to monitor the phenology of California oak/grass savanna and open grassland across spatial scales. Agricultural and Forest Meteorology, 237-238, 311-325. https://doi.org/10.1016/j.agrformet.2017.02.026

Lubczynski, M.W. (2009). The hydrogeological role of trees in water-limited environments. Hydrogeology Journal, 17, 247-259. https://doi.org/10.1007/s10040-008-0357-3

Meinzer, O.E. (1923). *Outline of ground-water hydrology*. US Geol. Survey Water Supply Paper 494. U.S. Govt. Print. Off., Washington D.C.

Nadal-Romero, E., Petrlic, K., Verachtert, E., Bochet, E., Poesen, J. (2014). Effects of slope angle and aspect on plant cover and species richness in a humid Mediterranean badland. Earth Surface Processes and Landforms,39,1705-1716. https://doi.org/10.1002/esp.3549

Nimmo, J.R. (2012). Preferential flow occurs in unsaturated conditions. Hydrological Processes 26: 786-789. https://doi.org/10.1002/hyp.8380

Ng, E., & Miller, P. (1980). Soil Moisture Relations in the Southern California Chaparral. Ecology, 61, 98-107. https://doi.org/10.2307/1937160

Nyberg, L. (1996). Spatial variability of soil water content in the covered catchment at Gårdsjön, Sweden. Hydrological Processes, 10, 89–103. https://doi.org/10.1002/(SICI)1099-1085(199601)10:1<89::AID-

HYP303>3.0.CO;2-W

Olea, L., & San Miguel-Ayanz, A. (2006). The Spanish dehesa. A traditional Mediterranean silvopastoral system linking production and nature conservation, in: Loveras, A., González-Rodriguez, A., Vázquez-Yañez,O.(eds.*),Proceedings of 21st General Meeting of the European Grassland Federation*,Badajoz (Spain),pp.1-15.

Or, D., Lehmann, P., Shahraeeni, E., Shokri, N. (2013). Advances in soil evaporation physics-a review. Vadose Zone Journal,12,1-16. https://doi.org/10.2136/vzj2012.0163

Peel, M., Finlayson, B., & McMahon, T. (2007). Updated world map of the Köppen-Geiger climate classification. Hydrology and Earth Systems Science, 11, 1633–1644. https://doi.org/10.5194/hess-11-1633-2007

Pelletier, J.D., Barron-Gafford, G.A., Gutiérrez-Jurado, H., Hinckley, E.-L, S., Istanbulluoglu, E., McGuire, L.A., Niu, G.-Y., Poulos, M.J., Rasmusen, C., Richardson, P., Swetnam, T.L., Tucker, G. (2018). Which way do you lean? Using slope aspect variations to understand Critical Zone processes and feedbacks. Earth Surface Processes and Landforms, 43), 1133-1154. https://doi.org/10.1002/esp.4306

Penna, D., Borga, M., Norbiato, D., & Fontana, G. D. (2009) Hillslope scale soil moisture variability in a steep alpine terrain. Journal of Hydrology. 364, 311–327, doi: 10.1016/j.jhydrol.2008.11.009, 2009.

Persico, R., Cataldo, A., De Benedetto, E. (2019). Chapter 3 - Time-domain reflectometry: Current uses and new possibilities. In R. Persico, S. Piro & Neil Linford (Eds.), *Innovation in near-surface Geophysics* (pp.59-96). https://doi.org/10.1016/B978-0-12-812429-1.00003-9.

Philip, J.R. (1993). Approximate analysis of the borehole permeameter in unsaturated soil. Water Resources Research 21, 1025-1033. https://doi.org/10.1029/WR021i007p01025

Poulos, M.J., Pierce, J.L., Flores, A.F., Benner, S.G. (2012). Hillslope asymmetry maps reveal widespread, multi-scale organization. Geophysical Research Letter 39, L06406, doi:10.1029/2012GL051283.

R Core Team (2018). *R: A language and environment for statistical computing*. R Foundation for Statistical Computing, Vienna, Austria. Available online at https://www.R-project.org/.

Rempe, D.M., & Dietrich, W.E. (2018). Direct observations of rock moisture, a hidden component of the hydrologic cycle. Proceedings of the National Academy of Sciences, 115(, 2664-2669. https://doi.org/10.1073/pnas.1800141115

Richardson, P.W., Perron, J.T., Miller, S.R. & Kichner J.W. (2020). Unraveling the mysteries of asymmetric topography at Gabilan Mesa, California. Journal of Geophysical Research. 125, e2019jF0025378, https://doi.org/10.1029/2019JF005378

Rodriguez-Iturbe, I., Porporato, A., Ridolfi, L., Isham, V., Cox, D.R. (1999). Probabilistic modelling of water balance at a point: the role of climate, soil and vegetation. Proceedings of the Royal Society of London, Series A 455: 3789-3805. https://doi.org/10.1098/rspa.1999.0477

Román-Sánchez, A., Vanwalleghem, T., Peña, A., Laguna, A., & Giráldez, J.V. (2018). Controls on soil carbon storage from topography and vegetation in a rocky, semi-arid landscapes. Geoderma, 311, 159-166. https://doi.org/10.1016/j.geoderma.2016.10.013

Salve, R., D. M. Rempe, and W. E. Dietrich (2012), Rain, rock moisture dynamics, and the rapid response of perched groundwater in weathered, fractured argillite underlying a steep hillslope, Water Resource Research., 48, W11528, doi:10.1029/2012WR012583.

Schmidt, L., & Rempe, D. (2020). Quantifying dynamic water storage in unsaturated bedrock with borehole nuclear magnetic resonance. Geophysical Research Letters, 47, e2020GL089600. https://doi.org/10.1029/2020GL089600

Scholes, R.J., Archer, S.R. (1997). Tree-grass interactions in savannas. Annual Reviews of Ecology and Systematics. 28: 517-544. https://doi.org/10.1146/annurev.ecolsys.28.1.517

SENTINEL-2. (2020). Retrieved 3 March 2020, from https://sentinel.esa.int/web/sentinel/missions/sentinel-2

Skierucha, W., Wilczek, A., Szypłowska, A., Sławiński, C., & Lamorski, K. (2012). A TDR-based soil moisture monitoring system with simultaneous measurement of soil temperature and electrical conductivity. Sensors, 12, 13545–13566. doi:10.3390/s121013545

Topp, G.C., Davis, J.L., & Annan, A.P. (1980). Electromagnetic determination of soil water content: Measurements in coaxial transmission lines. Water Resources Research, 16), 574-582. https://doi.org/10.1029/WR016i003p00574

Yetemen, O., Istanbulluoglu, E., & Duvall, A.R. (2015). Solar radiation as a global driver of hillslope asymmetry: Insights from an ecogeomorphic landscape evolution model. Water Resources Research, 51(12), 9843-9861. https://doi.org/10.1002/2015WR017103

Zapata-Rios, X., Brooks, P.D., Troch, P.A., McIntosh, J., & Guo, Q. (2016). Influence of terrain aspect on water partitioning, vegetation structure and vegetation greening in high-elevation catchments in northern New Mexico. Ecohydrology. 9, 782-795. https://doi.org/10.1002/eco.1674

Chapter 3

Modelling the effect of catena position and hydrology on soil chemical weathering

MODELLING THE EFFECT OF CATENA POSITION AND HYDROLOGY ON SOIL CHEMICAL WEATHERING

Published as: García-Gamero, V., Vanwalleghem, T., Peña, A., Román-Sánchez, A. and Finke, P.A.: Modelling the effect of catena position and hydrology on soil chemical weathering, SOIL Discuss. [Preprint], https://doi.org/10.5194/soil-2021-78, in review, 2021.

ABSTRACT

The sensitivity of chemical weathering to climatic and erosional forcing is well established at regional scales. However, soil formation is known to vary strongly along catenas where topography, hydrology, and vegetation cause differences in soil properties and possibly chemical weathering. This study applies the SoilGen model to evaluate the link between topographic position and hydrology with the chemical weathering of soil profiles on a north-south catena in southern Spain.

Pedogenesis was measured and simulated in seven selected locations over a 20,000-year period. A good correspondence between simulated and measured chemical depletion fraction (CDF) was obtained (R^2=0.47). An important variation in CDF values along the catena was observed, although the position along the catena alone, nor by the slope gradient, explained this variation well. However, the hydrological variables explained the observed trends better. A positive trend between CDF data and soil moisture and infiltration and a negative trend with water residence time was found.

The model sensitivity was evaluated with a large precipitation gradient (200-1,200 mm yr^{-1}). While a marked depth gradient was obtained for CDF with precipitation up to 800 mm yr^{-1}, a uniform depth distribution was obtained with precipitation above 800 mm yr^{-1}. The basic pattern for the response of chemical weathering to precipitation is a unimodal curve, with a maximum around a mean annual precipitation value of 800 mm yr^{-1}. Interestingly,

this corroborates similar findings on the relation of other soil properties to precipitation and should be explored in further research.

3.1. Introduction

The spatial variability of soil properties is conditioned by the five main soil forming factors: Climate, Organisms, Relief, Parent material, and Time (Jenny, 1941). Differences in the spatial and temporal distribution of these factors cause both long and short-scale spatial heterogeneity. In recent years, different soil formation models have been developed that explain the landscape or long-scale soil variability well. Such models range from simple mechanistic soil depth (Minasny & McBratney, 2001) to more complex schemes that link different forming and erosion-deposition processes, for example, MILESD or LORICA (Temme & Vanwalleghem, 2016; Vanwalleghem et al., 2013). However, the short-scale variability, or catena effect, has received much less attention. The interlocking of specific soil and vegetation associations at different landscape positions was first described by Milne (1935) and is widely used in soil science (Borden et al., 2020). The soil catena can be understood from the retention and movement of water and chemical elements linked to topography and vegetation (Reuter & Bell, 2001). Recently, Ferrier and Perron (2020) constructed a numerical model for the coevolution of topography, soils, and soil mineralogy that allowed them to conclude that the hillslope scale has a critical importance in the response of chemical weathering rates to changes in tectonics and climate. However, most existing soil formation models do not account for hydrology, nor for chemical weathering reactions. For example, the models marm3D (Cohen et al., 2010) and SSSPAM (Welivitiya et al., 2019) linked landscape and pedogenesis processes for catena spatial scales, but while they represent physical weathering and armouring well, they did not account for chemical weathering. At present, the only models of soil genesis with the capability of simulating water flow, physical and chemical weathering, and chemical equilibriums are one-dimensional, for example, SoilGen (Opolot et al., 2015). Despite this limitation, such

models have been applied successfully at the landscape scale, by modelling the different landscape positions independently. Finke (2012) for example modelled 3 soil profiles on different topographic positions in the loess belt of Belgium. Finke et al. (2013) modelled the spatial variation of soil horizons at 108 locations in a 1,329 ha large forest area in the same loess belt region. However, there is still needed to further test these one-dimensional models against field data from different environments, and especially, to test their capabilities to model chemical weathering.

Field studies have shown the importance of chemical weathering in the overall soil formation processes, and have shown that physical erosion and chemical weathering are tightly coupled (Riebe et al., 2004) as the main processes in eroding environments. The combination of these processes determines the total denudation rate (Riebe et al., 2001). The contribution of chemical weathering (W) to the total denudation rate (D), W/D, can be inferred by comparing the concentration of immobile elements in soil and bedrock, through the chemical depletion fraction (CDF) (Riebe et al., 2001).

There is an ongoing debate in the scientific community to whether chemical weathering is limited by physical erosion and the supply of fresh particles (e.g Larsen et al., 2014) or whether it is limited by reaction kinetics (e.g. Gabet & Mudd, 2009). Generally, it is assumed from models and field studies in different environments that soil weathering is supply-limited when erosion rates are low, and kinetically limited when erosion rates increase, as the shorter soil residence times imply that minerals do not stay in the soil long enough to become fully weathered. Larsen et al. (2014) compiled data from the New Zealand Alps, among the world's most rapidly eroding mountain areas, and still found a positive relation between physical erosion rates and chemical weathering, indicating supply-limited conditions. On the other hand, is well established that climate and specifically water availability is also an important factor affecting chemical weathering rates (e.g. Maher, 2011). Climatic factors affect significantly because of the dependency of the chemical

weathering types of water to drive the chemical alteration of rocks and are potentially accelerated by high temperatures because it affects the kinetics reactions and solubilities (Duarte et al., 2018). Schoonejans et al. (2016) confirmed the significant relation of chemical weathering to rainfall, by measuring CDF along a climatic gradient in a semiarid environment in the Southern Betic Cordillera (Spain). Whereas much of soil weathering research has focused much on the critical control of physical erosion rates on chemical weathering, more recent research by Calabrese and Porporato (2020) stresses the control of wetness. They suggest that water-limited environments are kinetically limited. Globally, they calculate 61% of the land to be kinetically-limited, while only 1% would be supply-limited. If their findings can be confirmed, it would imply that climatic conditions and soil hydrology are much more important than previously assumed. In any case, these authors point out that the factors affecting chemical weathering need to further be disentangled (Calabrese & Porporato, 2020).

However, the relation between weathering and water availability is not limited to precipitation and evapotranspiration but is also related to other factors such as infiltration or topography, and even vegetation. Along a catena, the hydrology is considerably different depending on the position (Chadwick et al., 2013). Brantley et al. (2017) developed a conceptual model to link chemical weathering reaction fronts to hillslope hydrology. Knowing how difficult it is for hydrologists to select models, they developed a conceptual model to relate reaction fronts with water flow inside hillslopes, exemplified with field data for shale, granite, and diabase. Riebe et al. (2004) made measurements on 42 study sites with highly variable climate regimes and they showed that the degree of chemical depletion increases systematically with temperature and precipitation. Dahlgren et al. (1997) in their work developed along an altitudinal transect in the Sierra Nevada in California (USA) found the maximum degree of chemical weathering with intermediate levels of precipitation and temperature. Dixon et al. (2016), along 60 km of a north-south toposequence in the Waitaki

Valley in the South Island of New Zealand, marked with an important precipitation gradient, identified a pedogenic threshold at mean annual precipitation of ~800 mm yr^{-1}. Samouëlian and Cornu (2008) pointed out the role of water in soil formation and how the soil moisture regime variation and its influence on soil formation processes were not included in several models. Indeed, the soil moisture dynamics related to the topographical position has been studied by several authors, such as Salve et al. (2012), who have monitored this and other variables for 4 years with multiple measurement devices on a hillslope in coastal Mendocino County, in northern California, USA. Mudd & Furbish (2006) presented a hillslope model that couples the evolution of topography and soil thickness by using immobile minerals. They assessed the importance of hydrology on the rate of chemical weathering in hillslope soils. Yoo et al. (2007) developed a model that integrated the Riebe et al. (2001) method and tested it with experimental data from a watershed in south-eastern Australia for simultaneously quantifying the rates of chemical weathering and soil transport as a function of hillslope position. Afterward, this work was expanded by Yoo et al. (2009). They quantified soil chemical weathering rates along a grass-covered hillslope in the Tennessee Valley in Coastal California (USA) and began to elucidate the mechanisms that control the topographical dependence on chemical weathering being the next step includes hydrology into the model. Langston et al. (2011) explored the role of hydrology in saprolite formation through 2-D numerical calculations on two idealized slopes, north (NFS) and south-facing (SFS), respectively, in the Boulder Creek watershed, Colorado (USA). Highlighting the importance of time and hillslope aspect in the formation of the saprolite and the need to couple hydrologic models with reactive-transport models to better understand the distribution of chemical weathering intensity. Braun et al.(2016) presented a model for the formation of regolith on geological timescales by chemical weathering, pointing out that this process has long been neglected in favor of hillslopes physical processes by geomorphologists, this process also being the mechanism that leads to the formation of

aquifers from the unweathered bedrock (Lachassagne & Wyns, 2011). Previously, the weathering zone had been considered the one located over the groundwater level. However, Lebedeva & Brantley (2020) formulated a simplified weathering model to explore relationships between weathering and the water table taking into account the unsaturated and the saturated zone. Because of the need to couple hydrology with chemical weathering to understand spatial variability in soil formation, this study applied the SoilGen model (Finke & Hutson, 2008) to different pedons and different hydrological conditions along a catena in a Mediterranean catchment in southern Spain. Finke & Hutson (2008) created the SoilGen model to reconstruct soil development based on present knowledge. It is a 1-D solute transport extended with various soil development processes such as physical and chemical weathering, clay migration, cycles of various elements including that of C and bioturbation, where soil forming-factors (climate, organisms, relief, parent material, and time) serve as initial and boundary conditions to recreate soil formation over various parent materials. The specific objectives were: (i) to evaluate differences in simulated soil development between two opposing, north-south facing, hillslopes, from 20,000 years before present to present; (ii) to relate soil development to differences in hydrological dynamics and (iii) to evaluate, through sensitivity analysis, the capability of the SoilGen model to simulate soil development in a Mediterranean catchment in granitic parent material.

3.2. Materials and methods

3.2.1. Study site

The study site is located in a semi-natural area of oak-woodland savanna or 'dehesa' (a traditional Mediterranean silvopastoral system, Olea & San Miguel-Ayanz, 2006) in Cardeña, within the Sierra Morena mountain range, in southern Spain (38.20° N; 4.17° W, 700 m a.m.s.l.) (Fig.3.1). Seven locations were chosen along a north-south catena, each

separated at a distance between 50 and 100 m on two opposite hillslopes. A summary of the characteristics of the locations is given in Table 3.1. A full soil profile description was made at each point, and soil samples were taken for chemical analysis up till the bedrock. Next, five soil moisture sensors were installed in each profile at different depths between 5 and 45 cm. For details on the soil hydrology dynamics, see García-Gamero et al. (2021).

According to the Köppen-Geiger climate classification (Peel et al., 2007), the area has a continental Mediterranean climate (BSk) with an average annual rainfall of 878 mm (1981-2010), with cold winters and long, dry summers. The mean annual air temperature is 15.3 °C, the coldest month is January, with a mean monthly temperature of 7°C, and the hottest July, with a mean monthly temperature of 25.4°C (Carpintero et al., 2020).

Soils in the catchment are derived from Los Pedroches batholith parent material, which consists of a main granodioritic unit, several granite plutons, and an important acid-to-basic dike complex (Carracedo et al., 2009). These fall into three classifications: Regosols, Leptosols, and Cambisols according to the FAO-UNESCO World Reference Base (IUSS Working Group WRB, 2015). The texture class ranges from sand to sandy loam with a soil depth generally ranging between 0.5 m along the south aspect part of the transect and 1.0 m along the northern part of the transect (Román-Sánchez et al., 2018), according to soil observations.

Vegetation in a dehesa includes sparse trees, holm and cork oaks, shrubs, retama, and annual grasses such as *Lolium* sp., *Bromus* sp., and *Trifolium* sp., with maximum production in spring and a non-vegetative period in summer (Olea & San Miguel-Ayanz, 2006).

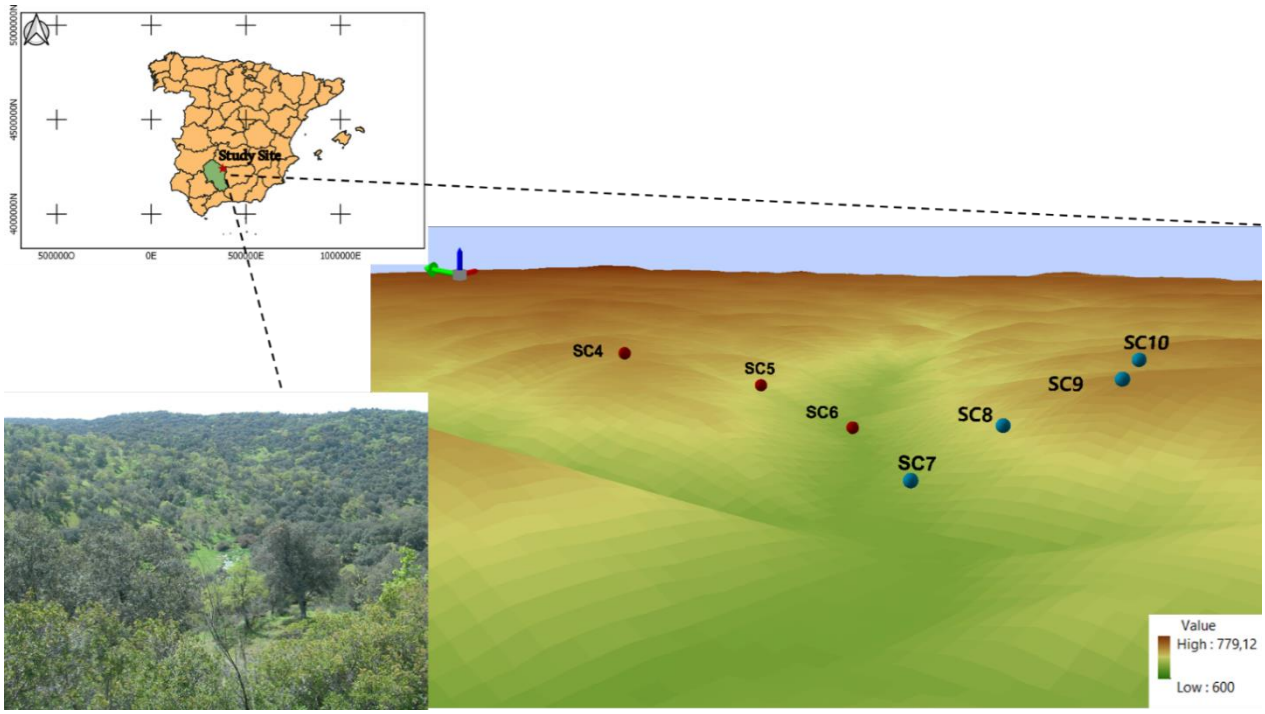

Figure 3.1. General location map of the study area and a detailed terrain map showing the location of the seven analyzed soil profiles along the catena with two opposing north-south facing slopes (respectively NFS and SFS, blue and red dots). The inset photo shows a landscape view of the study area. Note the green arrow indicates the north.

Table 3.1. Characteristics of the seven locations (SC4-SC10) in the study site.

	SC4	SC5	SC6	SC7	SC8	SC9	SC10
Latitude	38° N	38° N	38° N	38° N	38° N	38° N	38° N
Slope (°)	4	20	14	4	27	19	2
Upslope bearing (°)	35	27	40	55	61	66	53
Downwind bearing (°)	225	225	225	225	225	225	225

3.2.2. Testing of modelled soil hydrology

SoilGen simulates over millennium scales the flow of water, heat, solutes, and CO_2 in unconsolidated geomaterials by numerically solving partial differential equations (the Richards equation, heat flow equation, advection-dispersion equation, and C02-diffusion equation respectively) (Finke & Hutson, 2008).

Given the importance of water fluxes for soil formation in general and chemical weathering specifically, the model was tested for its ability to simulate the soil moisture dynamics accurately. For this, the current soil profile characteristics in 7 locations were used to run the model over a two-year period in which soil moisture was measured, i.e., 2016 and 2017. The soil moisture sensors started to collect data at the end of 2016 so for the first part of the year the simulations were adapted using precipitation and evapotranspiration data from 2017. This could be considered a spin-up (because the initial soil moisture profile was not known).

To account for interception by vegetation, we reduced the daily precipitation by a fixed value of 2 mm, as suggested by Laio et al. (2001). These changes resulted in a reduction of the measured precipitation during the calibration period of 718.7 mm to 525.4 mm.

Model-to-data correspondence was tested by comparing simulated values with measured values of soil moisture content, by the R^2 and the Nash-Sutcliffe Efficiency (NSE).

3.2.3. Model Inputs

The tested model was then run at the seven soil profile location for long-term simulations (20,000 years). This simulation period represents the residence time of the soil profile based on field measurements with Optically-Stimulated Luminescence (Román-Sánchez et al., 2019). Table 3.2 summarizes the main model parameters and initial values. Figure 3.2 depicts the temporal variation of boundary inputs if time series were reconstructed over the simulation period. In order to represent correctly the Mediterranean climate variability, the climate data reconstructions were obtained by combining a mean temperature, precipitation, or evapotranspiration from the pollen-based dataset by Davis et al. (2003), with the observed year-to-year variability of modern weather observations.

Table 3.2. Inputs for the SoilGen Model.

Group	Input Variable or Parameter	Dimensions	As Initial Condition	Time series, in Typical Year	Time Series, Annual	Source for Data and/or Method
Climate	Temperature	°C	Yes	Weekly average and daily amplitude	January and July averages	Davis et al., 2003; Cardeña weather data
	Precipitation	mm	-	Daily depth, intensity, and chemical composition of rain	Annual sum	Davis et al., 2003; Cardeña weather data
	Potential evapotranspiration	mm	-	Weekly total	Annual sum	Hargreaves & Samani, 1985
Organisms	Vegetation type	-	-	-	Vegetation type, rooting depth, and C input as litter	Olea & San Miguel-Ayanz, 2006; Unpublished data from Santa Clotilde 'dehesa'
	Bioturbation	Mg ha^{-1} yr^{-1}	-	-	Yearly depth distribution	Gobat et al., 1998, p. 122
Relief	Slope angle	degree	Yes			DEM; (García-Gamero et al., 2021)
	Slope aspect	degree	Yes			DEM; (García-Gamero et al., 2021)
	Wind direction	degree	Yes			Cardeña weather data
Parent material	Clay/Silt/Sand	Mass %	Yes			Granite: 7.0/17.4/75.6 Unpublished data from analyzed horizons in Santa Clotilde 'dehesa'
	OC	Mass %	Yes			0.17 %
	Ca, Mg, Na, K, Al, SO_4, Cl, Alkalinity in solution	mmol dm^{-3}	Yes			Unpublished data
	Ca, Mg, Na, K, Al, H on exchange complex and CEC	mmol+ kg^{-1}	Yes			Unpublished data from analyzed horizons in Santa Clotilde 'dehesa'
	$CaCO_3/CaSO_4$	Mass %	Yes			0.01/0% Unpublished data from analyzed horizons in Santa Clotilde 'dehesa'
	Gapon exchange coefficients	$(mol\ dm^{-3})^{1/n\ -1/m}$	Yes			De Vries and Posch (2003)
	Ca, Mg, Na, K, Al in primary minerals	$mol^{+}\ kg^{-1}$	Yes			Unpublished data from Santa Clotilde 'dehesa'

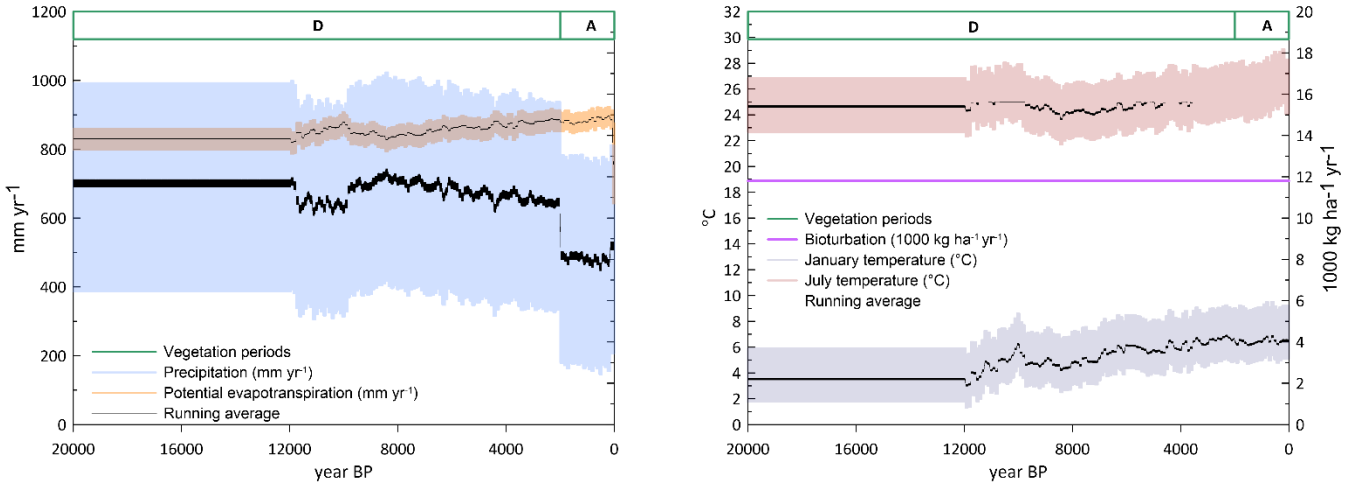

Figure 3.2. Boundary conditions for the soil modelling, representing reconstructed climate and vegetation change over the last 20,000 years, the left panel shows precipitation and evapotranspiration, the right panel shows temperature. The bandwidth indicates the year-to-year variability in the climate data, and the bold, black line indicates the 25 year running average. A= Agriculture, D= Deciduous wood.

3.2.4. Chemical weathering

Chemical depletion fraction (CDF), expressing the total fractional mass lost to chemical weathering, is a widely used indicator of the degree of chemical weathering of a soil profile (Dixon et al., 2009; Riebe et al., 2001):

$$CDF = 1 - \frac{Z_r^{ROCK}}{Z_r^{SOIL}}$$

where Zr^{ROCK} is the Zr concentration in the bedrock and Zr^{SOIL} is the Zr concentration in the soil. CDF values close to zero indicate the absence of weathering, as the Zr concentration of the soil is equal to that of the parent material. Values closer to 1 indicate higher chemical weathering, as the weathering of mobile elements results in a relative increase of the immobile Zr in the soil profile (Yoo et al., 2011).

CDF values were measured in the field by sampling each soil profile and comparing it to the minimum value registered in the soil profile (Table 3.3). The chemical analyzes were performed on a PHILIPS model PW 2404 wavelength-based X-ray fluorescence

spectrometer (WDS) with a 4 kW rhodium anode tube. For the determination of trace elements, the Pro-trace program of the PANalytical company was used, based on calibration curves that include both geological patterns and reference patterns of the program itself. The samples were prepared in a tablet pressed at 40 tons for two minutes. The amount of sample used was 10 g mixed with a solution of Elvacite, in a proportion of 10 g of sample with 4 ml of solution.

The SoilGen model was then used to model the measured CDF values, assuming one completely inert (0-weathering rate) mineral, and to explore the sensitivity of the CDF to variations of precipitation. The effect on model results of a marked gradient of precipitation, between 200 and 1,200 mm, has been evaluated at the SC10 location, because of its position at the hilltop, representative of the larger plateau area.

We conducted the performance evaluation by selecting various statistical indicators to conduct a quantitative analysis: the fraction of predictions within a factor or two (FAC2), the fractional bias (FB), the root mean square error (RMSE), and the normalized mean square error (NMSE).

Table 3.3. Chemical composition of the seven soil profiles (SC4-SC7). Values are averaged over the total soil profile depth. Mean measured Chemical Depletion Fraction, CDF.

Location	Soil profile depth (m)	SiO_2	Al_2O_3	Fe_2O_3	MnO	MgO	CaO	Na_2O	K_2O	TiO_2	P_2O_5	L.O.I	Zr	CDF
						%							ppm	
SC4	0.44	70.8	16.5	2.3	0.03	1.12	0.56	2.6	4.4	0.40	0.12	0.75	148.0	0.19
SC5	0.60	66.7	17.0	5.1	0.06	1.7	0.28	2.2	4.6	0.83	0.11	1.0	284.9	0.04
SC6	0.55	68.0	16.8	3.9	0.07	1.2	0.27	1.9	5.3	0.69	0.11	1.4	314.2	0.13
SC7	0.97	69.8	16.5	2.6	0.07	1.1	0.46	2.9	4.4	0.48	0.11	1.1	181.3	0.26
SC8	0.47	62.2	18.7	5.7	0.11	3.1	0.51	1.6	4.7	1.03	0.15	1.7	294.0	0.20
SC9	0.57	69.1	17.1	2.8	0.05	1.3	0.45	2.9	4.2	0.48	0.11	1.2	166.6	0.19
SC10	0.51	69.9	16.6	2.7	0.03	1.1	0.61	3.3	4.0	0.46	0.15	1.1	160.6	0.19

3.3. Results and discussion

3.3.1. Model testing and results

The model was tested using in-situ soil moisture observations, in order to check that the model represents well the soil profile's hydrological balance before modelling chemical weathering reactions and material fluxes. The model was adjusted for rainfall interception by vegetation. Figure 3.3 shows the R^2 values, with the best correlation determined by the daily precipitation reduced by a fixed value of 2 mm and interception evaporation fraction of 0. Consequently, all further simulations were carried out using this combination. The results are shown in Fig. 3.4, which compares the daily values of simulated and measured soil moisture content across a period of 1 year and 1-month (from November-2016 to December-2017) at the SC4 location, at the hilltop of SFS. Soil moisture values, both observed and simulated, vary between approximately 0.05 (m^3m^{-3}) and 0.30 (m^3m^{-3}). The calibrated coefficient of determination (R^2) and the Nash-Sutcliffe Efficiency (NSE) index indicate a good fit of SoilGen to the observations, with values of 0.85 and 0.78, respectively. Overall, most values fall close to the 1:1 line, although there is a small overprediction of low soil moisture values and underprediction of high soil moisture values. However, given the complex soil conditions and variable Mediterranean climate, this prediction can be considered a valid representation of the actual soil hydrological dynamics.

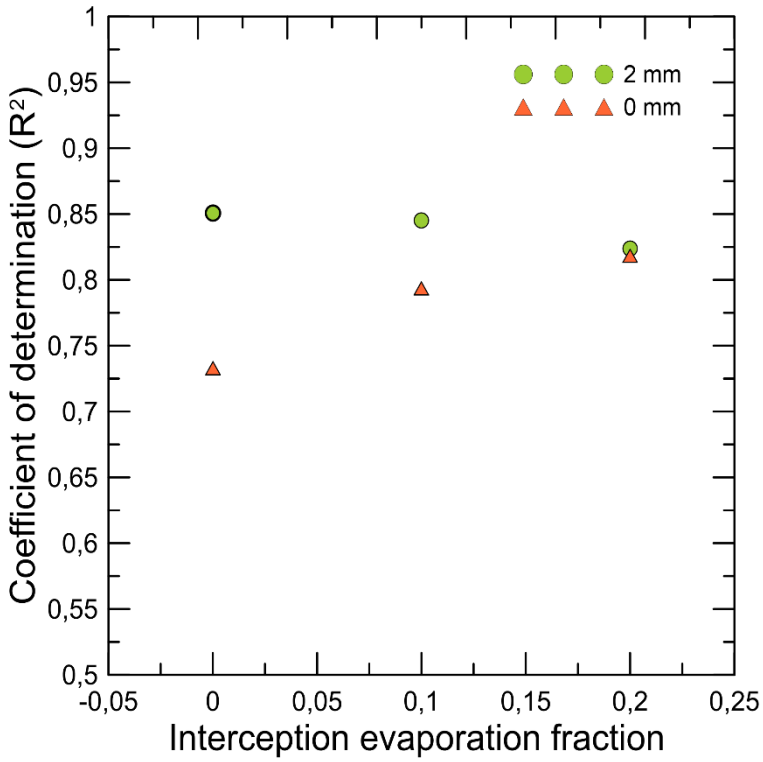

Figure 3.3.Coefficient of determination (R^2) calculated for different Interception evaporation fraction with the daily precipitation reduced by a fixed value of 2 mm and without reduction or 0 mm.

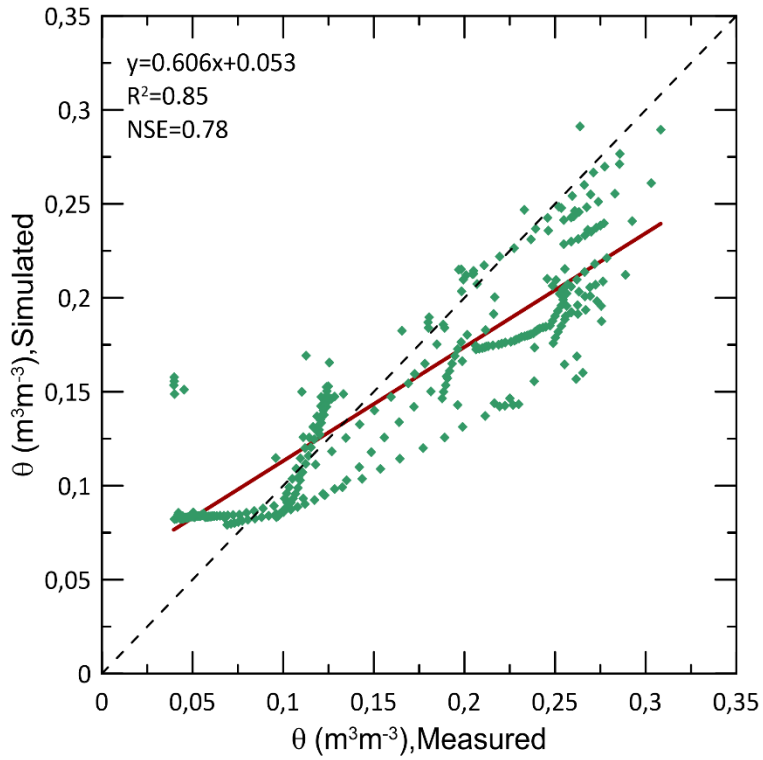

Figure 3.4. Relation between soil moisture content (θ) values simulated and measured at SC4 location. The coefficient of determination (R^2) and the Nash-Sutcliffe Efficiency (NSE) index are indicated.

A comparison between measured and modelled CDF values is shown in Fig. 3.5. Measured CDF values indicate an intermediate weathering of the soil profiles, with values ranging between 0.04 and 0.26. The highest chemical weathering was measured in the profiles SC7 and SC8. Simulations with SoilGen generally represent the trend in the measured data well, although the data show an overall trend for CDF to be overpredicted (Fig. 3.5), as the average slope of the regression line ($\mathrm{CDF}_{\mathrm{measured}} = 0.630 \cdot \mathrm{CDF}_{\mathrm{calculated}} + 0.011$) was significantly different from 1. The 1:1 solid line (perfect model) and the 1:0.5 and 1:2 dashed lines (FAC2) were added to the scatter plot (Fig. 3.5) to assist the interpretation of the results. The results of the statistical metrics (Table 3.4) met the criteria suggested by Kumar et al. (1993): the performance of a model can be deemed as acceptable if FAC2 ≥ 0.80, being the ideal value 1.0 (100%), NMSE ≤ 0.5, and -0.5 ≤ FB ≥ +0. 5. Taken this into account, the obtained FAC2, NMSE, and FB values are quite acceptable and equal to 0.86, 0.22 and -0.39, respectively. According to the FAC2 value, 86 % of simulated values were within a factor of two of the measured values. A negative value of FB indicates model overestimation whereas RMSE and NMSE do not account for over or underestimation but their ideal value is zero (Brancher et al., 2020). Note that the metric results shown are dimensionless because CDF is a non-dimensional quantity. The model, therefore, represents the measured trend in CDF values correctly, although there exists a positive bias. However, given the fact that the model is uncalibrated in terms of chemical reactions and with respect to the resulting soil properties, we consider this result to be satisfactory. Indeed, some degree of bias can be expected, in part since this 1-D model is not set up to handle possible lateral fluxes of water and chemical weathering products but also because of the large time scale of the modelled processes, a common problem in this type of soil formation studies (reference review paper by Opolot and Finke (2015)).

The low CDF in the SC5 location, considering the minimum Zr value measured in the soil profile, indicates that the complete soil profile is highly weathered. This is associated with

lower SiO_2 and higher MgO values with respect to the other locations (Table 3.3) and could be related to mafic intrusions because of differences in bedrock mineral composition which result in higher rock weatherability. Oeser et al. (2018), in their study along a steep climate and vegetation gradient in the Chilean Coastal Cordillera, attributed a high degree of weathering (CDF ≈ 0.4-0.5) in Santa Gracia sites to a more mafic composition of the bedrock. Further evidence corroborating the different rock composition at the SC5 site and its consideration as an outlier is given by the surface topography, as shown in Fig. 3.6. It can be seen that a small knickpoint is present just upslope of SC5, which could indicate indeed a higher weatherability around SC5.

Based on the chemical composition alone (Table 3.3), also the SC8 location is characterized by low SiO_2 and high MgO values, corresponding to mafic rocks. However, the simulated CDF at this location does not deviate as much from the measured values as in SC5. This location on the NFS shows denser vegetation than location SC5 on the SFS (Fig. 3.6), due to the higher water availability on the NFS (García-Gamero et al., 2021). Oeser & von Blanckenburg (2020) pointed out that the presence of denser vegetation might counteract a potential weathering increase in their study along the climate and vegetation gradient in the Chilean Coastal Cordillera. This could explain why SC8 is not an outlier, similar to SC5.

While the underlying reasons for any deviations between modelled and measured CDF values are certainly complex, they will be explored below in more detail, in order to try to establish systematic relations between CDF and topographic and hydrological variables.

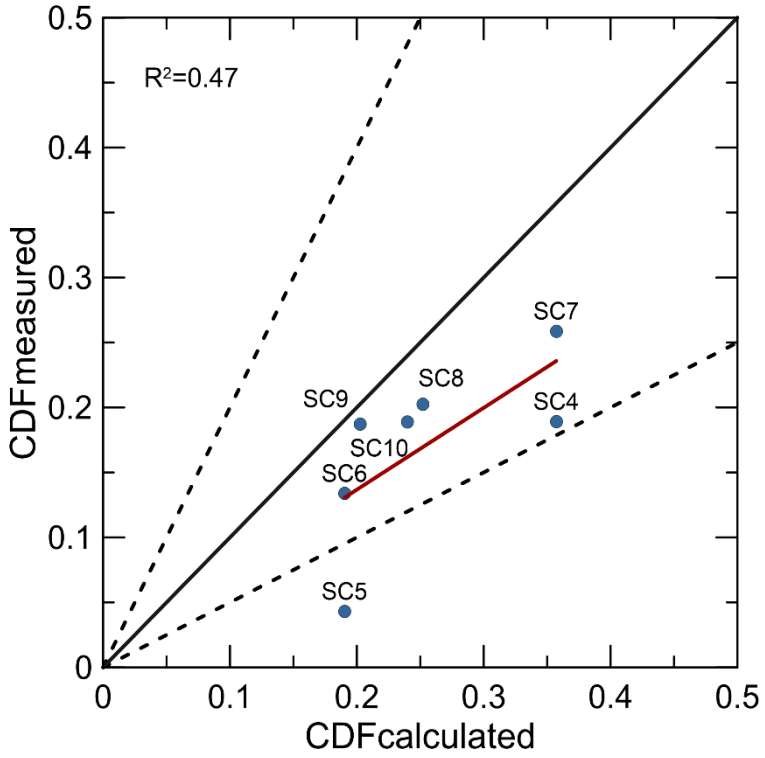

Figure 3.5.Relation between CDF values calculated based on simulations and measured based on field samples. The 1:1 line (solid) represents the perfect model and the 1:0.5 and 1:2 lines (dashed) embrace the data within a factor of two (FAC2). The coefficient of determination (R^2) is indicated.

Table 3.4. Statistical metrics of performance evaluation comparing measured and calculated CDF. n: number of observations, FAC2: Fraction of predictions within a factor of 2, FB: Fractional bias, RMSE: Root mean square error, NMSE: Normalized mean square error.

n	FAC2	FB	RMSE	NMSE
7	0.86	-0.39	0.099	0.22

3.3.2. Topographic and hydrological effect in CDF

The SoilGen model was applied to test the hypothesis that CDF values could be explained by landscape position and simulated by a simple one-dimensional model. Any deviations can then be analyzed to identify model shortcomings and future needs for model improvement.

To analyze the effect of topographic position along the catena, measured and simulated CDF values together with the conceptual model of the subsurface of the Critical Zone (the

zone of the Earth surface that extends from the top of the canopy to the bottom of the groundwater) in the study site are shown in Fig. 3.6. As mentioned in Fig. 3.5, simulated and measured CDF values generally have the same trend, except for SC5. Higher simulated values were observed on the hilltop, SC4, and the valley bottom, SC7, followed by location SC8 in the middle slope of the NFS (Fig. 3.6). These locations were among those with the lowest local slope gradient, except for SC8.

The position along the toposequence alone did not explain well the spatial variation of the CDF, so it must be concluded that its variation is due to other factors that are considered in the model and will be analyzed.

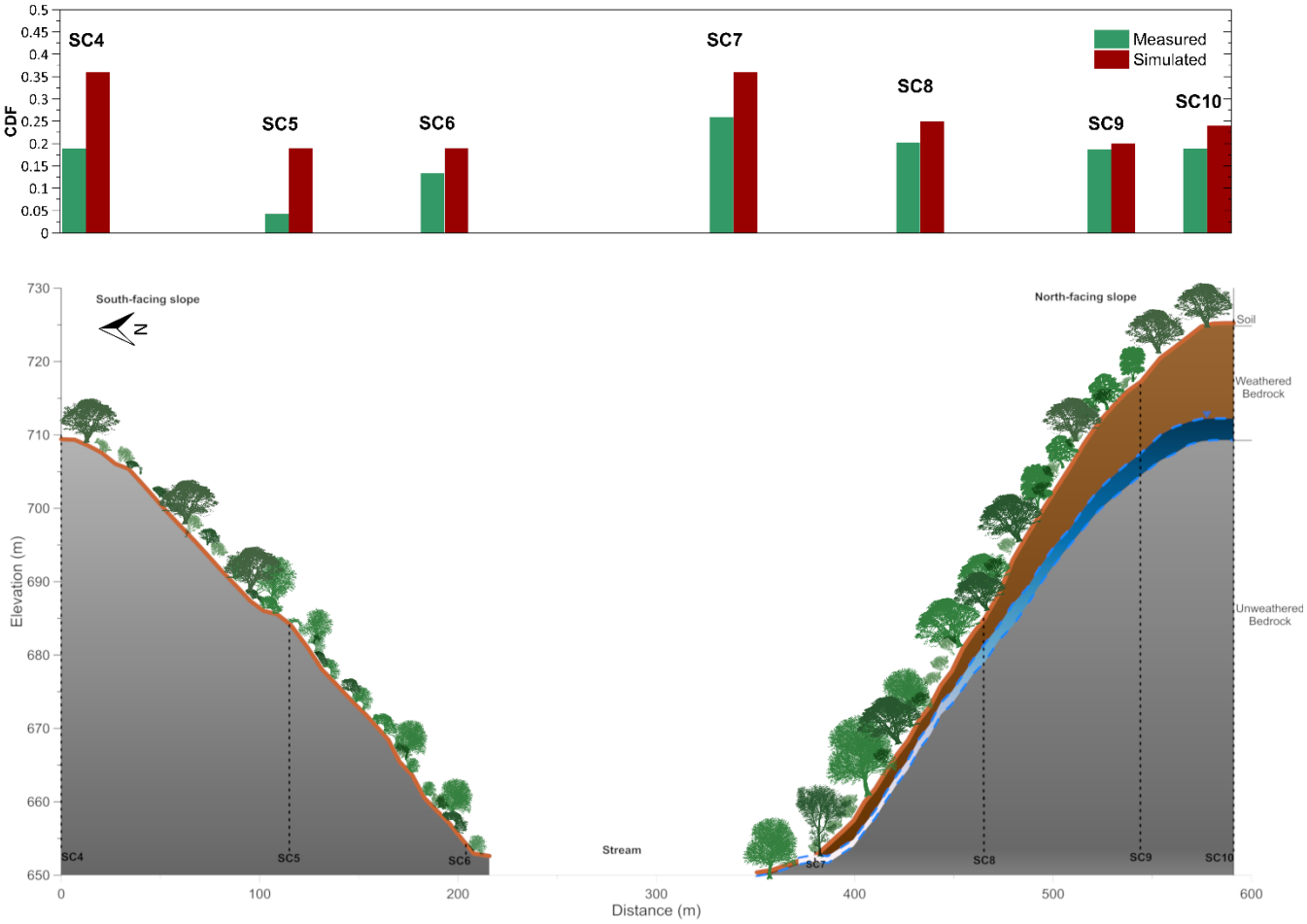

Figure 3.6.Variation of measured (green bars) and simulated (red bars) chemical depletion fraction (CDF) (top panel) along the studied north-south catena, including a schematic representation (bottom panel) of the vegetation, surface topography, soil, weathered bedrock, and unweathered bedrock. On the NFS we also distinguish a seasonal groundwater table (blue).

The relation of CDF values with different external factors was considered in Fig. 3.7. The variation of CDF along the toposequence was related to local slope gradient (Fig. 3.7a) and because the role of soil water hydrology on chemical weathering with hydrological parameters, i.e., infiltration (I, $m^3\ yr^{-1}$) (Fig. 3.7b), average moisture content (θ, m^3m^{-3}) (Fig. 3.7c), and water residence time (RT, yr) (Fig. 3.7d). The hydrological parameters were derived from the simulations.

The results indicated an absence of correlation with the current slope (Fig 3.7a), although the highest CDF values were found for two soil profiles with a low slope gradient (SC4 and SC7), this was not the case for SC10. On the other hand, the data indicate a positive relationship with average moisture content and infiltration. This implies that higher infiltration leads to higher chemical weathering. A negative relation was observed with residence time, implying that a faster throughflow of reactive water from rainfall speeds up the weathering process. The absence of statistically significant relations for slope and these hydrological parameters indicates the complexity of the modeled processes. One reason for this is the long-time scale of modelling, and the current topography might not have been constant during the full period of weathering. This problem is also recurrent in simulations of historical soil erosion (Peeters et al., 2006).

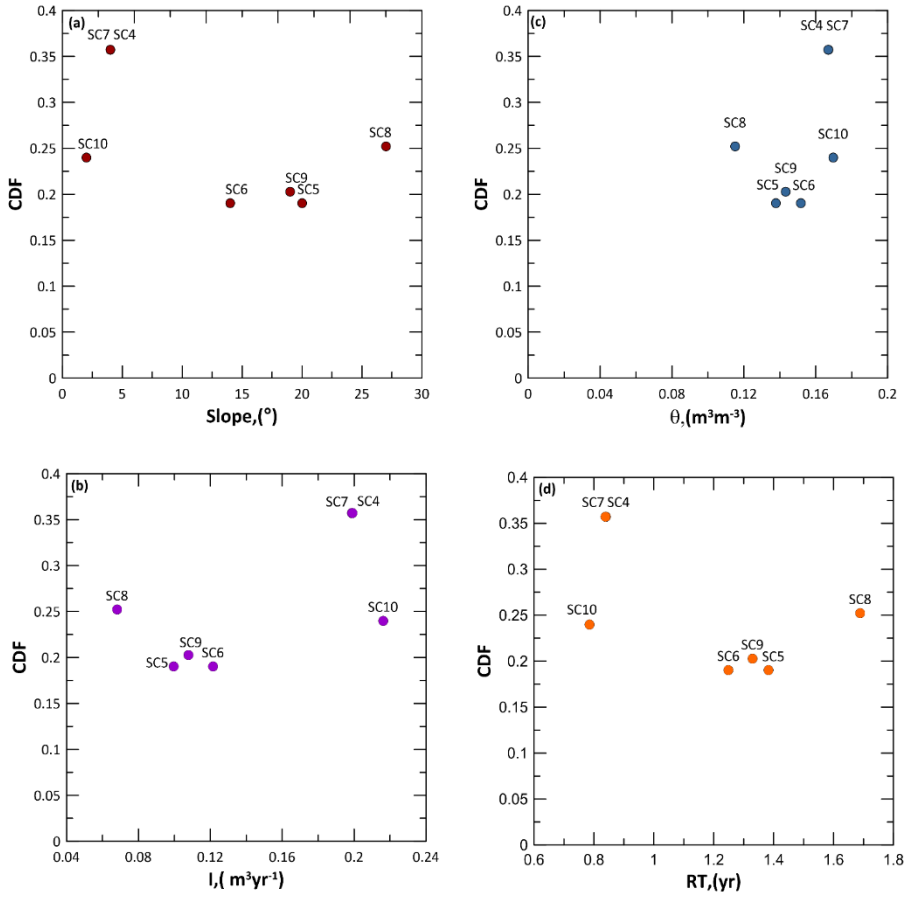

Figure 3.7.Relation between CDF values and (a) Local gradient slope (°) (b) Infiltration, I (m^3yr^{-1}), (c) average soil moisture, q (m^3m^{-3}) and (d) Water Residence Time, RT (yr).

The good relation between chemical weathering and hydrological variables corroborates previous studies that concluded the hydrological control on chemical weathering to be dominant (Maher, 2010; Maher & Chamberlain, 2014). These authors indicate that natural systems can generally be considered to be transport-controlled, where the reaction rate of chemical weathering processes depends mostly on the departure from the equilibrium. This departure is controlled by the water flow rate through the profile and how fast or slow weathered products are exported from the soil profile. In other words, in transport-controlled weathering systems, flow rates and solubility by definition will be the dominant control on mass removal. As natural systems are difficult to characterize fully, not much field data has been collected corroborating this so far. Some studies, like Schoonejans et al. (2016) found a positive relation between chemical weathering and rainfall along a climatic

gradient in southern Spain. However, the results of this study, both measured and modelled CDF values, are among the first to find differences in chemical weathering in different landscape positions along a catena. In this study area, rainfall is homogeneous, but the differences in infiltration can be purely attributed to differences in exposition and landscape position. Further studies will be needed, not only at the landscape or regional scale but also at a shorter spatial scale, such as this catena-scale study to elucidate these hydrological effects in more detail. Some authors have pointed to important feedbacks with plants, that definitely can have a significant impact on soil hydrology and perhaps also a direct influence on chemical weathering processes (Cipolla et al., 2021; Porada et al., 2016).

The results of this study are in contrast with observations by Molina et al. (2019) on 10 toposequences in a High Andean catchment. They observed only a marginally significant topographic control on chemical weathering extent, while our data varies considerably between landscape positions. Rather than topography, Molina et al. (2019) concluded that vegetation exerted an important control, as they found highly significant differences in chemical weathering extent between vegetation communities. In their study, however, they compared very different vegetation types, ranging from forest to grass and cushion-forming plants. In our study, vegetation is more similar between SFS and NFS, although vegetation is denser on the latter. Although counterintuitively, in previous work in the study site to characterize the hydrological dynamics using soil moisture sensors and piezometers, García-Gamero et al. (2021) observed very similar surface hydrological dynamics between the NFS and SFS. In fact, daily soil moisture storage change differences between both opposing slopes did not suggest more interception on the NFS (García-Gamero et al., 2021), despite the denser vegetation. The denser vegetation cover on the NFS only caused it to dry out somewhat earlier during the year compared to the SFS. However, subsurface water dynamics were found to be significantly different, with a deeper weathered bedrock on the NFS (Fig. 3.6) that allows seasonal water storage and a significant lateral water flow.

The model SoilGen could be further improved by taking into account lateral fluxes of water and sediment. The one-dimensional SoilGen model does not consider lateral fluxes by definition. These lateral water fluxes on the NFS can explain the higher measured CDF values in SC9, SC8 and particularly in SC7. The points located along this north-facing hillslope all receive an additional lateral water influx, which is greatest for SC7 at the bottom of the hillslope. This lateral water flux can accelerate the chemical weathering and is not considered in the one-dimensional model. At present, as far as the authors know, no soil profile formation model exists that has this capability. On the other hand, on the SFS soils are shallower and this lateral connectivity does not exist. The other profile on the SFS, SC6 however does behave as expected and is characterized by the lowest CDF values, except for SC5 above mentioned, both measured and simulated. To take into account these lateral fluxes goes beyond the objectives of this paper that aims to model chemical weathering with a simple model, but future modelling efforts should be pointed in this direction.

3.3.3. Climatic effect on chemical weathering: Sensitivity Analysis

After analyzing the variability in soil formation along the north-south oriented catena, the effect of a simulated precipitation gradient (200-1,200 mm) on the CDF was studied, at one fixed, representative location, SC10 (Fig. 3.8).

The lowest CDF values throughout the profile correspond to the lowest precipitation value of 200 mm, as expected. For this precipitation value, there is very little difference of CDF with depth. Increasing precipitation to 400 mm leads to a sudden increase in the weathering of the top 40 cm of the profile, with a marked depth gradient and similar CDF values in depth compared to the 200 mm case. A precipitation increase to 600 mm does not change the CDF-depth pattern much, although the weathering front lowers. For P=800mm the weathering and CDF values in depth increase markedly. However, for P > 800 mm, the CDF values are again lower and are all characterized by a uniform depth distribution (Fig. 3.8).

These simulated depth patterns are comparable to those measured in the eastern part of the Betic Cordillera located in Southeast Spain by Schoonejans et al. (2016).

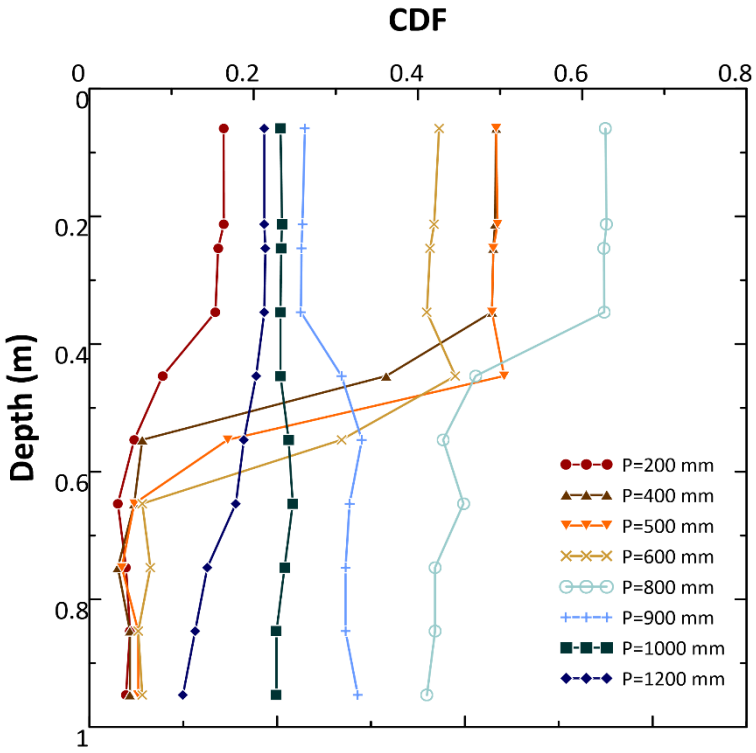

Figure 3.8. Weathering intensity (expressed by the chemical depletion fraction, CDF) of a soil profile under different annual rainfall (P). Profiles are simulated in the SC10 location, at the hilltop.

Figure 9 then shows the total CDF, averaged over the entire soil depth, i.e., 1 m of the soil profile. The results from this study, represented by the blue dots, showed an increased weathering up to 800 mm, but after this critical value, the profiles were less weathered. Moreover, in Fig. 3.9 CDFs of this study are compared to a global data compilation of granitic soil-mantled hillslopes (Schaller & Ehlers, 2021). Also, this global dataset seems to indicate that high weathering rates measured as CDF are not obtained with the highest precipitation values, but rather with intermediate precipitation. With precipitations less than 800 mm, a substantial part of the year will have a precipitation deficit. This means that leaching is of less importance and concentrations of cations released by weathering in the soil solution will be high. One theory often applied to quantify weathering is the transition state theory (TST). In the quantification of weathering fluxes by TST, the dissolution rate of

a mineral is the product of the rate parameter (which is often a function of pH) and the degree of saturation of the soil solution with respect to the dissolving mineral. Drier climates often result in a higher pH and a higher degree of saturation, which both (and certainly in combination) lead to lower weathering rates for most minerals. The decreasing weathering rates imply decreasing CDF values with lower precipitation. On the other hand, an explanation for the right part of the curve, where CDF values decrease with increasing precipitation is less straightforward. Possibly, with increasing precipitation surplus, travel times of water may be shorter and then contact time with the minerals is shorter, which slows down the dissolution rate. Additionally, vegetation will be lusher, and then the nutrient pump may prevent leaching of some elements. Both will decrease the CDF.Therefore, we observed two behaviours in this study, one with precipitation up to 800 and the other with precipitation above 800 mm.There are two aspects: an inverse dependence between weathering rate and residence time is reflected on the left side of the curve which agrees with the results obtained from data assembled from different previous publications by Maher (2010). On the other hand, the CDF values increase to a particular threshold and start to decrease as the residence time decreases, which is reflected on the right part of the curve. This denotes that the chemical weathering rate increases with longer residence time (Ameli et al., 2016).

This threshold or maximum weathering correspondent to intermediate precipitation is coincident with the maximum generalization of Albrecht's curve, which is shown in Fig. 3.9 by the grey shaded area. Huston (2012) pointed out the link between climate and soil formation and properties that scientists such as William Albrecht generalized 80 years ago. Albrecht's curve (e.g. Albrecht, 1957) is a rule that illustrated the effect of precipitation on soil-forming processes and soil properties (Huston, 2012). In this diagram, which presents a maximum in the center, the effect of a precipitation gradient on the rates of physical, chemical, and biological processes that affect pedogenesis and important soil properties

are shown. Different later works that have studied soil properties and weathering along a marked precipitation gradient (e.g. Chadwick et al., 2003) confirmed Albrecht's curve. Similarly, Dixon et al. (2016) in their study for chemical weathering in postglacial soils of New Zealand found an important pedogenic threshold coincident at mean annual precipitation of ~800 mm·yr·1, very similar to the threshold value that was identified in this sensitivity analysis. Oeser & von Blanckenburg (2020) on the other hand, in their study in the EarthShape Critical Zone located along the Chilean Coastal Cordillera, found no correlation between the degree of weathering and mean annual precipitation. Therefore, they pointed out that a competitive effect seems to offset the expected increase in the rate of weathering with precipitation. Huston (2012) even related this concept of the Albrecht curve to ecosystem trends. He analyzed global variations in soil properties, Net Primary Productivity and biodiversity as a function of precipitation. He found similar, unimodal curves with maximum values for soil properties such as total exchangeable bases and found that the maximum corresponded to the point where precipitation is equal to the evapotranspiration rate. Given the importance of soil properties and chemical weathering of soil profiles for ecosystem response, these results can be far-fetching consequences and should be explored further with more simulations and profile data.

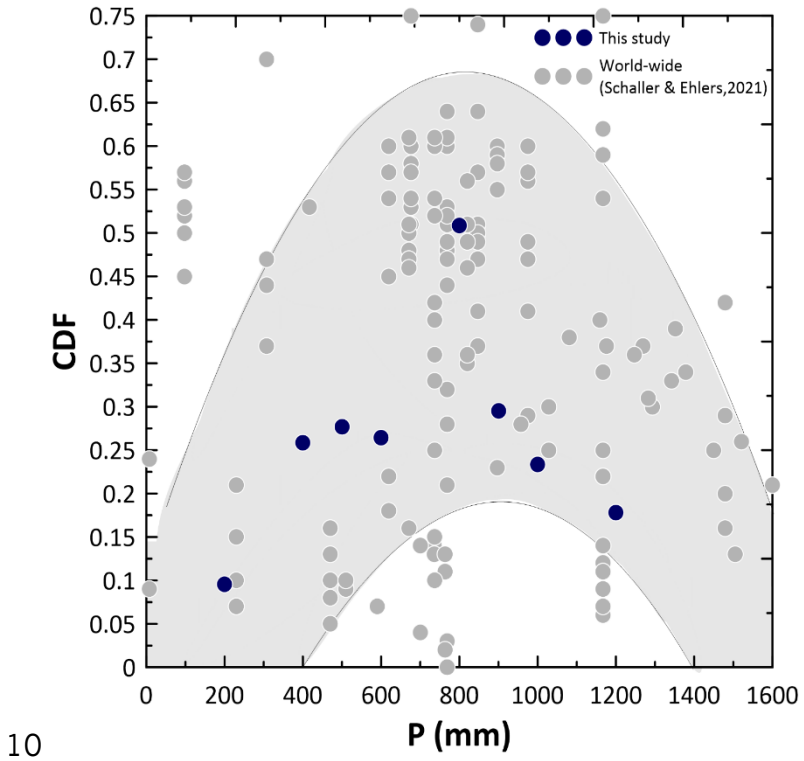

Figure 3.9.Chemical weathering (CDF) versus annual precipitation. The expected trend is indicated by the shaded area and follows a parabolic pattern with maximum chemical weathering for intermediate precipitation. Observations from this study are depth-averaged (blue dots). Observations from other study sites situated in granitic soil-mantled hillslopes (grey dots) are from a review by Schaller & Ehlers (2021).

3.4. Conclusions

The effect of topographic position and hydrology on chemical weathering was analyzed in soils formed on granites under a Mediterranean climate. Chemical depletion fraction was measured and modelled in seven locations, selected along a north-south oriented catena in southern Spain. The model SoilGen was used to simulate pedogenesis and the measured chemical weathering status over a 20,000-year period.

Despite the complexity of the catena and the hydrological conditions, a good correspondence was obtained between modelled and measured CDF. The variability of CDF values was explained better by hydrological variables than by topography. No clear relation to the catena position was found. No relation with slope gradient was observed. However, the CDF data did indicate a positive relation to the hydrological variables of soil moisture

and infiltration, and a negative relation to water residence time. In addition, differences between measured and simulated CDF values could be attributed to lateral water fluxes that are not considered in the model.

The model sensitivity was evaluated with different precipitation regimes. The results showed a marked depth gradient for rainfall under 800 mm for the CDF, but it showed a uniform depth distribution for precipitation above 800 mm. For the profile average chemical weathering, maximum values were observed for intermediate precipitation values, around 800 mm.

3.5. References

Albrecht, W. A. (1957). Soil Fertility and Biotic Geography. *Geographical Review*, *47*(1), 86. https://doi.org/10.2307/212191

Ameli, A. A., Beven, K., Erlandsson, M., Creed, I. F., McDonnell, J. J., & Bishop, K. (2016). Primary weathering rates, water transit times, and concentration-discharge relations: A theoretical analysis for the critical zone. *Water Resources Research*, 942–960. https://doi.org/10.1002/2016WR019448.

Borden, R. W., Baillie, I. C., & Hallett, S. H. (2020). The East African contribution to the formalisation of the soil catena concept. *Catena*, *185*(November 2019). https://doi.org/10.1016/j.catena.2019.104291

Brancher, M., Hieden, A., Baumann-Stanzer, K., Schauberger, G., & Piringer, M. (2020). Performance evaluation of approaches to predict sub-hourly peak odour concentrations. *Atmospheric Environment: X*, *7*(April), 100076. https://doi.org/10.1016/j.aeaoa.2020.100076

Brantley, S. L., Eissenstat, D. M., Marshall, J. A., Godsey, S. E., Balogh-Brunstad, Z., Karwan, D. L., Papuga, S. A., Roering, J., Dawson, T. E., Evaristo, J., Chadwick, O.,

McDonnell, J. J., & Weathers, K. C. (2017). Reviews and syntheses: On the roles trees play in building and plumbing the critical zone. *Biogeosciences*, *14*(22), 5115–5142. https://doi.org/10.5194/bg-14-5115-2017

Braun, J., Mercier, J., Guillocheau, F., & Robin, C. (2016). A simple model for regolith formation by chemical weathering. *Journal of Geophysical Research: Earth Surface*, 2140–2171. https://doi.org/10.1002/2016JF003914.Received

Calabrese, S., & Porporato, A. (2020). Wetness controls on global chemical weathering. *Environmental Research Communications*, *2*(8), 085005. https://doi.org/10.1088/2515-7620/abad7b

Carpintero, E., Andreu, A., Gómez-Giráldez, P. J., Blázquez, Á., & González-Dugo, M. P. (2020). Remote-Sensing-Based Water Balance for Monitoring of Evapotranspiration and Water Stress of a Mediterranean Oak – Grass Savanna. *Water*.

Carracedo, M., Paquette, J. L., Alonso Olazabal, A., Santos Zalduegui, J. F., de García de Madinabeitia, S., Tiepolo, M., & Gil Ibarguchi, J. I. (2009). U-Pb dating of granodiorite and granite units of the Los Pedroches batholith. Implications for geodynamic models of the southern Central Iberian Zone (Iberian Massif). *International Journal of Earth Sciences*, *98*(7), 1609–1624. https://doi.org/10.1007/s00531-008-0317-0

Chadwick, O. A., Gavenda, R. T., Kelly, E. F., Ziegler, K., Olson, C. G., Crawford Elliott, W., & Hendricks, D. M. (2003). The impact of climate on the biogeochemical functioning of volcanic soils. *Chemical Geology*, *202*(3–4), 195–223. https://doi.org/10.1016/j.chemgeo.2002.09.001

Chadwick, O. A., Roering, J. J., Heimsath, A. M., Levick, S. R., Asner, G. P., & Khomo, L. (2013). Shaping post-orogenic landscapes by climate and chemical weathering. *Geology*, *41*(11), 1171–1174. https://doi.org/10.1130/G34721.1

Cipolla, G., Calabrese, S., Valerio, L., & Porporato, A. (2021). Modeling rock-dissolution reactions coupled to plant , soil moisture , and carbon dynamics. *Advances in Water Resources*, *December 2020*, 103934. https://doi.org/10.1016/j.advwatres.2021.103934

Cohen, S., Willgoose, G., & Hancock, G. (2010). The mARM3D spatially distributed soil evolution model: Three-dimensional model framework and analysis of hillslope and landform responses. *Journal of Geophysical Research: Earth Surface*, *115*(4), 1–16. https://doi.org/10.1029/2009JF001536

Dahlgren, R. A., Boettinger, J. L., Huntington, G. L., & Amundson, R. G. (1997). Soil development along an elevational transect in the western Sierra Nevada, California. *Geoderma*, *78*(3–4), 207–236. https://doi.org/10.1016/S0016-7061(97)00034-7

Davis, B. A. S., Brewer, S., Stevenson, A. C., Guiot, J., Allen, J., Almqvist-Jacobson, H., Ammann, B., Andreev, A. A., Argant, J., Atanassova, J., Balwierz, Z., Barnosky, C. D., Bartley, D. D., De Beaulieu, J. L., Beckett, S. C., Behre, K. E., Bennett, K. D., Berglund, B. E. B., Beug, H. J., ... Zernitskaya, V. P. (2003). The temperature of Europe during the Holocene reconstructed from pollen data. *Quaternary Science Reviews*, *22*(15–17), 1701–1716. https://doi.org/10.1016/S0277-3791(03)00173-2

DeVries, W., & Posch, M. (2003). Derivation of cation exchange constants for sand loess, clay and peat soils on the basis of field measurements in the Netherlands. In *Alterra-rapport* (Vol. 701). Alterra Green World research.

Dixon, J. ., Heimsath, A. M., & Amundson, R. (2009). The critical role of climate and saprolite weathering in landscape evolution. *Earth Surface Processes and Landforms*, *34*, 1507–1521. https://doi.org/10.1002/esp.1836

Dixon, J. L., Chadwick, O. A., & Vitousek, P. M. (2016). Climate-driven thresholds for chemical weathering in postglacial soils of New Zealand. *Journal of Geophysical*

Research: Earth Surface, 1619–1634. https://doi.org/10.1002/2016JF003864

Duarte, I. M. R., Gomes, C. S. F., & Pinho, A. B. (2018). Chemical Weathering. In P. T. Bobrowsky & B. Marker (Eds.), *Encyclopedia of Engineering Geology.Encyclopedia of Earth Sciences Series.* Springer,Cham. https://doi.org/https://doi.org/10.1007/978-3-319-73568-9_49

Ferrier, K. L., & Perron, J. T. (2020). The importance of hillslope scale in responses of chemical erosion rate to changes in tectonics and climate. *American Geophysical Union*. https://doi.org/10.1029/2020JF005562

Finke, P A, Vanwalleghem, T., Opolot, E., Poesen, J., & Deckers, J. (2013). Estimating the effect of tree uprooting on variation of soil horizon depth by confronting pedogenetic simulations to measurements in a Belgian loess area. *Journal of Geophysical Research: Earth Surface*, *118*, 2124–2139. https://doi.org/10.1002/jgrf.20153

Finke, Peter A. (2012). Modeling the genesis of luvisols as a function of topographic position in loess parent material. *Quaternary International*, *265*, 3–17. https://doi.org/10.1016/j.quaint.2011.10.016

Finke, Peter A, & Hutson, J. L. (2008). Modelling soil genesis in calcareous loess. *Geoderma*, *145*, 462–479. https://doi.org/10.1016/j.geoderma.2008.01.017

Gabet, E. J., & Mudd, S. M. (2009). A theoretical model coupling chemical weathering rates with denudation rates. *Geology*, *37*(2), 151–154. https://doi.org/10.1130/G25270A.1

García-Gamero, V., Peña, A., Laguna, A. M., Giráldez, J. V., & Vanwalleghem, T. (2021). Factors controlling the asymmetry of soil moisture and vegetation dynamics in a hilly mediterranean catchment. *Journal of Hydrology*, *598*(October 2020), 126207. https://doi.org/10.1016/j.jhydrol.2021.126207

Gobat, J.-M., Aragno, M., & Matthey, W. (1998). *Le Sol Vivant*. Les Presses polytechniques et

universitaires romandes.

Hargreaves, G. H., & Samani, Z. A. (1985). Reference Crop Evapotranspiration from Temperature. *Paper - American Society of Agricultural Engineers*, 96–99.

Huston, M. A. (2012). Precipitation, soils, NPP, and biodiversity: Resurrection of Albrecht's curve. *Ecological Monographs*, *82*(3), 277–296. https://doi.org/10.1890/11-1927.1

Jenny, H. (1941). *Factors of soil formation: A System of Quantitative Pedology*. McGraw-Hill Book Company Inc.

Kumar, A., Luo, J., & Bennett, G. F. (1993). Statistical evaluation of Lower Flammability Distance (LFD) using four hazardous release models. *Process Safety Progress*, *12*(1), 1–11. https://doi.org/10.1002/prs.680120103

Lachassagne, P., & Wyns, R. (2011). Review article The fracture permeability of Hard Rock Aquifers is due neither to tectonics , nor to unloading , but to weathering processes. *Terra Nova*, 145–161. https://doi.org/10.1111/j.1365-3121.2011.00998.x

Langston, A. L., Tucker, G. E., Anderson, R. S., & Anderson, S. P. (2011). Exploring links between vadose zone hydrology and chemical weathering in the Boulder Creek critical zone observatory. *Applied Geochemistry*. https://doi.org/10.1016/j.apgeochem.2011.03.033

Larsen, I. J., Almond, P. C., Eger, A., Stone, J. O., Montgomery, D. R., & Malcolm, B. (2014). Reports 11. *Science*, *343*(February), 637–641.

Lebedeva, M. I., & Brantley, S. L. (2020). Lebedeva Marina (Orcid ID: 0000-0003-4987-4182) Relating the depth of the water table to depth of weathering. *Earth Surface Processes and Landforms*, 0–3. https://doi.org/10.1002/esp.4873

Maher, K. (2010). The dependence of chemical weathering rates on fl uid residence time. *Earth and Planetary Science Letters*, *294*(1–2), 101–110.

https://doi.org/10.1016/j.epsl.2010.03.010

Maher, K. (2011). The role of fluid residence time and topographic scales in determining chemical fluxes from landscapes. *Earth and Planetary Science Letters*, *312*(1–2), 48–58. https://doi.org/10.1016/j.epsl.2011.09.040

Maher, K., & Chamberlain, C. P. (2014). Hydrologic Regulation of Chemical. *Science*, *1502*. https://doi.org/10.1126/science.1250770

Milne, G. (1935). Some suggested units of classification and mapping particularly for East African soils. *Soil Research - Bodenkundliche Forschung, Supplement to the Proceedings of the International Union of Soil Science IV*, 183–198.

Minasny, B., & McBratney, A. B. (2001). A rudimentary mechanistic model for soil formation and landscape development II. A two-dimensional model incorporating chemical weathering. *Geoderma*, *103*(1–2), 161–179. https://doi.org/10.1016/S0016-7061(01)00075-1

Molina, A., Vanacker, V., Corre, M. D., & Veldkamp, E. (2019). Patterns in Soil Chemical Weathering Related to Topographic Gradients and Vegetation Structure in a High Andean Tropical Ecosystem Journal of Geophysical Research : Earth Surface. *JGR Earth Surface*.

Mudd, S. M., & Furbish, D. J. (2006). Using chemical tracers in hillslope soils to estimate the importance of chemical denudation under conditions of downslope sediment transport. *Journal of Geophysical Research: Earth Surface*, *111*(2). https://doi.org/10.1029/2005JF000343

Oeser, R. A., Stroncik, N., Moskwa, L. M., Bernhard, N., Schaller, M., Canessa, R., van den Brink, L., Köster, M., Brucker, E., Stock, S., Fuentes, J. P., Godoy, R., Matus, F. J., Oses Pedraza, R., Osses McIntyre, P., Paulino, L., Seguel, O., Bader, M. Y., Boy, J., ...

von Blanckenburg, F. (2018). Chemistry and microbiology of the Critical Zone along a steep climate and vegetation gradient in the Chilean Coastal Cordillera. *Catena*, *170*(June), 183–203. https://doi.org/10.1016/j.catena.2018.06.002

Oeser, R. A., & Von Blanckenburg, F. (2020). Do degree and rate of silicate weathering depend on plant productivity? *Biogeosciences*, *17*(19), 4883–4917. https://doi.org/10.5194/bg-17-4883-2020

Olea, L., & San Miguel-Ayanz, A. (2006). The Spanish dehesa, a traditional Mediterranean silvopastoral system. *21st General Meeting of the European Grassland Federation*, *April*, 1–15.

Opolot, E., & Finke, P. A. (2015). Evaluating sensitivity of silicate mineral dissolution rates to physical weathering using a soil evolution model (SoilGen2.25). *Biogeosciences*, *12*(22), 6791–6808. https://doi.org/10.5194/bg-12-6791-2015

Opolot, E., Yu, Y. Y., & Finke, P. A. (2015). Modeling soil genesis at pedon and landscape scales: Achievements and problems. *Quaternary International*, *376*, 34–46. https://doi.org/10.1016/j.quaint.2014.02.017

Peel, M. C., Finlayson, B. L., & McMahon, T. A. (2007). Updated world map of the Köppen-Geiger climate classification. *Hydrology and Earth System Sciences*, *11*, 1633–1644.

Peeters, I., Rommens, T., Verstraeten, G., Govers, G., Van Rompaey, A., Poesen, J., & Van Oost, K. (2006). Reconstructing ancient topography through erosion modelling. *Geomorphology*, *78*(3–4), 250–264. https://doi.org/10.1016/j.geomorph.2006.01.033

Porada, P., Lenton, T. M., Pohl, A., Weber, B., Mander, L., Donnadieu, Y., Beer, C., Po, U., & Kleidon, A. (2016). High potential for weathering and climate effects of non-vascular vegetation in the Late Ordovician ¨. *Nature Communications*, 1–13. https://doi.org/10.1038/ncomms12113

Reuter, R. J., & Bell, J. C. (2001). Soils and Hydrology of a Wet-Sandy Catena in East-Central Minnesota. *Soil Science Society of America Journal*, *65*(5), 1559–1569. https://doi.org/10.2136/sssaj2001.6551559x

Riebe, C. S., Kirchner, J. W., & Finkel, R. C. (2004). Erosional and climatic effects on long-term chemical weathering rates in granitic landscapes spanning diverse climate regimes. *Earth and Planetary Science Letters*, *224*, 547–562. https://doi.org/10.1016/j.epsl.2004.05.019

Riebe, C. S., Kirchner, J. W., Granger, D. E., & Finkel, R. C. (2001). Strong tectonic and weak climatic control of long-term chemical weathering rates. *Geological Society of America*, *29*(6), 511–514.

Román-Sánchez, A., Vanwalleghem, T., Peña, A., Laguna, A., & Giráldez, J. V. (2018). Controls on soil carbon storage from topography and vegetation in a rocky, semi-arid landscapes. *Geoderma*, *311*, 159–166. https://doi.org/10.1016/j.geoderma.2016.10.013

Román-Sánchez, Andrea, Reimann, T., Wallinga, J., & Vanwalleghem, T. (2019). Bioturbation and erosion rates along the soil-hillslope conveyor belt, part 1: Insights from single-grain feldspar luminescence. *Earth Surface Processes and Landforms*, *44*(10), 2051–2065. https://doi.org/10.1002/esp.4628

Salve, R., Rempe, D. M., & Dietrich, W. E. (2012). Rain, rock moisture dynamics, and the rapid response of perched groundwater in weathered, fractured argillite underlying a steep hillslope. *Water Resources Research*, *48*(11), 1–25. https://doi.org/10.1029/2012WR012583

Samouëlian, A., & Cornu, S. (2008). Modelling the formation and evolution of soils, towards an initial synthesis. *Geoderma*, *145*(3–4), 401–409. https://doi.org/10.1016/j.geoderma.2008.01.016

Schaller, M., & Ehlers, T. A. (2021). Vegetation and climate effects on soil production , chemical weathering , and physical erosion rates. *Earth Surface Dynamics*, *April*, 1–26.

Schoonejans, J., Vanacker, V., Opfergelt, S., Ameijeiras-Mariño, Y., & Christl, M. (2016). Kinetically limited weathering at low denudation rates in semiarid climatic conditions. *Journal of Geophysical Research: Earth Surface*, 336–350. https://doi.org/10.1002/2015JF003626

Temme, A. J. A. M., & Vanwalleghem, T. (2016). LORICA - A new model for linking landscape and soil profile evolution: Development and sensitivity analysis. *Computers and Geosciences*, *90*, 131–143. https://doi.org/10.1016/j.cageo.2015.08.004

Vanwalleghem, T., Stockmann, U., Minasny, B., & McBratney, A. B. (2013). A quantitative model for integrating landscape evolution and soil formation. *Journal of Geophysical Research: Earth Surface*, *118*(2), 331–347. https://doi.org/10.1029/2011JF002296

Welivitiya, W. D. D. P., Willgoose, G. R., & Hancock, G. R. (2019). A coupled soilscape-landform evolution model: Model formulation and initial results. *Earth Surface Dynamics*, *7*(2), 591–607. https://doi.org/10.5194/esurf-7-591-2019

Yoo, K., Amundson, R., Heimsath, A. M., Dietrich, W. E., & Brimhall, G. H. (2007). Integration of geochemical mass balance with sediment transport to calculate rates of soil chemical weathering and transport on hillslopes. *Journal of Geophysical Research*, *112*. https://doi.org/10.1029/2005JF000402

Yoo, K., Mudd, S. M., Sanderman, J., Amundson, R., & Blum, A. (2009). Spatial patterns and controls of soil chemical weathering rates along a transient hillslope. *Earth and Planetary Science Letters*, *288*(1–2), 184–193. https://doi.org/10.1016/j.epsl.2009.09.021

Yoo, K., Weinman, B., Mudd, S. M., Hurst, M., Attal, M., & Maher, K. (2011). Evolution of

hillslope soils: The geomorphic theater and the geochemical play. *Applied Geochemistry*, *26*(SUPPL.), 149–153. https://doi.org/10.1016/j.apgeochem.2011.03.054

Chapter 4

Temporal Stability analysis of soil moisture content in a hilly Mediterranean catchment

TEMPORAL STABILITY ANALYSIS OF SOIL MOISTURE CONTENT IN A HILLY MEDITERRANEAN CATCHMENT

ABSTRACT

Understanding the drivers of soil moisture variability and temporal stability (TS) in different climates and environments is relevant for improving our knowledge about the hydrological functioning and its relationship with soil formation in natural and semi-natural Mediterranean environments. This study analyses soil moisture measured across two opposing slopes in a *dehesa* (oak-woodland savannah) farm in Sierra Morena near Cardeña (Córdoba). Temporal stability analysis of soil moisture showed that the sites located on the north-facing slope (NFS) exhibited greater temporal stability at the different depths (0.05, 0.15, 0.25, 0.35 y 0.45 m) at which soil moisture was monitored than on the south-facing slope (SFS) and in the valley bottom. Indeed, locations SC6 and SC7 in the valley bottom on the SFS and NFS, respectively, exhibited the highest SDRD values. Principal Component Analysis (PCA) was used to reduce the dimensions of the data set, with the first two PCs explaining 97.5 % of the total variance. PC_1 explained 92.5 % of the variance and could be related to climatic conditions, while PC_2 explained 5.1 % of the variance and could be linked to topography and its influence on the hydrology of both slopes. When the PCA is performed by depth PC_1 remained the dominant pattern, although PC2 became more important in deeper soil layers. The results of this study are relevant for understanding the soil hydrology of the shallow sloping soils that characterize *dehesa* farms in Mediterranean environments.

4.1. Introduction

Soil moisture, the main indicator of the soil water storage state in the water cycle, is a key variable for the exchange of mass and energy between the soil surface and the

atmosphere (e.g.Henderson-Sellers, 1996). The large temporal and spatial variability of soil moisture has been widely studied under a wide range of environmental conditions to improve climate and hydrological modelling, optimize sensor networks or validate remote sensing measurements (Brocca et al., 2010; Robinson et al., 2008). Vachaud et al. (1985) introduced the concept of temporal stability (TS) of soil moisture to appreciate its persistence at different locations within a field. The TS of the soil moisture has been used at different spatial and temporal scales, exploring the role of different soil, landscape, climate and vegetation characteristics on its evolution. Martínez-Fernández and Ceballos (2003) evaluated the TS of soil moisture over an area of 1,285 km^2 in the northwest of the Iberian Peninsula using three years of data finding that dry soil was more stable than wet soil. Similarly, Brocca et al. (2009) detected a good persistence of the TS of soil moisture on three characteristic sites of an inland region of central Italy grouped by the slopes greater than 0.07-0.08, upslope drainage areas, other slope values, and elevation. In that work, the stability of soil moisture in flat areas was smaller than that of the other groups. In the colder, semi-arid steppe of Inner Mongolia, China, with chernozem soils rich in organic carbon, Zhao et al. (2010) found that the soil moisture was more stable under wet than under dry conditions, and the stability was dependent on the grazing intensity. Among other differences, the soil organic carbon content in Zhao et al. (2010) was greater than in Martínez-Fernandez and Ceballos (2003), except nearby the riverbeds.

Vanderlinden et al. (2012) in a complete and detailed review warned about the risk of considering only the isolated influence of factors such as measurement design, topography, soil, vegetation, and climate on the TS of soil moisture because interactions occur among them. A similar conclusion was reached by Fry and Guber (2020) in their study at an agricultural field in Mason, South Central Michigan (USA). Nevertheless, Fry

and Guber (2020) indicated that topography and hydrology had a dominant influence over the other factors.

To disentangle the influence of the main factors in the spatiotemporal variability of soil moisture the Empirical Orthogonal Function (EOF) or, the equivalent, Principal Component Analysis (PCA) can be performed (e.g. Martini et al., 2017).

PCA allows identifying patterns in the soil moisture dataset and their relationship to landscape features (Jawson and Niemann, 2007). The method became popular in other scientific fields such as meteorology (Kim, 1996) and has been applied in Hydrology from the field-scale (Yoo & Kim, 2004) to 10,000 km^2 encompassing the sub-humid part of Oklahoma State (USA) (Kim & Barros, 2002), to reduce the dimensionality of soil moisture datasets.

This work focuses on a granitic rock area in the south of the Iberian Peninsula, where the influence of aspect on soil moisture has been studied in two opposing hillslopes (García-Gamero et al., 2021). The observed differences in the structure of the critical zone across the study area require further study considering a larger number of monitoring locations, that allow an analysis of the TS of soil moisture across both hillslopes. The specific objectives of this work were: (i) to study the temporal pattern at each of the monitoring locations and the whole dataset, (ii) to analyze how these patterns differ as a function of depth, (iii) to investigate the change in TS of soil moisture under different soil moisture conditions, and (iv) to identify patterns in the measured soil moisture dataset and the factors that control their spatiotemporal variability using PCA.

4.2. Material and methods

4.2.1. Study area

The study was performed in a Mediterranean Catchment in Cardeña (Córdoba), southern Spain (38.2º N; 4.17º W). Two opposing hillslopes shown in Figure 4.1 were selected for the installation of a soil moisture sensor network. The land use at the site was oak-woodland savannah or '*dehesa*', a semi-natural system composed of oaks (*Quercus* spp.) and annual grasses such as *Lolium* sp., *Bromus* sp., and *Trifolium* sp., (Olea and San Miguel-Ayanz, 2006). The entire catchment is underlain by granite and granodiorite units (Carracedo et al., 2009). Soil texture ranged from sandy to sandy loam (Román-Sánchez et al., 2018). The average soil properties of the studied locations are shown in Table 4.1. Based on observations recorded in soil profile pits and during instruments installation, depth to bedrock ranged from 0.6 m on the south-facing slope (SFS) to 9.5 m on the north-facing slope (NFS). Elevation of the rolling terrain ranged from 650 to 725 m.a.s. l. Four basic landforms were identified (Fig. 4.1): (i) Hilltop, (ii) SFS with a wooded grassland, (iii) NFS a closed canopy of evergreen oaks, and (iv) Valley bottom where the Martin-Gonzalo creek flows, an affluent of the Guadalquivir River.

The regional climate is classified as continental Mediterranean (BSk) in the Köppen-Geiger diagram (Peel et al., 2007), with a mean annual rainfall of 878 mm (from 1981 to 2010), cold winters, and dry, long summers. The mean annual air temperature is 15.3 °C, with the coldest month being January, with a mean monthly temperature of 7 °C, and the hottest July, with a mean monthly temperature of 25.4 °C (Carpintero et al., 2020).

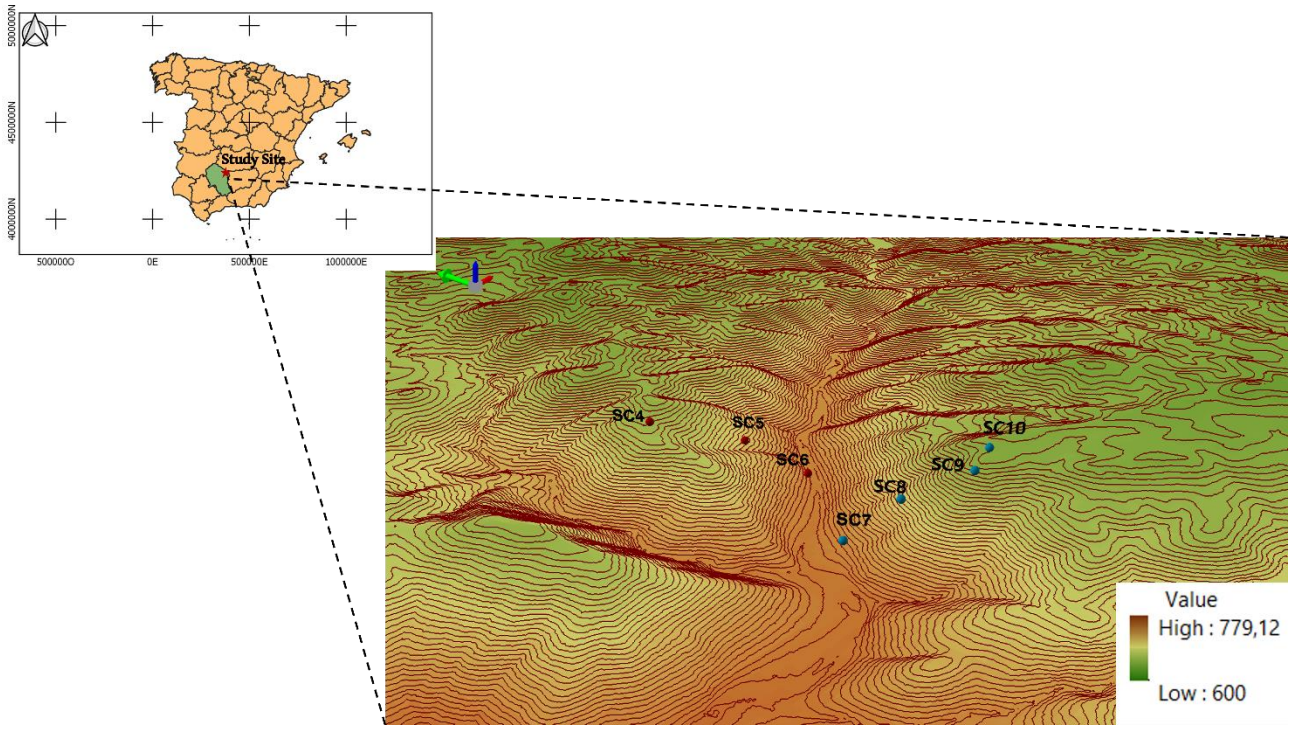

Figure 4.1. Location of the study site in Cardeña (Córdoba) in southern Spain with the monitoring locations situated on two opposing hillslopes (rendered three-dimensionally). The locations on the SFS (SC4-SC6) are in red and those on the NFS (SC10-SC7) are in blue. Contour lines are plotted for a 2 m interval.

Table 4.1. Weighted 0-0.5-m mean of the sand, silt, and clay fractions and organic matter content (OM) at the seven soil moisture monitoring locations.

Location	Sand	Silt	Clay	OM
	Without coarse fraction, %			%
SC4	73.5	20.1	6.4	1.16
SC5	83.1	12.0	4.9	0.54
SC6	69.5	22.4	8.1	1.21
SC7	76.1	15.6	8.3	1.02
SC8	61.3	29.0	9.7	1.09
SC9	75.2	19.4	5.4	1.16
SC10	81.5	14.3	4.2	1.27

4.2.2. Soil moisture monitoring

Soil moisture measurement and data normalization were performed as described in García-Gamero et al. (2021). Soil moisture, θ, measured at each depth in the 0–0.50 m profile was normalized as an effective saturation ratio (e.g. Brutsaert 2005):

$$s = \frac{\theta - \theta_{mín}}{\theta_{max} - \theta_{mín}} \quad (4.1)$$

Soil moisture was monitored at the seven locations represented in Fig 4.1 (SC4-SC10) at 0.05, 0.15, 0.25, 0.35, and 0.45 m depth, except for SC4 and SC5 where the shallow profile prevented sensor installation at the two deepest and the deepest depths, respectively. To understand the hydrological connectivity and the spatial pattern of soil moisture the sites were split by hillslope; four of them were located on NFS (SC10-SC7) and three on the SFS (SC4-SC6). The monitoring period comprised almost 3 years, from 29 November 2016 to 8 November 2019. Measurements were made each 30 min from November 2016 to early January 2018, and at 10 min intervals from January 2018 to November 2019. In this study, daily averaged data were used.

Soil moisture dynamics was represented by the mean (Eq.4.2) and the standard deviation (Eq.4.3) calculated separately for each depth and location during the complete monitoring period as:

$$\bar{s_i} = \frac{1}{N_j}\sum_{j=1}^{N_j} s_i^j \,, \quad (4.2)$$

where s_i^j is the effective saturation ratio at location *i* at time *j*; $\bar{s_i}$ is the time-averaged effective saturation ratio at location *i*.

$$SD_i = \sqrt{\frac{1}{N_J - 1}\sum_{J=1}^{N_J}\left(s_i^j - \bar{s_i}\right)^2}, \quad (4.3)$$

where SD_i is the standard deviation of the effective saturation ratio at location *i*.

4.2.3. Temporal stability of soil moisture content

To quantify the deviation of soil moisture from soil moisture averaged across the 7 locations for time moments *j*, separately for each depth and location, the relative difference (RD_i) was calculated (Vachaud et al., 1985):

$$RD_i^j = \frac{\left(s_i^j - \overline{s^j}\right)}{\overline{s^j}}, \quad (4.4)$$

where s_i^j is the effective saturation ratio of a given depth at the location *i* at time *j*. $\overline{s^j}$ is the average effective saturation ratio of a given depth for time moment *j* for the 7 monitoring locations. The mean relative difference (MRD_i) was calculated from *RD*:

$$MRD_i = \frac{1}{N_j}\sum_j^{N_j} RD_i, \quad (4.5)$$

where N_j is the number of monitoring days. In this regard, the daily datasets included only those days for which data were available at each depth and the 7 locations, i.e., 7 data per day.

A positive MRD for a monitoring location indicates that the location is wetter than the mean, whereas a negative MRD indicates that the location is drier than the mean.

The estimation of the standard deviation of the RD_i is used to quantify the TS of soil moisture content in these locations. The standard deviation ($SDRD_i$) was computed for each depth and location:

$$SDRD_i = \sqrt{\frac{1}{N_j - 1}\sum_{j=1}^{N_j}\left(RD_i^j - MRD_i\right)^2} \quad (4.6)$$

Small $SDRD_i$ values indicate a greater TS of soil moisture pattern in these locations. All analyses in this study were performed using R-Studio software (RStudioTeam, 2020).

4.2.4. Principal Component Analysis

A correlation analysis using the Spearman rank correlation coefficient, as an alternative technique to the Pearson correlation to address nonnormality (Wilks, 2011) was used to assess the relationship between the soil moisture content at different locations. To discriminate the underlying factors responsible for soil moisture content variability and to analyze the correlation between variables, a PCA was performed. This analysis

transforms an original set of variables into a reduced set of uncorrelated variables that retain most of the information of the original variables, Principal Components (PCs).

The results are evaluated based on the *loadings* of the PCs that indicate the relevance of each variable in each PC and the *scores* of each observation that indicates the distance from the origin to each projection. For more details on PCA, see the work by Perry and Niemann (2007).

The input variables were the daily and profile and depth-averaged soil moisture content data from the whole dataset. Values greater than or equal to 0.5 are considered to belong to the wet period, values less than or equal to 0.25 corresponded to the dry period, and the rest are confined in the intermediate period. The PCA of the normalized data set was implemented with the R-Studio package factoextra (ver. 1.0.7).

4.3. Results and discussion

4.3.1. Soil moisture content dynamics

Soil moisture at the 7 locations showed great temporal variability, typical for a Mediterranean climate (Fig.4.2). Overall, temporal patterns of effective saturation ratio were similar for the 7 locations at each depth but deferred as a result of topographic position, e.g., SC7, located in the valley bottom, at depth of 0.05 m from October 2017 to June 2018.

Overall, the temporal variability in soil moisture decreased with depth. Soil moisture is more stable deepest in the soil profile than near the surface. However, the differences between some locations are accentuated with depth, such as locations SC7 and SC8 from October 2017 to December 2017, where the variability in measured soil moisture increases.

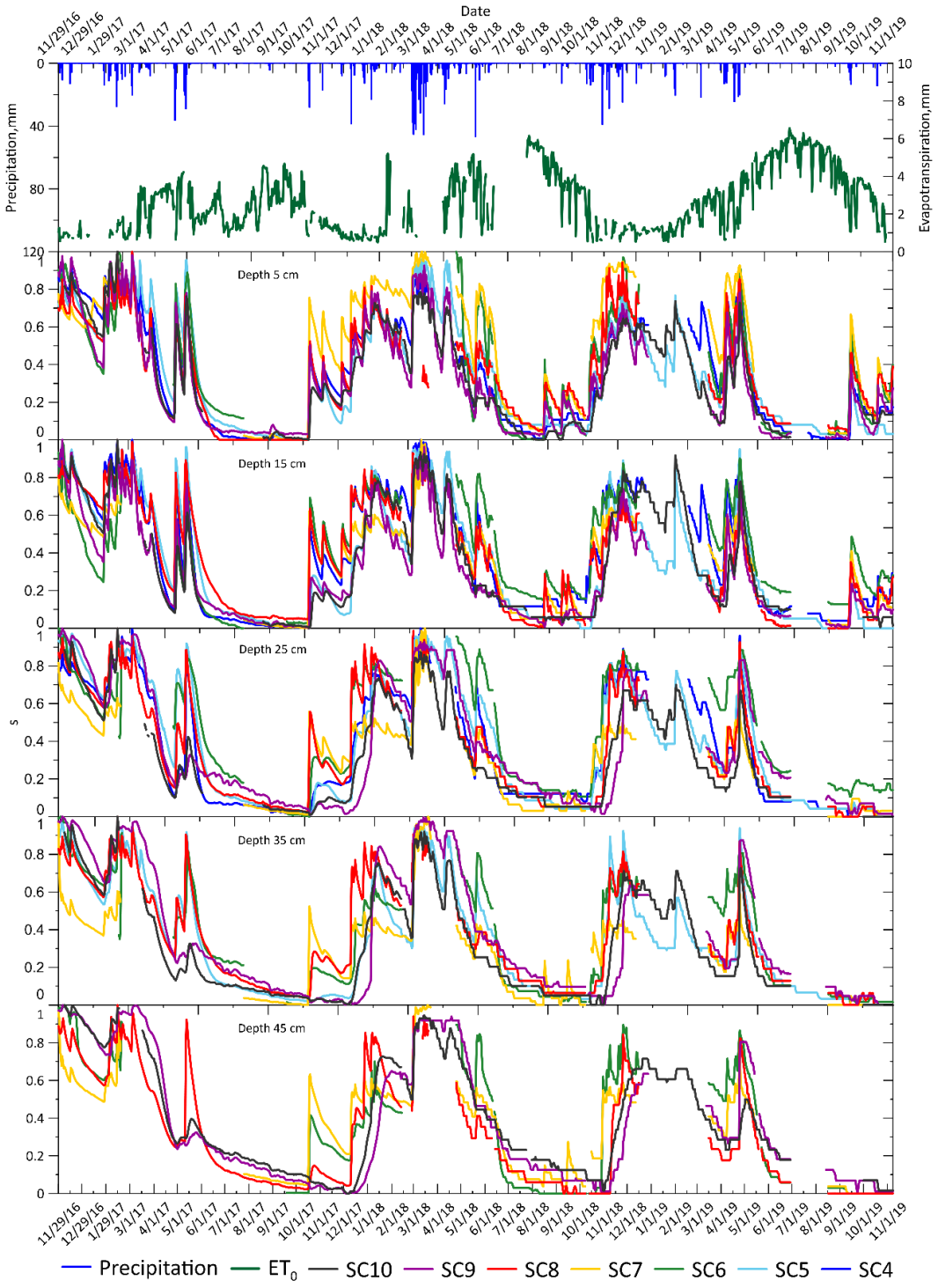

Figure 4.2. Evolution of effective saturation ratio, *s*, for the different locations and depths during the study period. Daily precipitation *P*, and reference evapotranspiration, ET_0, are shown in the top panel.

Figure 4.3 shows depth-averaged and standard deviation (SD) of *s*, at the seven locations:

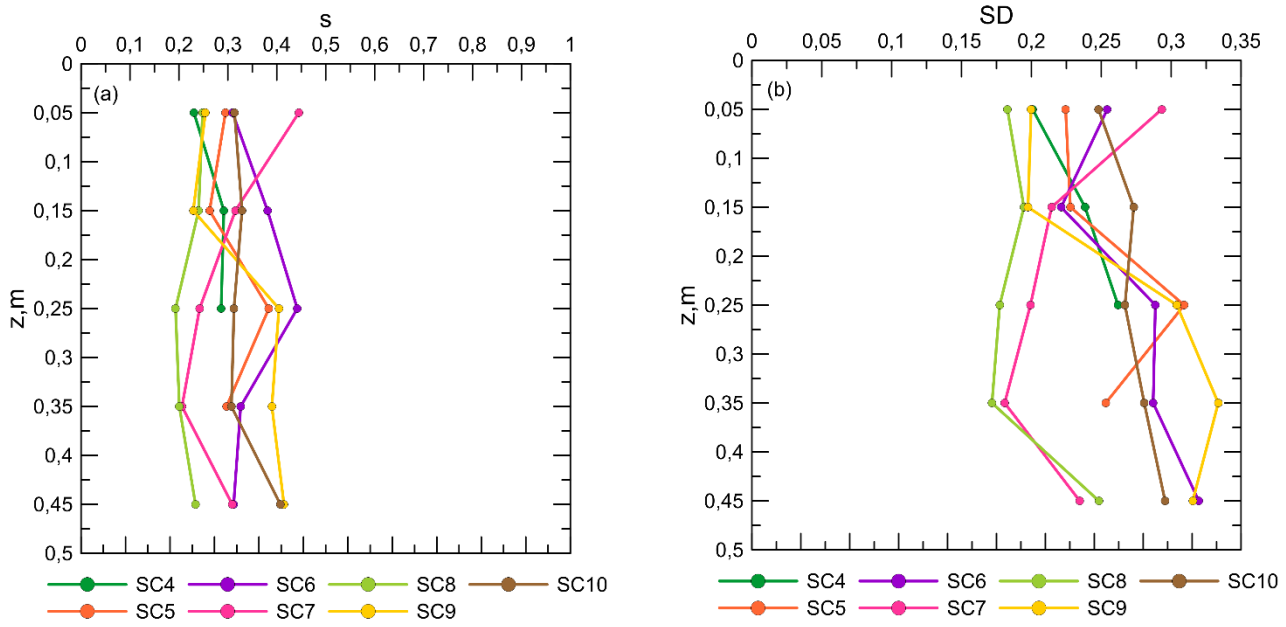

Figure 4.3. Mean effective soil saturation (s) and standard deviation (SD) for different depths at locations SC4-SC10.

The greatest values of the mean and standard deviation of s were observed at 0.05 m depth for SC7, in the bottom of the valley near the Martin Gonzalo Creek on the NFS (Fig.4.3), possibly due to topographical position. Conversely, the smallest values corresponded to SC4, on the hilltop on the SFS.

At 0.15 m and 0.25 m the greatest mean values occurred also at the valley bottom but on the SFS, at location SC6, where the SD was smaller at 0.15 m, as compared to the deeper soil layers below 0.25m. At 0.15 m, locations SC8 and SC9, in the middle and upper slope on the NFS, respectively, had the smallest mean *s*. This could be attributed to the structure of the critical zone on this slope with a highly weathered zone extending down to 9.5 m in the middle of the NFS, where fractures and/or macropores can facilitate unsaturated preferential flow (Nimmo et al., 2012), as opposed to the structure of the critical zone on the SFS where the bedrock is found at 0.6 m depth (García-Gamero et al., 2021).

However, at 0.35 and 0.45 m depth, the largest *s* was observed at the upper NFS at location SC9, which also exhibited the highest SD as a result of the relative hydrological disconnection with respect to the other locations. Conversely, the smallest *s* was found at the mid-slope position SC8, at 0.35 and 0.45 m depth, possibly as a result of vertical and lateral preferential water flow (García-Gamero et al., 2021; Zhang et al., 2018).

These observations suggest a different response to both between locations as a function of topography, and within locations as a function of depth.

4.3.2. Temporal stability of soil moisture

Figure 4.4 shows the MRD and SDRD, represented by error bars, for the whole period at, 0.05 (4.4a), 0.15 (4.4b), 0.25 (4.4c), 0.35 (4.4d) and 0.45 m (4.4e). For each of the 5 depths, the average SDRD (±standard deviation) was 0.33 (±0.07), 0.36 (±0.13), 0.46 (±0.22), 0.59 (±0.24) and 0.61 (±0.14), showing that the variability between locations increased with depth, while the TS decreased with depth at each location.

Sites with relatively large SDRD were associated with the deepest sensors and with wet locations located at the valley bottom, *e.g.* SC6. The above-mentioned characteristics of the critical zone of the NFS would facilitate preferential downward unsaturated flow. In addition, at the lower part of the slope, *e.g.* SC7, runoff may be generated as a result of subsurface flow from both the vadose zone and saturated zone (exfiltration) which would also explain the large moisture variability at this location (García-Gamero et al., 2021). On the SFS, the unweathered, almost impervious bedrock with an irregular surface might divert the vertical water flow towards the bottom of the slope. This observation might indicate the feasibility of subsurface flow on the SFS although in previous comments this was not evident. In later chapter evidence of this flow will be shown. However, although pit SC6 is very close to the Martín Gonzalo Creek its behavior differs from that of the analog pit SC7 what might be due to the absence of a clear

underground connection. In this regard, Lin (2006) found that the soil moisture of most monitoring sites located along the valley floor at the Shale Hills Critical Zone Observatory in Pennsylvania (USA) exhibited greater values than the catchment average. In this study, also location SC6 shows greater soil moisture values, except at 0.05 m where it is location SC7, which shows the highest values, and at 0.45 where it is location SC9. On the contrary, location SC10, at the hilltop of the NFS, shows smaller soil moisture values, except at 0.15 and 0.45 m. At the latter depth, the situation is reversed the location SC10 shows wetter values than the mean.

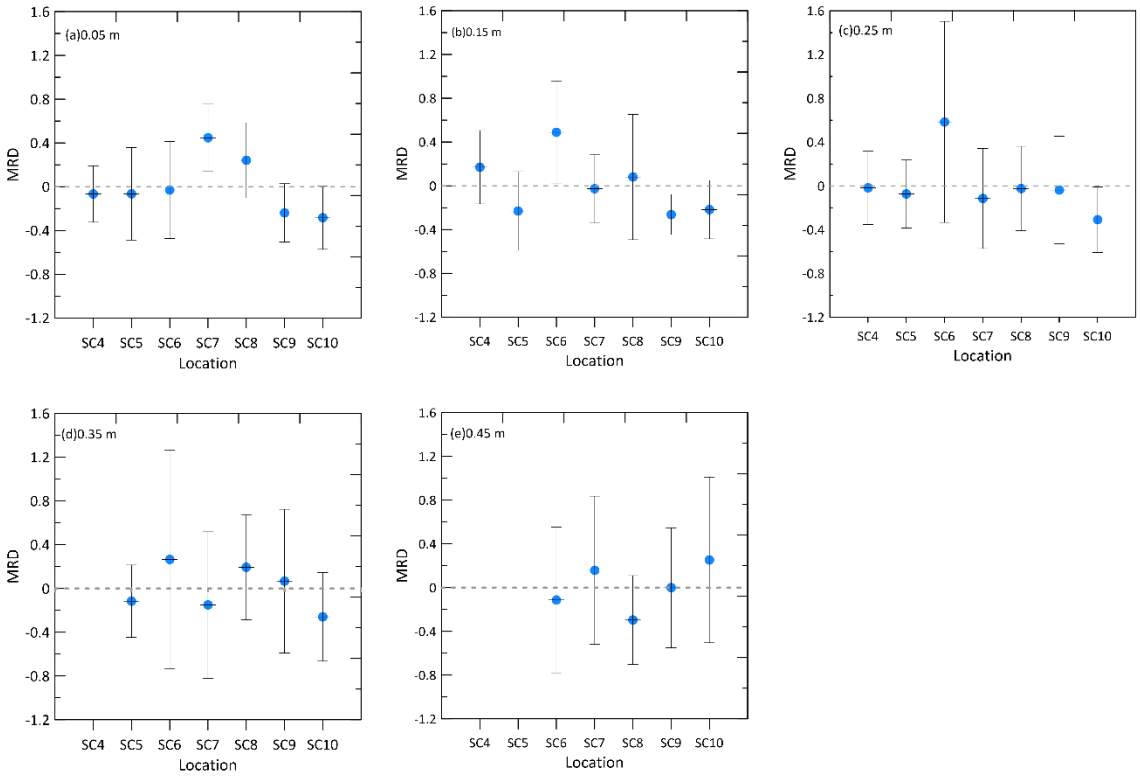

Figure 4.4. Mean relative differences (*MRD*) with their standard deviation (vertical bars) for soil moisture at five depths (0.05, 0.15,0.25, 0.35 y 0.45 m) at locations SC4 to SC10.

Figure 4.5 depicts MRD and SDRD values as a function of depth. The location SC6 stands out as the wettest point for the whole study area, except for the 0.05 and 0.45 m depths. Conversely, SC10 is the driest location with soil moisture below the mean value,

except for 0.15 and 0.45 m, being SC10 wetter than the mean at the latter depth.

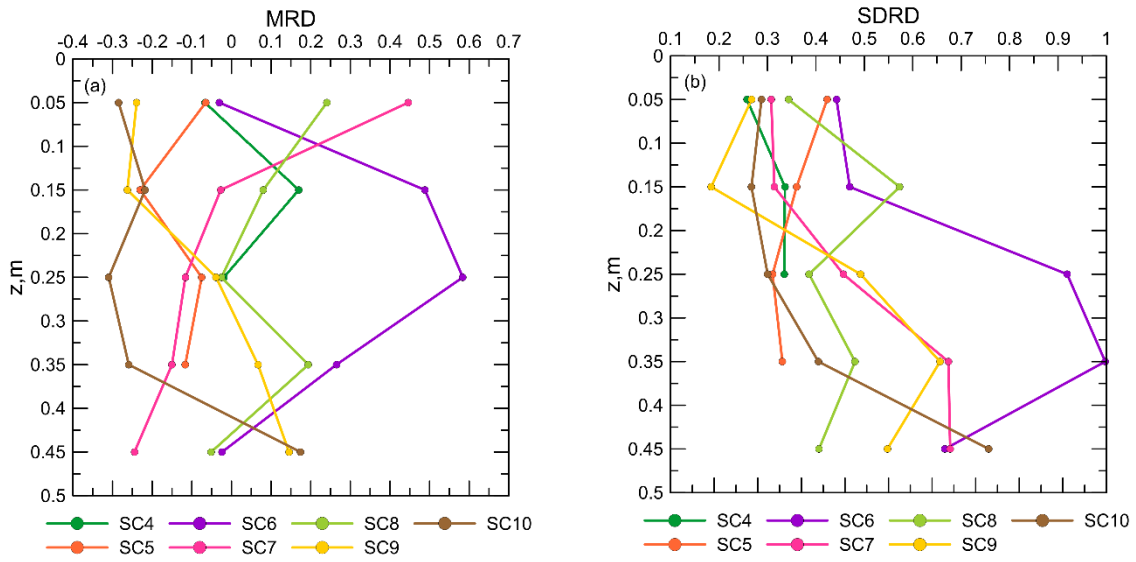

Figure 4.5. Relationships between the mean value of the relative differences (MRD) (a), and their standard deviation (SDRD) (b) with depth for the 7 locations (SC4-SC10).

Considering the MRD values, the most "representative" locations and depths for the catchment and the study period are SC6 at 0.05 m, SC7 at 0.15 m, SC4 at 0.25 m, and SC9 at 0.35 m and 0.45 m. However, the SDRD values identify other "representative" locations that are temporally more stable than the rest. Locations SC6 and SC7 show the highest SDRD values. In general, the more stable points are found on the NFS for the different depths, similar to the findings of Zhao et al. (2010) (Fig. 4.4 and Fig. 4.5): SC4 at 0.05 m; SC9 at 0.15 m; SC10 at 0.25 m; SC5 at 0.35 m and SC8 at 0.45 m. The above-mentioned characteristics of the critical zone of the NFS result in a significantly lower soil water residence time on this slope as compared to the SFS. Martínez-Fernández and Ceballos (2003) pointed out that the profiles with a higher percentage of sand are those that are temporally more stable due to the limited capacity of sandy soils to retain water, and, consequently, the driest soils. Thus, due to the characteristics observed on the NFS, these locations are expected to be temporally more stable.

4.3.2.1. Two different temporal stability conditions

Figure 4.6a through 4.6e shows the results for a selected wet-up period (from 07 December 2016 to 13 February 2017) and Figure 4.7a through 4.7b show the results for a selected dry-down period (from 14 June 2018 to 24 July 2018). The locations fluctuate between positive and negative values of MRD depending on the depth and do not maintain their rank, particularly during the dry period. In general, the MRD shows a stronger TS for most locations at each depth during the wet period than during the dry one (Fig. 4.6 and Fig. 4.7).

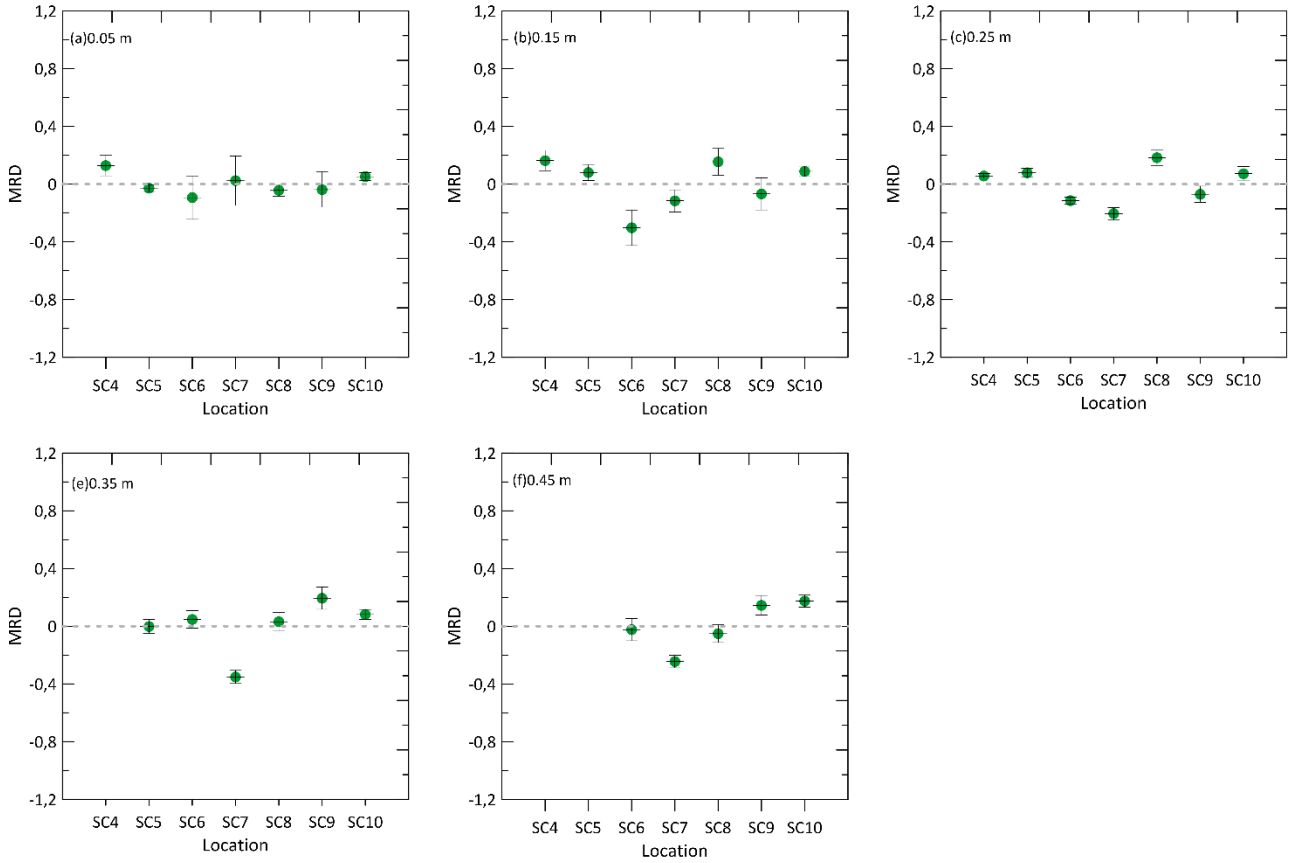

Figure 4.6. Mean relative differences (MRDs) with their standard deviation (vertical bars) for soil moisture in a wet-up period at five depths (0.05, 0.15,0.25, 0.35 y 0.45 m) in seven plots.

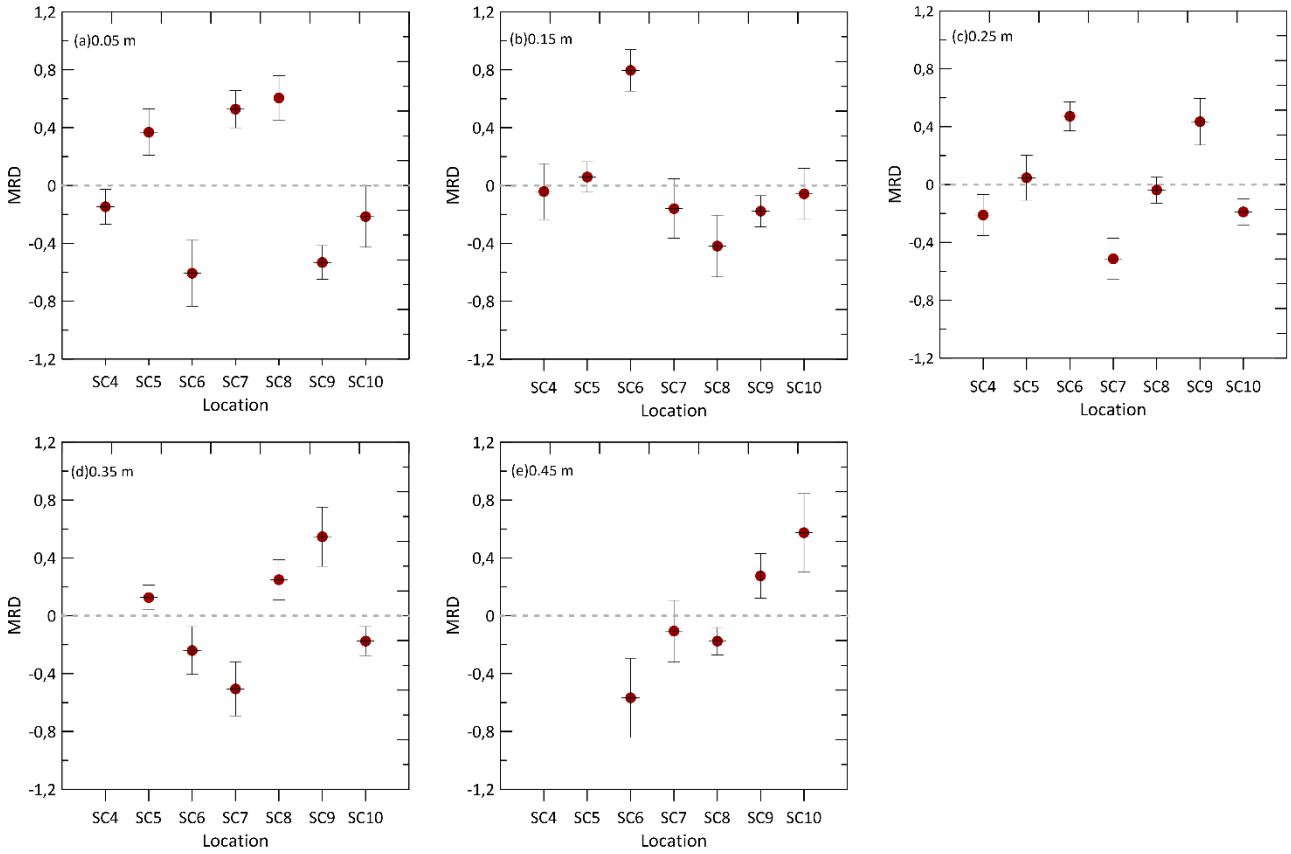

Figure 4.7. Mean relative differences (MRDs) with their standard deviation (vertical bars) for soil moisture in a dry-down period at five depths (0.05, 0.15,0.25, 0.35 y 0.45 m) in seven plots.

Figure 4.8 shows the SDRD values as a function of depth for the complete monitoring period and the selected dry-down and wet-up periods for each of the monitoring sites (SC4-SC10). SDRD values are lower during the wet period than during the dry period at all locations except for point SC7 at 0.05 m. Therefore, in this case, TS of soil moisture was higher under dry conditions than under wet conditions. This result was consistent with Zhao et al. (2010).

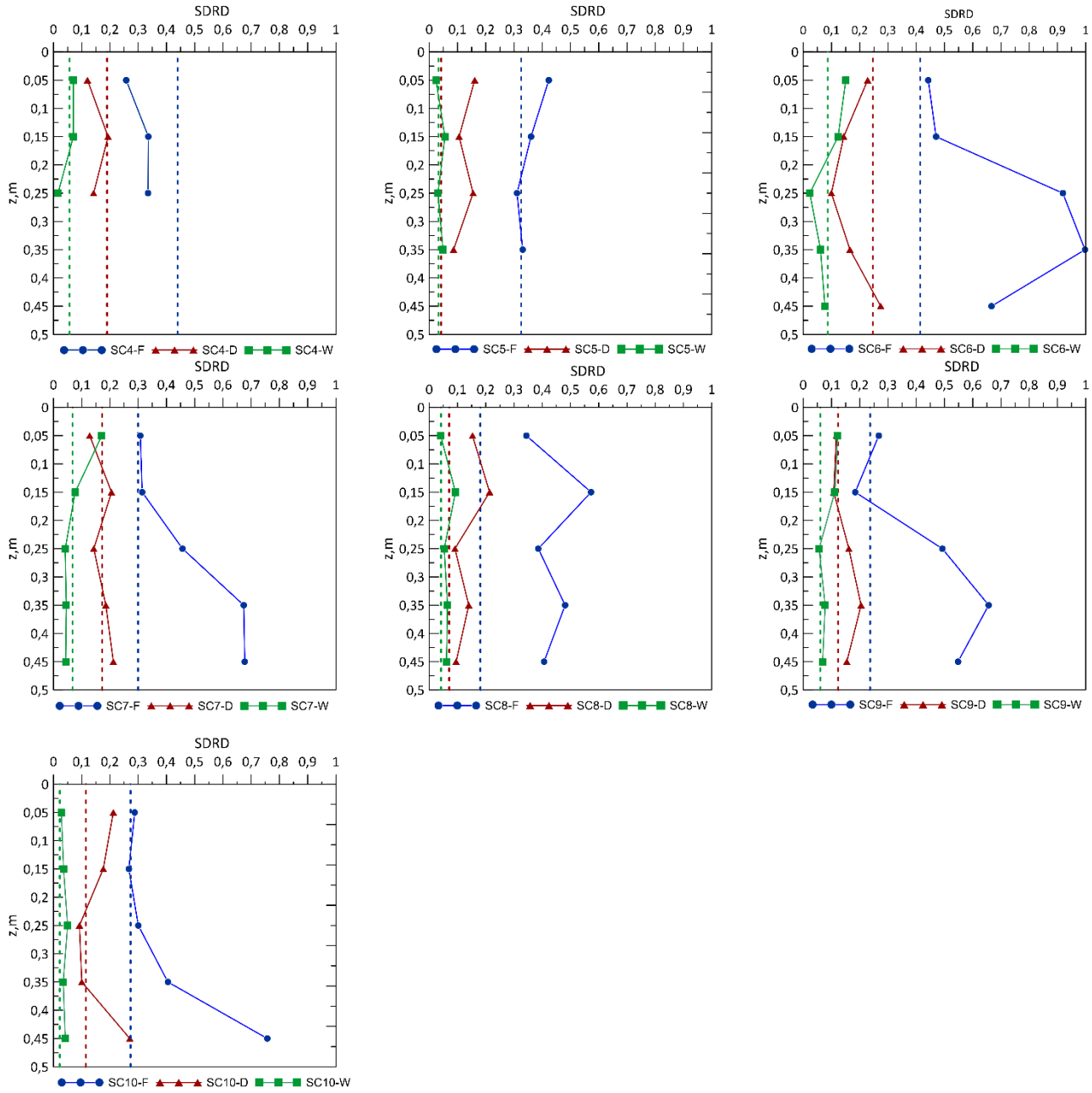

Figure 4.8. Relationships of the standard deviation of the relative difference (SDRD) for the whole (F), dry (D), and wet (W) monitoring period of soil moisture of the locations (a) SC4, (b) SC5, (c) SC6, (d) SC7 (e) SC8 (f) SC9 and (g) SC10 with depth in the two slopes. Dashed lines indicate SDRD calculated for the profile average *s* values.

Figure 4.9a shows the MRD plots for the profile-averaged soil moisture content from the 7 locations and the whole period. For the complete period, the differences between locations SC6 and SC7 and SC9 and SC10 in opposite topographic positions, the former in the valley bottom and the latter on the hilltop point out. (Fig.4.9a). SC8 is the representative location with the highest temporal stability for the whole study area,

considering the minimum value of SDRD. The MRD ranged from -0.25 to 0.27 and the SDRD from 0.18 to 0.44 at the locations wetter than the mean (SC4, SC6, SC7 and SC8), locations above the mean value, and from 0.24 to 0.33 in the locations drier than the mean (SC5, SC9 and SC10), locations below the mean value (Fig.4.9a).

Figure 4.9b and 4.9c shows the results for the studied wet-up and dry-down periods. The locations do neither maintain their ranks in dry nor in wet periods. We found that SDRD were in the order wet<dry<whole study period.

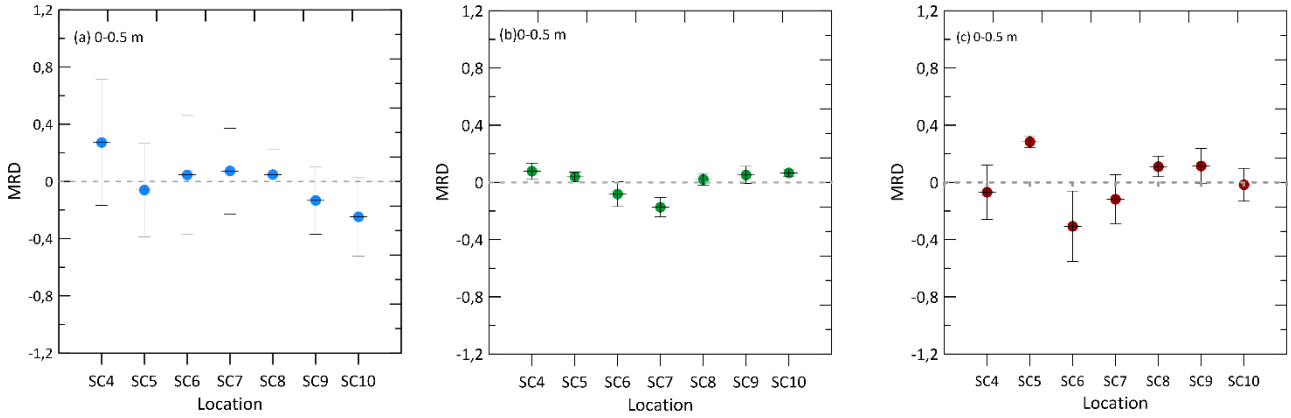

Figure 4.9. Mean relative differences (MRDs) with their standard deviation (vertical bars) for (a) the full soil moisture periods, (b) in a wet-up period, and (c) in a dry-down period at profile average depth.

4.3.3. Analysis of the relationship between soil moisture series

Based on the 3- year daily and profile averaged *s* data, all soil moisture series measured at the 7 locations showed a strong positive correlation with a mean Spearman's correlation coefficient greater than 0.9 (Table 4.2). Note the strong correlation between SC6 and SC7 (0.92), both in the valley bottom on the SFS and on the NFS, respectively, and between SC9 and SC10 (0.98) at the upper slope and hilltop on the NFS, respectively. Correlations between locations at the hilltop and the valley bottom were substantially smaller (see numbers in bold in Table 4.2). Despite Spearman's correlation was considered, the results are very similar to those obtained with Pearson's correlation.

Table 4.2. The Spearman correlation coefficients among values of s determined at profile-depth averaged at the 7 observational locations (SC4-SC10). Coefficients in bold indicate the smallest correlation between hilltop and valley bottom locations.

	SC4	SC5	SC6	SC7	SC8	SC9	SC10
SC4	1.0						
SC5	0.92	1.0					
SC6	0.91	0.90	1.0				
SC7	0.96	0.90	0.92	1.0			
SC8	0.97	0.94	0.91	0.93	1.0		
SC9	0.90	0.96	**0.88**	**0.86**	0.93	1.0	
SC10	0.91	0.97	**0.86**	**0.85**	0.93	0.98	1.0
Mean	0.93	0.93	0.90	0.90	0.94	0.92	0.92

4.3.4. PCA of profile-averaged soil moisture

The computed percent of total variance explained by each PC is plotted in Fig. 4.10. There is a marked drop in the percentage of explained variation between PC_1 and the rest of PCs. Here, PC_1 explains a much greater proportion of the variance than the subsequent PCs. This result draws our attention to PC_1 and PC_2. The first two PC account for 97.5 % of the explained variance:

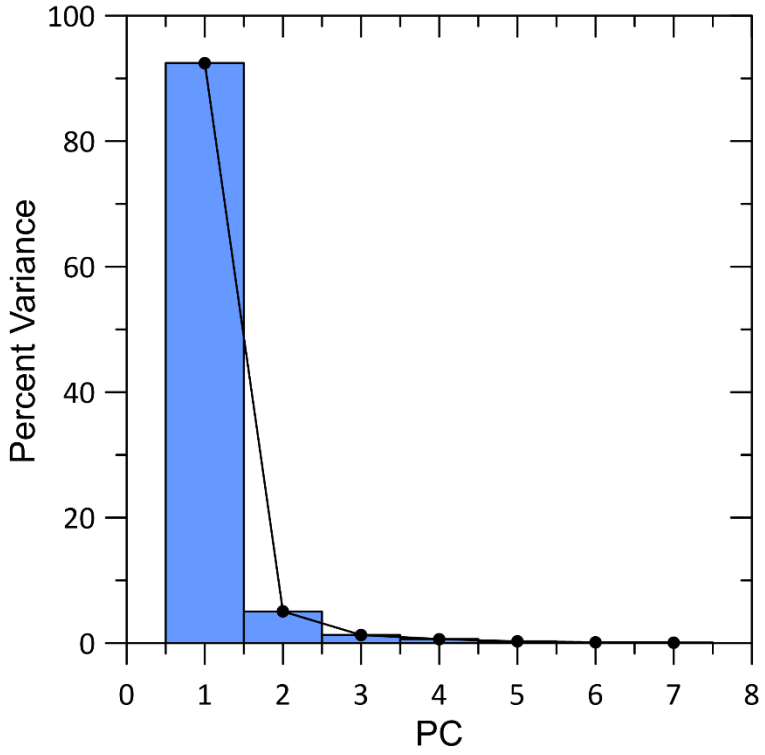

Figure 4.10. Scree plot with the percent variance explained by each principal component (PC).

The loadings reveal how the different variables contributed to each of the PCs (Table 4.3). PC_1 has similar negative loadings (≤ -0.37), negative correlation, for all variables (SC4_AVG-SC10_AVG). Therefore, no single variable significantly contributed to this PC, which might reflect climate influences on soil moisture. Therefore, all variables contributed in a similar way to explain a great percentage of variance. PC_2 has strong positive loadings, positive correlation, for SC9_AVG and SC10_AVG (≥ 0.46) whereas it has strong negative loadings for SC6_AVG and SC7_AVG (≤-0.48), which might be due to the hillslope hydrology or topographical effect.

Table 4.3. Loadings of Principal Component 1 (PC_1) and Principal Component 2 (PC_2). Large loadings are highlighted in boldface to emphasize the variables that contribute to each PC.

	PC_1	PC_2
SC4_AVG	**-0.384**	-0.083
SC5_AVG	**-0.387**	0.021
SC6_AVG	**-0.365**	**-0.540**
SC7_AVG	**-0.374**	**-0.479**
SC8_AVG	**-0.389**	0.109
SC9_AVG	**-0.372**	**0.462**
SC10_AVG	**-0.375**	**0.500**

The PCA map determined by the PC_1 and PC_2 displayed a general perspective of the measurements (Fig.4.11). The first two axes of the PCA accounted for 92.5 % and 5.1% of the total variation, respectively. The soil moisture observations showed clear clustering, in the biplot combining *scores* or the position of each observation in this new coordinate system and *loadings* to a PC, corresponding to the wet and dry periods. Overall, SC10_AVG and SC8_AVG are the variables that contribute more to the variability in both principal components.

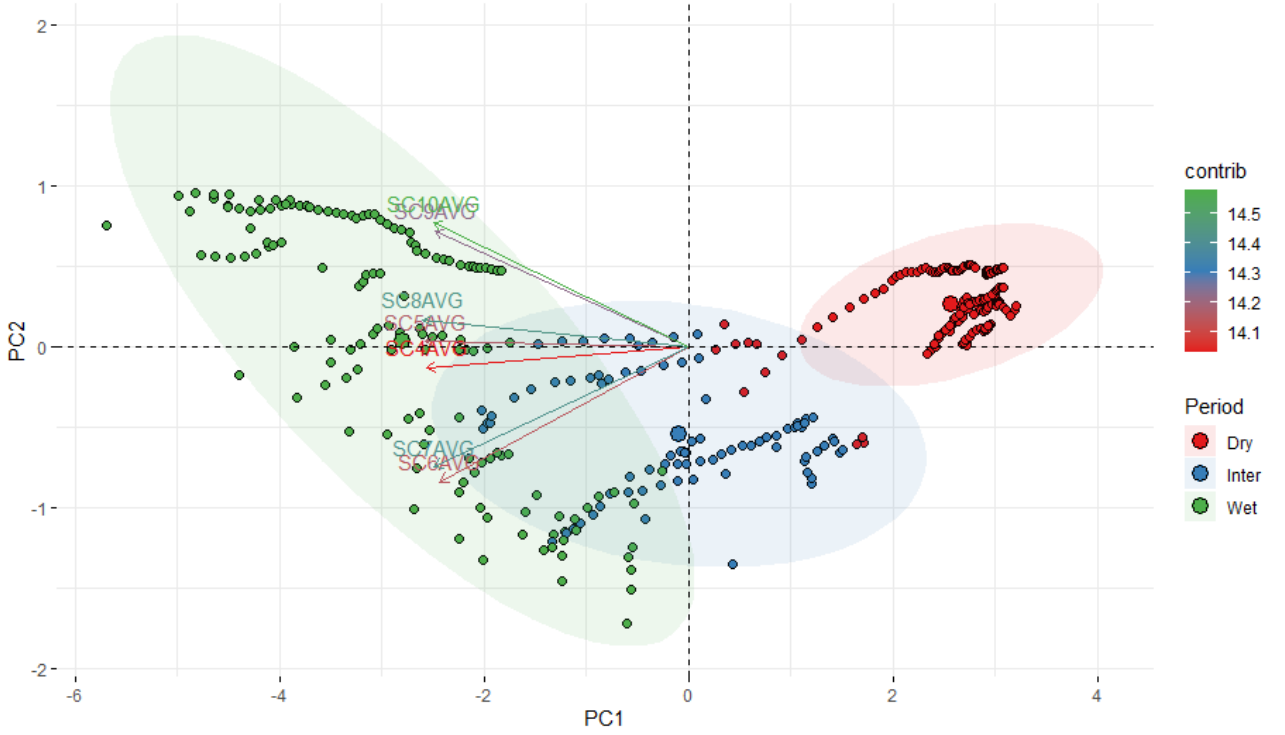

Figure 4.11. Principal component analysis (PCA) showing the two main axes of variability in soil moisture variables. Ellipse grouping observations by period: Dry, Inter, and Wet. The variables are indicated by arrows drawn from the origin, which indicate their 'weight' in different directions or loadings. The most contributing variables to the principal components can be highlighted according to a colour gradient.

The fact that 92.5 % of the variability had been captured by the PC_1 in Fig. 4.11 indicates that a single component can explain much of the overall soil moisture spatial and temporal pattern. The fact that the PCs divide the observations into three separated clusters, corresponding to dry, intermediate and wet periods, might indicate that PC_1 may correspond to the influence of climate on soil moisture. The fact that *loadings* have negative values for this PC and that the observations corresponding to the wet and dry periods have negative and positive values, respectively, on the x-axis, means that PC_1 may be interpreted because of a scarcity of rain, or drought, related to the seasonality of the Mediterranean climate, with a prolonged summer drought. This not only explains a large percentage of the variation in the data, above mentioned but also influences all the measurement locations examined.

PC_2, explaining 5.1 % of the total variance, the different loadings observed in table 4.3, that reflects the correlation values of table 4.2, and is shown also in figure 4.11, between the soil moisture near the valley bottom (SC6 and SC7) and the hilltop (SC9 and SC10) could be attributed to the distinct slope position and its influence on hillslope hydrology. At SC6 and SC7 a negative contribution was observed, suggesting a considerable effect of subsurface flow, while at SC9 and SC10 the opposite effect was observed.

The elevation of SC4 and SC10 was similar, although SC4 is in a flat area farther than site SC10 from the slope as shown in Fig. 4.1.

Kim and Barros (2002), in their study conducted to explain the spatial structure of soil moisture, examined large-scale images obtained during the Southern Great Plains 1997 (SGP'97) hydrology experiment (USA) and identified topography as the dominant factor for the spatial structure of soil moisture during rainfall. Yoo and Kim (2004) also found in their study of two soil moisture datasets of the SGP'97 hydrology experiment at the field scale that topography-related factors were important. However, both studies highlight that during inter-storm and dry-down periods other factors such as soil properties and vegetation dominate soil moisture evolution. To identify factors affecting soil moisture spatial variability, Choi et al. (2007) applied a PCA to 18 datasets from 9 experiments across the world and determined that soil factors, precipitation, and topography control this variability. A preceding work in this study area (Cardeña, southern Spain) showed a significant correlation of soil moisture with the Topographic Wetness Index (TWI) only under dry conditions, while for wet conditions the correlation was only significant with bulk density (García-Gamero et al., 2021).This study expands on the previous one by considering the complete soil moisture dataset, climate and topography were identified as dominant factors in our PCA.

4.3.5. Principal Components Analysis of soil moisture with depth

Figure 4.12 shows the PCA maps determined by the PC_1 (Dim1) and PC_2 (Dim2) to visualize the distribution of the observations at five different depths (0.05,0.15,0.25,0.35 and 0.45 m). Combining PC_1 and PC_2 accounted for more than 94 % of the variances, where PC_1 accounted for 90.9, 89, 87.7,86.2, and 84 % and PC_2 explained 5, 6.4, 6.4, 7.8, and 10.4 % at the five different depths (0.05,0.15,0.25,0.35 and 0.45 m). Although PC_1 still explained much of the variance at all depths, PC_2 became more important with depth. At the surface, the control of climate on soil moisture is evident through evapotranspiration and rainfall, but topography-related factors exert stronger controls on subsurface soil moisture as depth increased.

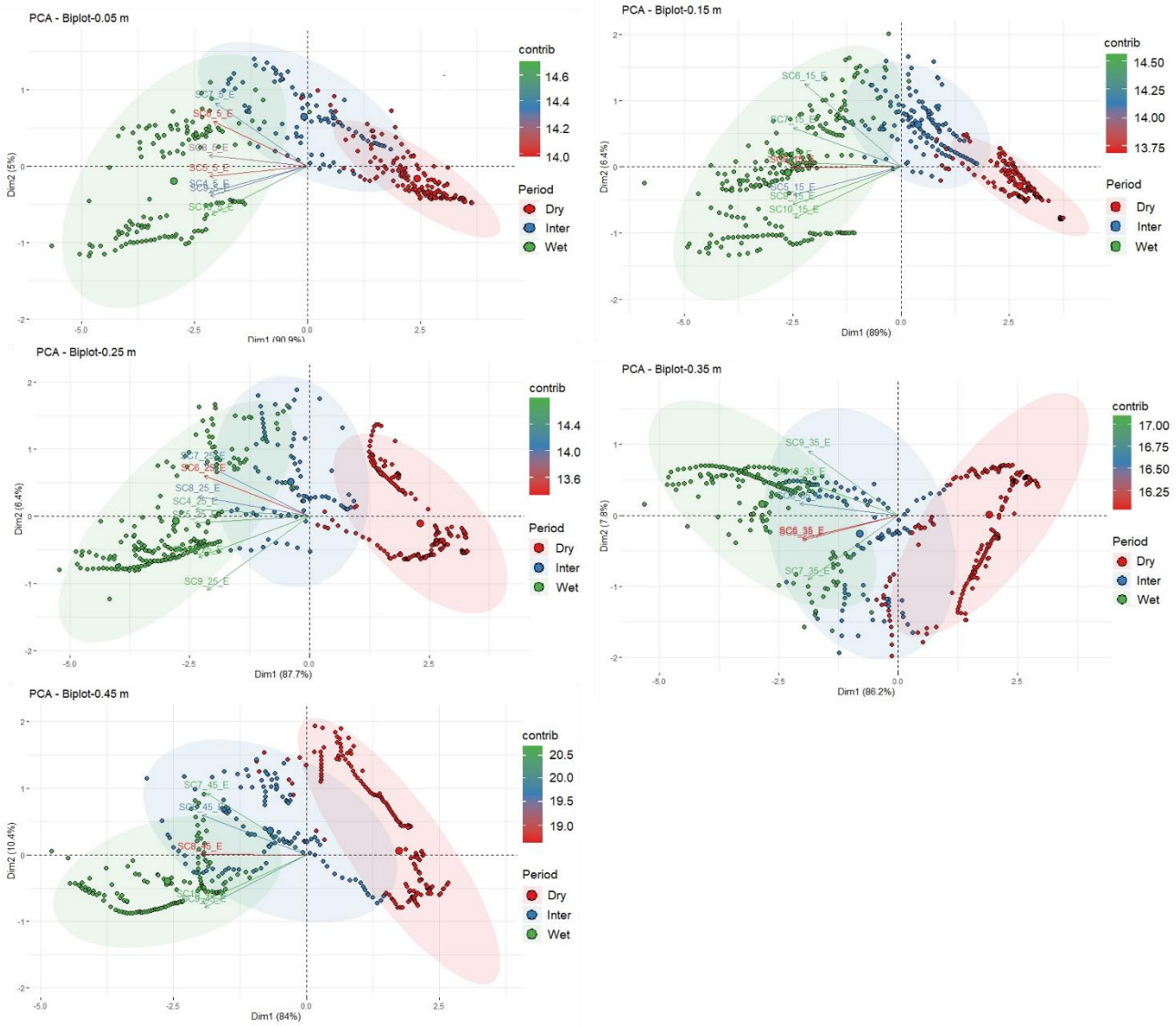

Figure 4.12. Principal component analysis (PCA) showing the two main axes of variability in soil moisture variables by depth (0.05,0.15,0.25,0.35 and 0.45 m). Ellipse grouping observations by period: Dry, Inter, and Wet. The variables are indicated by arrows drawn from the origin, which indicate their 'weight' in different directions or loadings. The most contributing variables to the principal components can be highlighted according to a color gradient.

4.4. Conclusions

In a Mediterranean oak-woodland savanna or 'dehesa', of southern Spain, soil moisture dynamics reflects the influence of the strong seasonality that characterizes this climate. The analysis of temporal stability (TS) of soil moisture on two opposing hillslopes shows that the monitoring locations situated on the NFS generally showed higher TS at the

different depths at which this variable was measured. Conversely, the soil moisture monitoring locations SC6 and SC7 showed lower TS, because of their position at the valley bottom. SC8, in the middle slope of NFS, is selected as the representative monitoring site within the study site. Considering the full dataset and the profile-averaged data the spatial pattern of soil moisture showed considerable TS which was stronger for wet than for dry conditions.

Two independent PCs were found to describe 97.5 % of the full dataset's variance and were important to describe the spatial and temporal variability of soil moisture. The dominant pattern PC_1, which explained 92.5 % of the variance, may be identified with climate. While PC_2, which explained 5.1 % responded to topographical attributes. When the PCA is conducted by depth, the PC_1 is still the dominant pattern (PC_1, σ^2_{PC1} = 0.91,0.89,0.88,0.86, and 0.84) although less variance was explained deeper into the profile. PC_2 became more relevant with depth (PC_2, σ^2_{PC2} = 0.05, 0.064, 0.064, 0.078, and 0.10), underlining the increasing importance of topography-related factors deeper into the soil profile.

4.5. References

Brocca, L., Melone, F., Moramarco, T., & Morbidelli, R. (2009). Soil moisture temporal stability over experimental areas in Central Italy. *Geoderma*, *148*(3–4), 364–374. https://doi.org/10.1016/j.geoderma.2008.11.004

Brocca, L., Melone, F., Moramarco, T., & Morbidelli, R. (2010). Spatial - temporal variability of soil moisture and its estimation across scales. *Water Resources Research*, *46*, 1–14. https://doi.org/10.1029/2009WR008016

Brutsaert, W. (2005). *Hydrology: An Introduction*. Cambridge University Press. https://doi.org/10.1017/CBO9780511808470

Carpintero, E., Andreu, A., Gómez-Giráldez, P. J., Blázquez, Á., & González-Dugo, M. P.

(2020). Remote-Sensing-Based Water Balance for Monitoring of Evapotranspiration and Water Stress of a Mediterranean Oak – Grass Savanna. *Water*.

Carracedo, M., Paquette, J. L., Alonso Olazabal, A., Santos Zalduegui, J. F., de García de Madinabeitia, S., Tiepolo, M., & Gil Ibarguchi, J. I. (2009). U-Pb dating of granodiorite and granite units of the Los Pedroches batholith. Implications for geodynamic models of the southern Central Iberian Zone (Iberian Massif). *International Journal of Earth Sciences*, *98*(7), 1609–1624. https://doi.org/10.1007/s00531-008-0317-0

Choi, M., Jacobs, J. M., & Cosh, M. H. (2007). Scaled spatial variability of soil moisture fields. *Geophysical Research Letters*, *34*(September 2006), 1–6. https://doi.org/10.1029/2006GL028247

Fry, J. E., & Guber, A. K. (2020). Temporal stability of fi eld-scale patterns in soil water content across topographically diverse agricultural landscapes. *Journal of Hydrology*, *580*(July 2019), 124260. https://doi.org/10.1016/j.jhydrol.2019.124260

García-Gamero, V., Peña, A., Laguna, A. M., Giráldez, J. V., & Vanwalleghem, T. (2021). Factors controlling the asymmetry of soil moisture and vegetation dynamics in a hilly mediterranean catchment. *Journal of Hydrology*, *598*(October 2020), 126207. https://doi.org/10.1016/j.jhydrol.2021.126207

Henderson-Sellers, A. (1996). Soil moisture: A critical focus for global change studies. *Global and Planetary Change*, *13*(1–4), 3–9. https://doi.org/10.1016/0921-8181(95)00034-8

Jawson, S. D., & Niemann, J. D. (2007). Spatial patterns from EOF analysis of soil moisture at a large scale and their dependence on soil , land-use , and topographic properties. *Advances in Water Resources*, *30*, 366–381. https://doi.org/10.1016/j.advwatres.2006.05.006

Kim, G., & Barros, A. P. (2002). Space-time characterization of soil moisture from passive microwave remotely sensed imagery and ancillary data. *Remote Sensing of Environment*, *81*(2–3), 393–403. https://doi.org/10.1016/S0034-4257(02)00014-7

Kim, K.-Y. (1996). Sensitivity of a linear detection procedure to the accuracy of empirical orthogonal functions. *Journal of Geophysical Research Atmospheres*, *101*(18), 23423–23432. https://doi.org/10.1029/96jd02383

Lin, H. (2006). Temporal Stability of Soil Moisture Spatial Pattern and Subsurface Preferential Flow Pathways in the Shale Hills Catchment. *Vadose Zone Journal*, *2000*, 317–340. https://doi.org/10.2136/vzj2005.0058

Martínez-Fernández, J., & Ceballos, A. (2003). Temporal Stability of Soil Moisture in a Large-Field Experiment in Spain ´. *Soil Sci Soc Am J*, 1647–1656. https://doi.org/10.2136/sssaj2003.1647

Martini, E., Wollschläger, U., Musolff, A., Werban, U., Zacharias, S., Martini, E., & Werban, U. (2017). Principal Component Analysis of the Spatiotemporal Pattern of Soil Moisture and Apparent Electrical Conductivity. *Vadose Zone J.*, *16*. https://doi.org/10.2136/vzj2016.12.0129

Nimmo, J. R., Survey, U. S. G., & Park, M. (2012). Preferential fl ow occurs in unsaturated conditions †. *Hydrological Processes*, *789*, 786–789. https://doi.org/10.1002/hyp.8380

Olea, L., & San Miguel-Ayanz, A. (2006). The Spanish dehesa, a traditional Mediterranean silvopastoral system. *21st General Meeting of the European Grassland Federation*, *April*, 1–15.

Peel, M. C., Finlayson, B. L., & McMahon, T. A. (2007). Updated world map of the Köppen-Geiger climate classification. *Hydrology and Earth System Sciences*, *11*, 1633–1644.

Perry, M. A., & Niemann, J. D. (2007). Analysis and estimation of soil moisture at the catchment scale using EOFs. *Journal of Hydrology*, 388–404. https://doi.org/10.1016/j.jhydrol.2006.10.014

Robinson, D. A., Campbell, C. S., Hopmans, J. W., Hornbuckle, B. K., Jones, S. B., Knight, R., Odgen, F., Selker, J., & Wendroth, O. (2008). Soil Moisture Measurement for Ecological and Hydrological Watershed-Scale Observatories: A Review. *Vadose Zone Journal*. https://doi.org/10.2136/vzj2007.0143

Román-Sánchez, A., Vanwalleghem, T., Peña, A., Laguna, A., & Giráldez, J. V. (2018). Controls on soil carbon storage from topography and vegetation in a rocky, semi-arid landscapes. *Geoderma*, *311*, 159–166. https://doi.org/10.1016/j.geoderma.2016.10.013

RStudioTeam. (2020). *RStudio: Integrated Development for R. RStudio, PBC, Boston, MA*. http://www.rstudio.com/

Vachaud, G., Passerat De Silans, A., Balabanis, P., & Vauclin, M. (1985). Temporal Stability of Spatially Measured Soil Water Probability Density Function. *Soil Science Society of America Journal*, *49*(4), 822–828. https://doi.org/10.2136/sssaj1985.03615995004900040006x

Vanderlinden, K., Vereecken, H., Hardelauf, H., Herbst, M., Martínez, G., Cosh, M. H., & Pachepsky, Y. A. (2012). Temporal Stability of Soil Water Contents: A Review of Data and Analyses. *Vadose Zone Journal*, *11*(4), vzj2011.0178. https://doi.org/10.2136/vzj2011.0178

Wilks, D. S. (2011). *Statistical methods in the atmospheric Sciences* (3rd ed.). Academic Press. https://doi.org/10.1016/B978-0-12-815823-4.09988-0

Yoo, C., & Kim, S. (2004). EOF analysis of surface soil moisture field variability. *Advances in*

Water Resources, *27*, 831–842. https://doi.org/10.1016/j.advwatres.2004.04.003

Zhang, H., Chang, J., Zhang, L., Wang, Y., Li, Y., & Wang, X. (2018). NDVI dynamic changes and their relationship with meteorological factors and soil moisture. *Environmental Earth Sciences*, *77*(16), 1–11. https://doi.org/10.1007/s12665-018-7759-x

Zhao, Y., Peth, S., Wang, X. Y., Lin, H., & Horn, R. (2010). Controls of surface soil moisture spatial patterns and their temporal stability in a semi-arid steppe. *Hydrological Processes*, *24*(18), 2507–2519. https://doi.org/10.1002/hyp.7665

Chapter 5

Evolution of soil moisture profiles during the early stages of infiltration and evaporation processes in a Mediterranean catchment

EVOLUTION OF SOIL MOISTURE PROFILES DURING THE EARLY STAGES OF INFILTRATION AND EVAPORATION PROCESSES IN A MEDITERRANEAN CATCHMENT

ABSTRACT

The edaphic and physiographic factors of watersheds characterize the main water recharge and discharge processes, which in their turn, are essential in the evolution of the landscape as, for instance, Tucker and Slingerland (1997) have shown.

The purpose of this chapter is to illustrate the early stages of recharge and discharge processes on soils located in two opposite slopes, one oriented towards the south, or toward the Equator in global terms, and another one oriented towards the north, or toward the Poles, of a granitic watershed of the Sierra Morena, close to the village of Cardeña, in the province of Córdoba. The soil profiles are saturated fast with the occurrence of some subsurface water flow due to the shallower depth of the former with respect to the latter. The percolation flow towards the underlying phreatic aquifer attenuates the profile saturation rate in the soils of the north-facing slope. The discharge processes evolve at a similar rate in the soils of the two hillslopes, at least in the early stages while the root water uptake by the vegetation is not too relevant.

5.1. Introduction

In mountain catchments where the topography divides slopes with different aspect concerning the solar radiation incidence, the so-called sunny and shady areas, the insolation received induces changes in the hydrological processes that, in turn, generate different ecosystems in them. The hydrological literature includes numerous examples such as Richardson et al. (2020) in California or Gutiérrez-Jurado et al. (2013) in New Mexico, both with marked differences between the two aspects. In a complete review, Pelletier et al. (2018) recommended the separation between water and temperature constraining conditions on the soil developed on different slopes, suggesting the denomination of

Equator-facing or Pole-facing slopes corresponding respectively to sunny or shady spots, as exposed by McMillan & Srinivasan (2015).

In the critical zone of Cardeña in the Sierra Morena of Córdoba, Spain, where the precipitation and temperature conditions enhance soil-forming processes (Román-Sánchez et al., 2018), some differences between vegetation and edaphic characteristics have been observed. In this work, these differences are explored by relating them to the evolution of soil moisture and biomass. García-Gamero et al. (2021) have detected different effects on the evolution of soil moisture, the vegetation, and on the recharge of the water table that delimits an aquifer occupying the fractures of the granitic rocks of the area, which seems limited to the north-facing slope.

The ongoing research in this critical zone continues to gather the information that allows us to explore in greater detail the behavior of the soil. This chapter includes the evolution of soil moisture profiles in response to rainfall and solar radiation and vertical vapor pressure gradients in the lower atmosphere following a period of rains.

5.2. Material and methods

The Santa Clotilde farm has been extensively described in other works (e.g., García-Gamero et al. 2021) so here we describe only the rain gauges that were installed along the opposite slopes and the methods of analysis of the profiles.

A network of capacitance sensors, CS655 (Campbell Scientific), which started recording on 24.11.2016, measured half-hourly soil moisture, electrical conductivity, and the temperature data.

Figure 5.1 shows the seven sensors pits along two opposite slopes, one Southeast faced, SC4-SC6, and the other one North faced, SC7-SC10. The depth of sensors was 0.05, 0.15, 0.25, 0.35, and 0.45 m.

Figure 5.1.Location of the study site.

Rain gauges were installed at five (SC10, SC8, SC7, SC6 and SC4) of the seven pits, to cover the slope. The rain gauges accurately measured rainfall depth activated by a bucket mechanism, with a collection area of 200 cm^2, a resolution of 0.2 mm, and an accuracy of ± 4%.

Solar panels with a maximum power of 15 W at 12 V supplied the required maintenance and data recording energy. Two measurements periods have been selected to show the recharge and discharge processes of the soil profiles. A very suitable recharge period from 27.02.2018 to 20.03.2018, when a prolonged autumn drought was truncated, leading to a rather wet spring throughout the Sierra Morena. Another period starting on 25.04.2019 allows us to explore the soil response to incipient evaporation.

5.3. Results and discussion

The records of the 5 rain gauges installed in the cross-section of the valley do not present any appreciable orography-induced differences as can be observed in the comparison of the daily rainfall of Figure 5.2. Figure 5.2 shows the rainless days and the detractions attributed to the vegetation interception. The approximation to the line 1:1 allows the estimation of the rainfall from anyone of the rain gauges in the rainy days, independent of the misfunctions of the other ones due to accidental blockage of the reception are by fallen leaves.

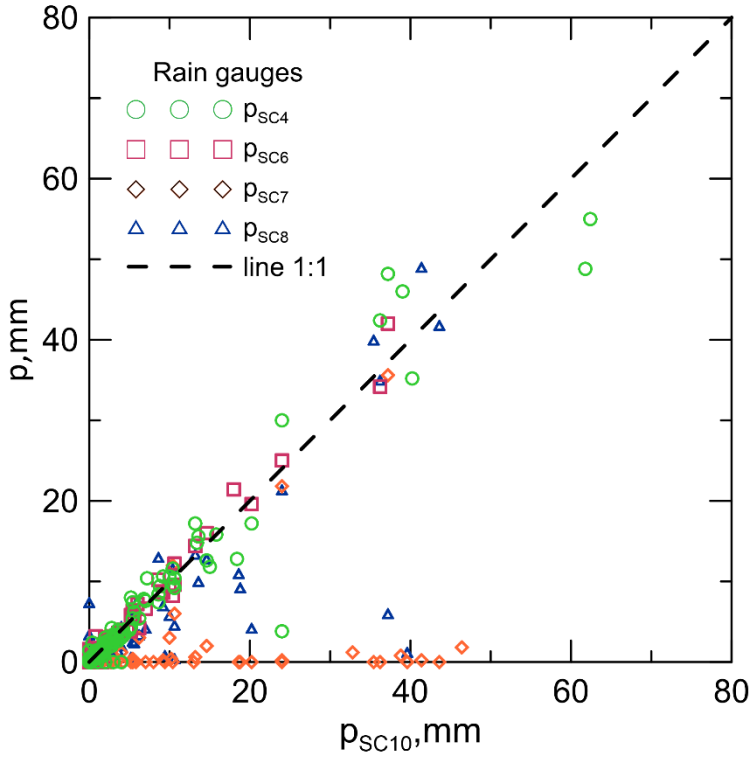

Figure 5.2.Comparison of daily rainfall, p_{scx}, recorded in the rain gauges at different locations, SCx.

The observed hyetographs during the recharge period on some February and March 2018 days, depicted in Fig. 5.3, seem to follow a similar pattern with some high-intensity rainfall, in some cases up to 80 mm h^{-1}, with a short duration, preceded and followed by pulses of lower intensity.

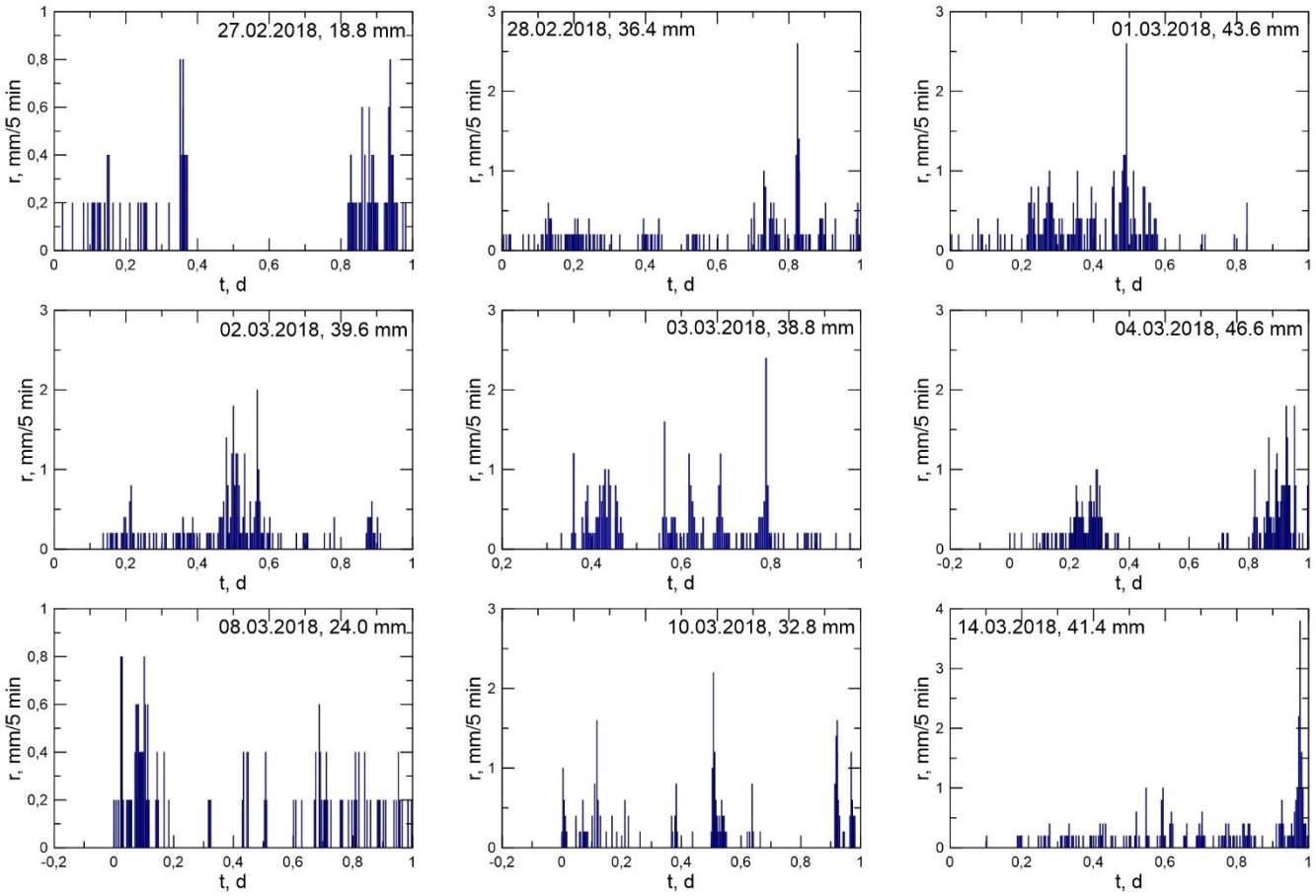

Figure 5.3. Hyetographs registered in rain gauge SC10 in February and March 2018.

Figure 5.4 shows the fast increase of moisture in all the soil profiles, until almost saturation, in this case at locations SC10, SC7 and SC5. In profile SC5 the moisture at the bottom increased almost suddenly between noon and midnight on March 1st, which could be attributed to a subsurface flow, from upslope given the reduced depth of the soil, underlain by unweathered granitic rocks. A similar effect may occur in profile SC7, although in this case, it is the bottom of the valley in which the subsurface flow of the Martin Gonzalo stream interfered. The increase in the soil moisture of the bottom of the soil profile, 0.45 m, started at noon of February 27, shortly after the rainfall began, with another great rain pulse after midnight of March 1st. The evolution of these profiles is similar to that of the computed profiles of Basha (2002, fig.1; 2011, fig. 3) and different from those of Vachaud and Tony (1971, fig. 7) obtained during infiltration trials in sand columns and analyzed later by Salvucci and Entekhabi, (1995, fig. 7). The rainwater in the SC10 profile was

moving relatively slower than in the experiments of Vachaud and Thony (1971) probably due to the lower rain intensity or the smaller size of the pores of the field soil and obstacles laid by the roots on them.

In the profiles of the SFS, soil development is limited, therefore it was not possible to install sensors at the depths indicated. The SC4 location barely reached 0.3 m and the SC5 location 0.40 m. On the other hand, on the NFS, depths of more than 1 m were reached, locations SC8, SC9, and SC10.

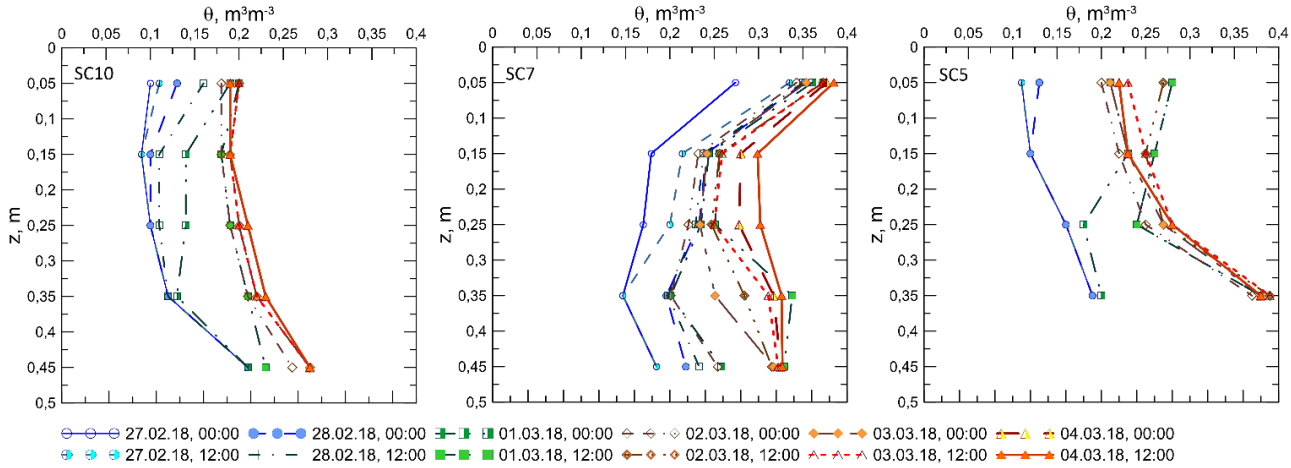

Figure 5.4.Evolution of the soil moisture profiles observed at locations SC10, SC7 and SC5 during the rainy period of late February and early March 2018.

From the above curves, it is possible to estimate the amount of water present and that which infiltrates into the soil profile (Fig. 5.5). In this period no data were collected for locations SC8 and SC6 due to a transmission failure of the sensors. Note that successive pulses of rain did not increase the volume of water retained in the soil profile, which could be due in part to reduced infiltration because the soil is saturated, in the case of profiles SC4 and SC5, or to fast transmission of water by percolation at the bottom to the underlying aquifer in the case of locations SC8, SC9, and SC10. The volume of water in the SC4 location, or, more appropriately, depth when expressed per unit area, is lower than that of the other soils due to its shallower depth.

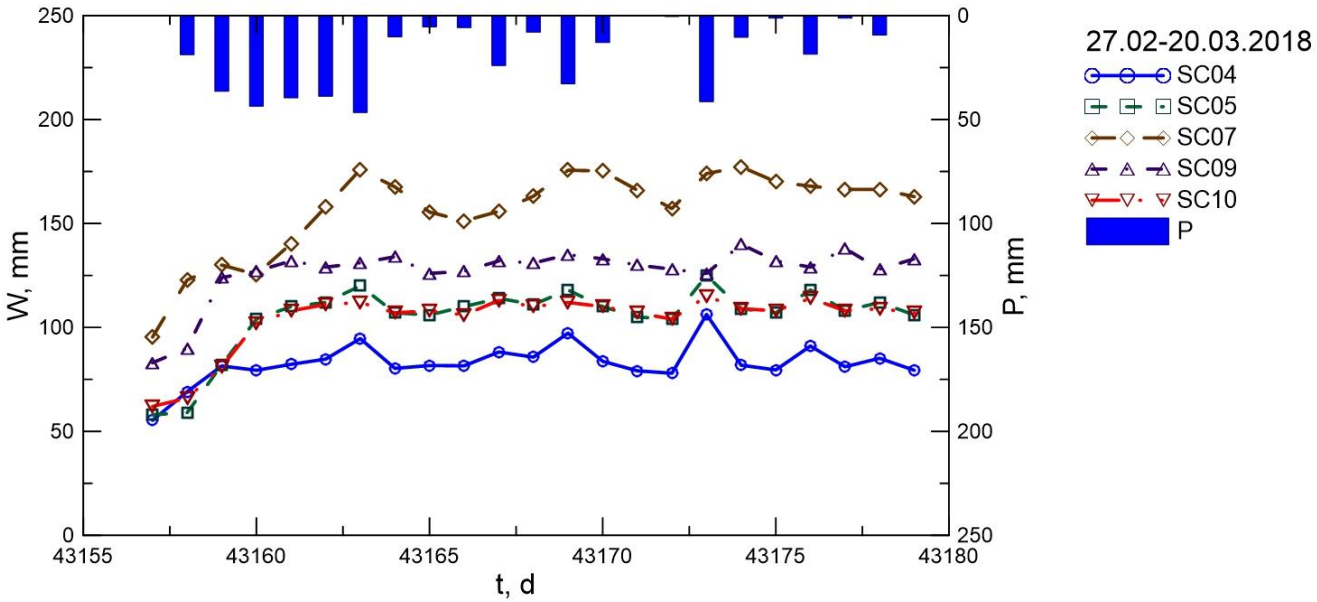

Figure 5.5. Soil moisture evolution observed at locations SC4-SC10 during the rainy period of the end of February and early March 2018.

Figure 5.6 shows the evolution of the soil moisture profiles, expressed as the effective saturation ratio, s, to better show the continuous refill of the soil pores.

Also noteworthy is the fast discharge of the soils when the daily rainy is reduced, especially in soil SC7, which could be attributed to a very fast horizontal redistribution due to the porosity of the medium, which is part of the phreatic aquifer connected to the Martín Gonzalo Creek stream bed. At this time of the year, with a not very high air temperature, and in such an elevated area, the influence of evaporation is scarce. In some profiles, there could be partial obstructions of some pores similar to what has been called the tipping-bucket, (Emerman, 1995) that allow the flow of water discretely. The evolution of the moisture profiles in the soil SC7 is similar to the measured profiles of Vachaud and Thony (1971, fig. 10), which could be attributed to the greater rainfall intensity of the latter laboratory experiment, 21.3 mm h^{-1}.

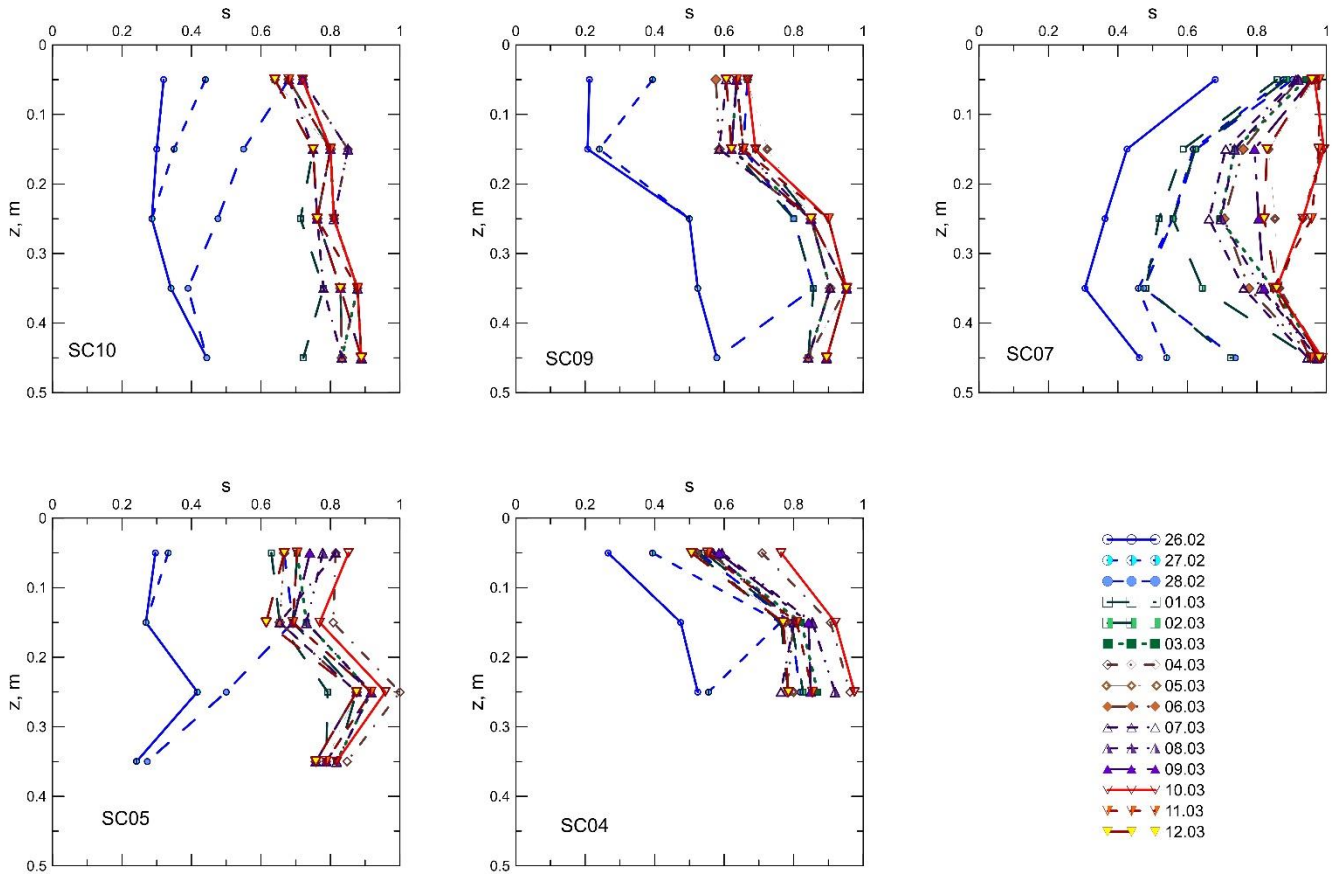

Figure 5.6. Evolution of the effective saturation ratio, s, observed at the different measurement locations during the rainy period at the end of February and beginning of March 2018.

Figure 5.7 shows the gradual discharge of the soil after a series of rain pulses in a drier and warmer period at location SC4. In this case, evaporation proceeds uniformly because of the particle size distribution of the soil with large pores and fissures well connected, which facilitated the flow of water towards the surface in response to the gradient of the potential. The profiles are different from those of the Vachaud and Thony (1971, fig. 4) trials, although the smaller curvature of the field profiles suggested a better gradation of the pore sizes than in the sand used in the laboratory experiment. Some changes are also observed in the intensity of evaporation due to thermal oscillations in the exterior due to the spacing of the successive profiles.

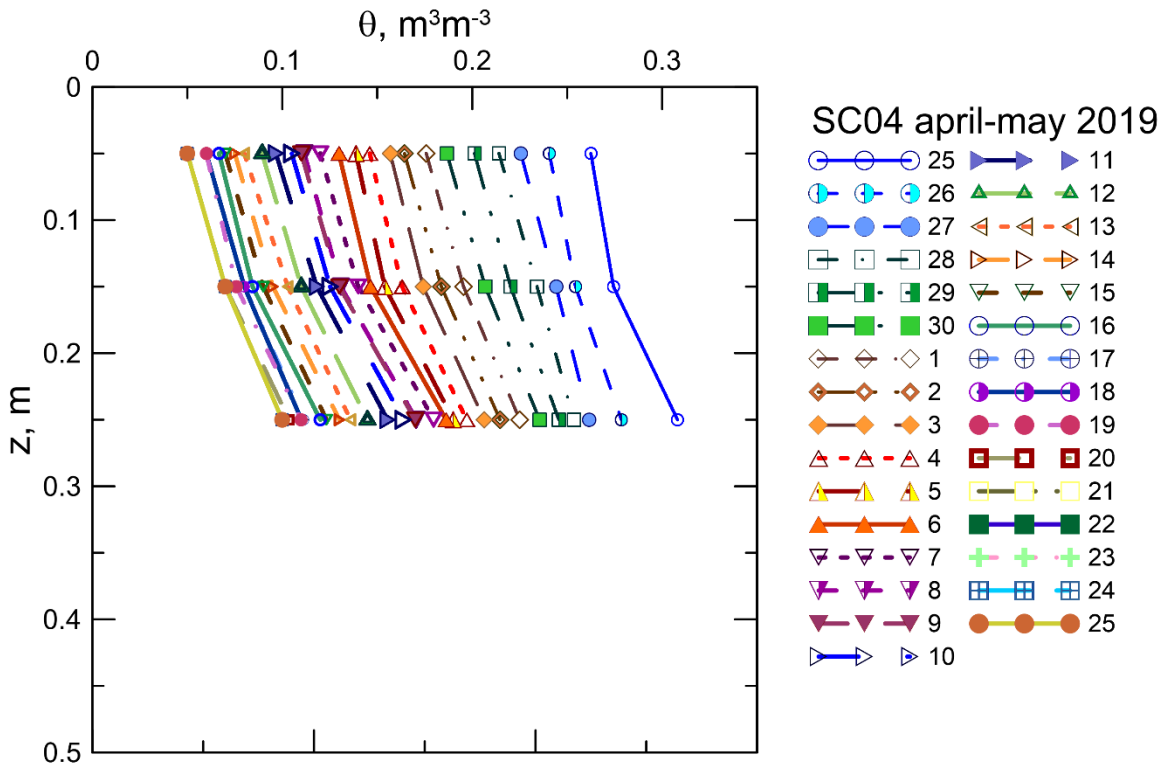

Figure 5.7.Evolution of the soil moisture profiles observed at location SC4 during the period without rain from April 25 to May 25, 2019.

By integration of the soil moisture profile, and further comparison of the water depth in successive days, it is possible to estimate the loss of moisture, attributable in these conditions to evaporation, in the broad sense, thus including evapotranspiration. Figure 5.8 shows the estimated daily evaporation intensity at location SC4 during the period without rainfall from April 25 to May 25. To compare these estimates with the potential or reference evaporation intensity, the calculated values of the reference evapotranspiration (ET_o) from meteorological data measured at a station near the study area, Adamuz, of the Andalusian Agroclimatic Information Network (RIA 2021), using the FAO method (Allen et al. 1988), have also been inserted in the figure.

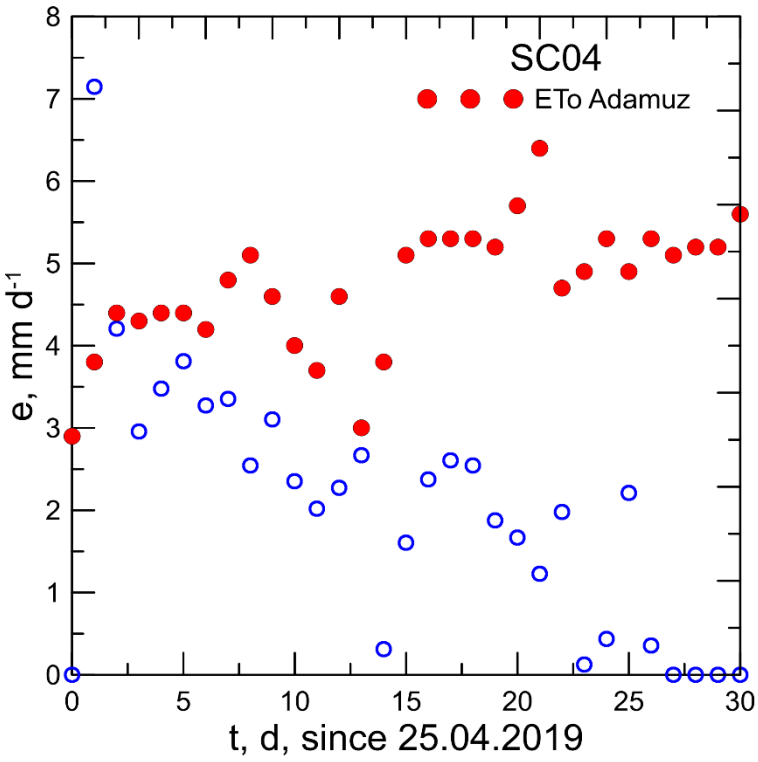

Figure 5.8. Daily evaporation evolution at location SC4 during the period without rain 25 April to 25 May 2019 (blue circles). Reference evapotranspiration calculated from meteorological data measured at the nearby Adamuz RIA station is shown as red circles.

The estimated values of evaporation intensity are sensibly similar to those calculated at the Adamuz station during the first days till the eighth day when it starts to decrease in what could be estimated as the beginning of the second phase of evaporation (Or et al. 2013). The decreasing trend of evaporation intensity, e, seems to follow the exponential equation of Brutsaert (2014), with the parameters of the initial intensity, time 0, eo, and the normalization time, κ:

$$e = 4.276 \cdot e^{-0.04176 \cdot t} \quad (5.1)$$

With a coefficient of determination R^2=0.6238 for the set of 22 data pairs. The reference intensity 4.28 mm d^{-1} coincides with the Adamuz data and the normalized time, the inverse of the coefficient in the exponent, 23.9 days is close to the time in which the second phase of evaporation is close to the end, as shown in Figure 5.8.

Figure 5.9 shows the water discharge in the period of Figure 5.7 but using effective saturation ratios. The control of the surface horizon on the evaporation rate, frequent in other soils as pointed out by some authors such as Kim and Lakshmi (2019) or Li et al. (2020) might not be very important in these field sites, since no differences were appreciated in the wetting profiles, figures 5.4 and 5.6, and dry-down figures 5.7 and 5.9. The memory of these soils, the time is taken for any anomaly, positive or negative, to dissipate (McColl et al. 2017) do not seem to be very high. On the other hand, there was not a large spatial variability in the soils, so, according to the criteria of Peterson et al. (2019), it is the average participation type, with reducing variation.

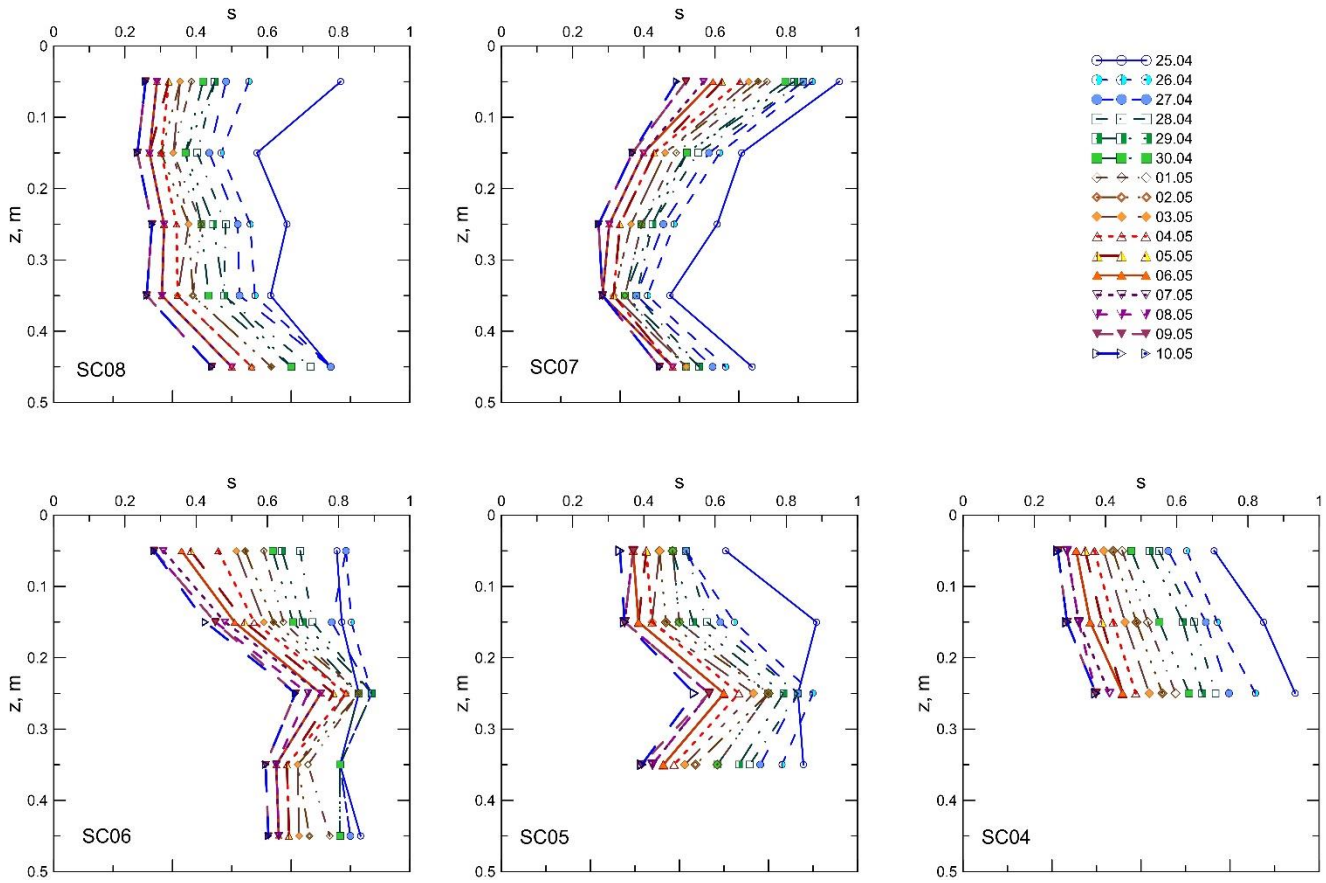

Figure5.9.Evolution of the effective saturation ratio, s, observed at the different measurements locations during the period without rain from April 25 to May 10, 2019.

5.4. Conclusions

The influence of the aspect of a slope on the hydrological processes that take place results in important modifications, not only in the soil but also in the vegetation that grows on them, in their formation, and the subsurface flow. Perhaps the influence is indirect, through the changes in soil moisture, as indicated by Berger and Entekhabi (2001), whose results stressed the relevance of the rainfall rate and the initial soil moisture for the generation of runoff at the watershed scale.

The evolution of the soil moisture profiles revealed the importance of the downslope subsurface flow of water.

Water flow in these soils is very fast both during infiltration and evaporation processes. It does not appear that the upper horizon can exert much control over the water cycle, although the vegetation can also contribute by shading the surface, homogenizing the extraction by the roots, and contributing to the formation of smaller pores.

5.5. References

Allen, R.G., L.S. Pereira, D. Raes y M. Smith, 1988. Crop evapotranspiration - Guidelines for computing crop water requirements. Irrig. Drain. Paper 56, FAO, Roma.

Basha, H.B. (2002). Burgers' equation: A general nonlinear solution of infiltration and redistribution. Water Resources Research. Vol. 38, doi:10.1029/2001WR000954.

Basha, H.B. (2011). Infiltration models for soil profiles bounded by a water table. Water Resources Research. Vol. 47, doi:10.1029/2011WR010872.

Berger, K.P., Entekhabi, D. (2001). Basin hydrologic response to distributed physiographic descriptors and climate. Journal of Hydrology. 247:169-182. https://doi.org/10.1016/S0022-1694(01)00383-3.

Brutsaert, W., 2014. Daily evaporation from drying soil: Universal parameterization with similarity. Water Resour. Res. 50, 3206-3215.

Emerman, S.H., 1995. The tipping bucket equation as a model for macropore flow. Journal of Hydrology. 171, 23-47. https://doi.org/10.1016/0022-1694(95)02735-8.

García-Gamero, V., Peña, A., Laguna, A. M., Giráldez, J. V., y Vanwalleghem, T. 2021. Factors controlling the asymmetry of soil moisture and vegetation dynamics in a hilly mediterranean catchment. Journal of Hydrology, 598(October 2020), 126207. https://doi.org/10.1016/j.jhydrol.2021.126207

Gutiérrez-Jurado, H. A., Vivoni, E. R., Cikoski, C., J. Harrison, J. B., Bras, R. L., y Istanbulluoglu, E. 2013. On the observed ecohydrologic dynamics of a semiarid basin with aspect-delimited ecosystems. Water Resources Research, 49, 8263–8284. https://doi.org/10.1002/2013WR014364

Kim, H y V. Lakshmi, 2019. Global dynamics of stored precipitation water in the topsoil layer from satellite and reanalysis data. Water Resour. Res. 55, 3328-3346

Li, Z., J. Vandenborght y K.M. Smits, 2020. The effect of the top soil layer on moisture and evaporation dynamics. Vadose Zone L. 19:e20049.

McColl, K.A., S.H. Alemohammad, R. Akbar, A.G. Konings, S. Yueh y D. Entekhabi, 2017. The global distribution and dynamics of surface soil moisture. Nature Geosci. 10, DOI: 10.1038/NGEO2868.

McMillan, H.K. y M.S. Srinivasan, 2015. Characteristics and controls of variability in soil moisture and groundwater in a headwater catchment. Hydrol. Earth Syst. Sci. 19, 1767-1786.

Or, D., P. Lehmann, E. D. Shahraeeni y N. Shokri, 2013. Advances in Soil Evaporation Physics—A Review. Vadose Zone J. doi:10.2136/vzj2012.0163

Pelletier, J. D., Barron-Gafford, G. A., Gutiérrez-Jurado, H., Hinckley, E. L. S., Istanbulluoglu, E., McGuire, L. A., Niu, G. Y., Poulos, M. J., Rasmussen, C., Richardson, P., Swetnam, T. L., Tucker, G. E. 2018. Which way do you lean? Using slope aspect variations to understand Critical Zone processes and feedbacks. Earth Surface Processes and Landforms, 43(5), 1133–1154. https://doi.org/10.1002/esp.4306

Peterson, A.M., W.H. Helgason, y A.M. Ireson, 2019. How spatial patterns of soil moisture dynamics can explain field-scale soil moisture variability: Observations from a sodic landscape. Water Resources Research 55, 4410-4426.

Richardson, P. W., Perron, J. . T., Miller, S. . R., y Kirchner, J. W. 2020. Unraveling the mysteries of asymmetric topography at Gabilan Mesa , California. American Geophysical Union, 0–2. https://doi.org/10.1029/2019JF005378

RIA, Portal de la Red de Inofrmación Agroclimática de Andalucía, IFAPA, https://www.juntadeandalucia.es/agriculturaypesca/ifapa/riaweb/web/ acceso el 27 de juio de 2021

Román-Sánchez, A., Vanwalleghem, T., Peña, A., Laguna, A., y Giráldez, J. V. 2018. Controls on soil carbon storage from topography and vegetation in a rocky, semi-arid landscapes. Geoderma, 311, 159–166. https://doi.org/10.1016/j.geoderma.2016.10.013

Salvucci, G.D., Entekhabi, D. (1995). Ponded infiltration into soils bounded by a water table. Water Resources Research. 31:2751-2759. https://doi.org/10.1029/95WR01954.

Tucker, G.E., Slingerland, R. (1997). Drainage basin responses to climate change. Water Resources Research. 33:2031-2047. https://doi.org/10.1029/97WR00409.

Vachaud, G., Thony, J.-L. (1971). Hysteresis during infiltration and redistribution in a soil column

at different initial water content. Water Resources Research 7:911-920. https://doi.org/10.1029/WR007i001p00111

Chapter 6

Temporal evolution of the piezometric level in a shallow aquifer in granitic soils

TEMPORAL EVOLUTION OF THE PIEZOMETRIC LEVEL IN A SHALLOW AQUIFER IN GRANITIC SOILS

ABSTRACT

The piezometric levels of a hillslope aquifer on a granitic formation have been measured during experimental research on the hydrological, rock weathering, and soil-forming processes, in the Cordovan part of Sierra Morena, near the village of Cardeña, Spain. Tectonic fractures and chemical and biological weathering induce the formation of macropores that enhance the fast circulation of water from the soil surface to the phreatic aquifer through the vadose zone.

The response of the water table to intense rain pulses is very quick. The large period between successive rain events allows the estimation of the Master Recession Curve using the water table fluctuation method, and a first approximation to the aquifer specific yield.

6.1. Introduction

The hillslopes channel the flow of both runoff water on the surface (D'Odorico & Rigon, 2003), and, through their macropores, cracks, and fissures (Jarvis et al., 2016), the infiltrated water through the vadose zone to the water table (Rempe & Dietrich, 2018). The two water flows belong to the Earth System Models discussed by Fan et al. (2019). At the same time, the circulation of water through the porous media reinforces an active chemical front that gradually weathers the vadose zone, contributing to the soil formation (*e.g.,* Brantley et al., 2017).

The groundwater recharge can be related to the occurrence of the rain pulses (e.g., Besbes & de Marsily, 1984). In semi-arid and arid areas, aquifer recharge is discontinuous, resulting from rain pulses (Healy & Cook, 2002). Once in the saturated zone, in the aquifer, water may evaporate into the atmosphere either by upward flows to the surface horizons, or

be absorbed by plant roots, transported to the stomata and, subsequently, transpired to the atmosphere (e.g., Meinzer, 1927; Schenk & Jackson, 2005), although extraction of water from deep aquifers is not very frequent. Alternatively, water can flow in the saturated zone to the aquifer boundary where it will be discharged into the surface fluvial network.

The depth of the water table, therefore, depends on the occurrence of rainfall events. Some works suggested the possible use of it as an indicator of climatic fluctuations (*e.g.*, Miguez-Macho et al., 2008).

The fluctuation of a shallow water table could be used for the estimation of the intensity of evapotranspiration as proposed by White in (1932) and adopted later with some improvements (Healy & Cook, 2002). Crosbie et al. (2005) adopted a time series method for the interpretation of the water table fluctuations, including the influence of some field observations like the Lisse effect (e.g. Weeks, 2002), caused by the presence of air in the aquifer. Later, Cuthbert (2010) introduced the solutions of the Boussinesq equation for water flow to explore not only the rainfall recharge but the slower water movement in the aquifer. The water table fluctuation methods give satisfactory results when compared with other methods for the estimation of watershed recharge (*e.g.* Labrecque et al., 2020).

The hillslope hydrogeology has been based on Boussinesq's equation as Brutsaert (2005, Chap. 10), among other workers properly described. Brutsaert (1994) proposed the use of a solution of one of the several linearization forms of the Boussinesq equation to derive a unit response function. The method was developed by the Ghent University group (*e.g.*, Pauwels & Uijlenhoet, 2018). Thereafter Dralle et al. (2014) integrated the linear Boussinesq equation with an auxiliary function, an exponential of a linear combination of time and space. More recently, Bartlett and Porporato (2018) have applied another function to integrate the same equation differently.

The physical and chemical importance of water flow on the slopes requires special attention in areas where advanced weathering processes can be observed, such as the Cardeña

surroundings in the Sierra Morena in Córdoba. This area can be considered a critical zone according to the accepted definition: "...a living, breathing, constantly evolving boundary layer where rock, soil, water, air, and living organisms interact. These complex interactions regulate the natural habitat and determine the availability of life-sustaining resources, including our food production and water quality" (https://czo-archive.criticalzone.org/national/research/the-critical-zone-1national/), refining the general definition to stress the relevance and the great rate of the weathering processes, as well as the risks posed by the large and frequent drought periods.

The purpose of this chapter is the analysis of the hydrological response of a hillslope to the rain pulses observed in an area of the Sierra Morena from November 2016 to November 2018.

6.2. Material and methods

6.2.1. Study site

The study site is located in Cardeña, northern region of Córdoba, within the Spanish natural park *Sierra de Cardeña y Montoro*, latitude 38.20° N, longitude 4.17° W, and elevation 700 m a.s.l. (Fig.6.1). This site belongs to a private farm, Santa Clotilde, an oak woodland savannah 'dehesa' in which the holm oak (*Quercus Ilex* L.) and annual grasses such as Lolium *sp*., *Bromus sp*., and *Trifolium sp*. are predominant.

The average annual precipitation is 878 mm (from 1981 to 2010) and the mean temperature is 15.3°C, January is the coldest month, with an average of 7°C, and July the hottest, with an average of 25.4°C (Andreu et al., 2013). The reference, or potential, annual average evapotranspiration is not very high due to the altitude of the area, 971 mm, which supports a green vegetation cover throughout most of the year. The climate is classified as Bsk, (semi-arid cold) in the Köppen-Geiger classification (Peel et al., 2007).

The soils in the study area are forming from granodiorite and granite materials of the Los Pedroches batholith(Carracedo et al., 2009). They belong to the Regosol, Leptosol, and Cambisol orders (IUSS Working Group WRB, 2014), or the Lithic Xerorthent subgroup in Soil Taxonomy (Soil Survey Staff, 1999). Their main textural classes are sandy and loamy-sandy, with high stoniness and a thickness between 0.5 and 1.0 m (Román-Sánchez et al., 2018).

Sensors were installed on two opposite north and south-facing slopes, respectively. On the first, a network of three piezometers was set up, figure 6.1 (c) and (d), at a depth of 18.20 m at the hilltop, 9.50 m on the mid slope, and 4.20 m at the hill base. The holes encasing the piezometers have a diameter of 0.076 m and are protected with PVC pipes in the first few meters. In the bottom of the piezometers, a pressure transducer (HOBO, Water level (30.5 m) Data Logger) was placed to measure the fluctuations of the water table and the water temperature at 15-minute intervals. Data was recorded over 2 years, from November 2016 to November 2018. During this period, the hydrological conditions of the site have changed not only due to seasonal cycles but to some intense rainy spells and prolonged droughts.

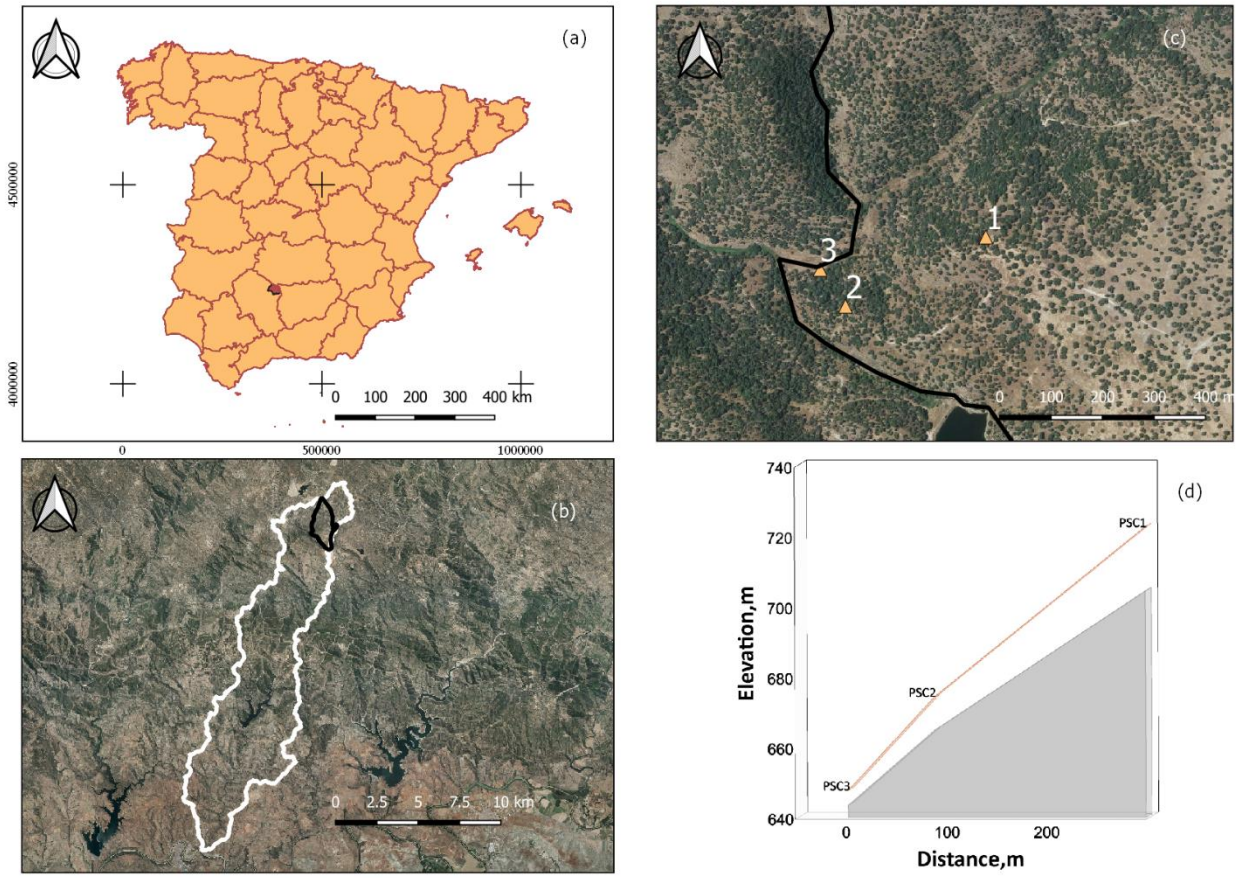

Figure 6.1. (a) Location of the Santa Clotilde farm in southern Spain, and (b) within the Martin Gonzalo watershed (c) the two hillslopes and (d) the longitudinal profile of the hillslope with groundwater flow, pointing out the less permeable bottom of the aquifer.

6.2.2. Estimation of the daily rainfall recharge

To evaluate precipitation-induced recharge, it is necessary first to detract the interception of the vegetation cover. Since the vegetation cover of the experiment site is a dehesa with sparse trees and grasses vegetation cover lasting almost the whole year, threshold values such as those adopted by Laio et al. (2001) of 2 mm for trees and 0.5 mm for grass vegetation can be assumed. A weighted average of 1.5 mm was detracted from the rain depth of every storm event.

The net rainfall water infiltrates into the soil. Given the coarse character of the soil and the rough surface, it is assumed that there is no runoff generated by rain excesses. This hypothesis is supported by the practical absence of runoff flow marks on the site.

The flow of infiltrated water through the soil to the underlying aquifers can be regulated

with a simple model based on a mass balance, or volume, admitting that at ambient temperature the density of the water is constant. Alley (1984) proposed the use of simple models such as the scheme of Thorntwaite and Mather, which reduces the soil to a bucket, similar to that of Milly (1994), but restricting the evapotranspiration rate to a linear function of the available soil moisture. In this way, the actual evapotranspiration rate decreases with the moisture content.

The daily input to the soil profile is the net rainfall, p_{nt}, equal to the rainfall depth, p_t, minus the actual potential evapotranspiration e_{0t}

$$p_{nt} = p_t - e_{0t} \tag{6.1}$$

If the net rainfall is nonnegative, $p_{nt} \geq 0$, the water content of the profile at the end of the day will be

$$\omega_t = \omega_{t-1} + p_{nt} \tag{6.2}$$

Nevertheless, if this value is greater than the maximum field capacity value, there is a recharge, rc_t

$$rc_t = (\omega_{t-1} + p_{nt}) - \omega_0 \tag{6.3}$$

The moisture of the profile is set to the maximum

$$\omega_t = \omega_0 \tag{6.4}$$

And the cumulative potential soil moisture loss is set to zero

$$ce_t = 0 \tag{6.5}$$

If on the contrary there is no recharge, the cumulative water loss is readjusted to the value

$$ce_t = -\omega_0 \ln\left(\frac{\omega_{t-1} + p_{nt}}{\omega_0}\right) \tag{6.6}$$

When the net rainfall is negative, $p_{nt} < 0$, the cumulative potential soil moisture loss increases

$$ce_t = ce_{t-1} - p_{nt} \tag{6.7}$$

There is no recharge, rc_t=0, and the water content in the soil profile will be

$$\omega_t = \omega_0 e^{-ce_t/\omega_0} \tag{6.8}$$

The values for soil moisture, ωt, recharge, rc_t, and cumulative potential water loss, ce_t, are summarized in Table 6.1.

Table 6.1. Recharge and cumulative potential water loss adjust in the model

ω_t	ω_t	rc_t	ce_t
$> \omega_0$	ω_0	$(\omega_{t-1} + p_{nt}) - \omega_0$	0
$\leq \omega_0$	ω_t	0	$ce_t = -\omega_0 \ln\left(\frac{\omega_{t-1} + p_{nt}}{\omega_0}\right)$

Because of the conditions of the study area, the value of potential evapotranspiration measured at the farm's meteorological station is reduced by 75% due to vegetation cover, and the maximum moisture in the 30 cm of the soil profile es estimated at 100 mm, based on the information obtained in the field by Díaz (2020). The excess of soil water is considered the daily recharge rate. There are alternative models which could be useful too (e.g., Sala et al. 1992, Schlaepfer et al. 2012),

6.2.3. A water budget in the aquifer to understand the fluctuations of the water table

The stored water in the aquifer, Scf, changes ΔS_{cf}, considering the baseflow rate, Q_{fb}, evapotranspiration rate from the water table, ET_{cf}, and a change at a fast flow, caused, among other causes by pumping, ΔQ_{cf}. Then the recharge rate, R, all [LT^{-1}], is evaluated as (Healy and Cook, 2002).

$$R = \Delta S_{cf} + Q_{fb} + ET_{Cf} + \Delta Q_{cf} \tag{6.9}$$

The water table fluctuation method, WTF, is based on equation (6.4), when the contribution of baseflow, the evapotranspiration from the water table, and pumping are negligible. A relationship between the recharge rate and the time change of the water table level over the impermeable base, h, [L], time, t, [T], using the specific yield of the aquifer, S_y, is

$$R = S_y \frac{dh}{dt} \approx S_y \frac{\Delta h}{\Delta t} \tag{7.0}$$

Although the specific yield of the aquifer is variable, as Childs (1960) and many other works (e.g. Hilberts et al. 2005, Dietrich et al. 2018) indicated, it could be assumed constant for a large area during a long period. Neuman (1987) strongly recommended the convenience of field measurements for the estimation of accurate specific yield values. For the application of the WTF method, the guidelines of Heppner and Nimmo (2005) refined by Nimmo et al. (2005) and contrasted by Heppner et al. (2007) and Allocca et al. are very convenient, as shown by Heppner et al. (2007) in a wet zone. Nimmo et al. (2015) have refined the method and Allocca et al. (2015) in a karst aquifer in southern Italy among many other hydrologists.

The master recession curve, or MRC, is a characteristic water table recession hydrograph that describes the behavior of the declining piezometric level near the observation site (Heppner and Nimmo 2005). Following the recommendations of Heppner and Nimmo (2005), the data were binned into reduced intervals. The simplest fitting function is a linear regression line with slope β and intercept α

$$\frac{dh}{dt} \approx \frac{\Delta h}{\Delta t} = \alpha + \beta h \tag{7.1}$$

Integrating equation (7.1), with the initial condition of the level h_0, in time t_0, a temporal variation of the piezometric levels is deduced,

$$h = -\frac{\alpha}{\beta} + (\alpha + \beta z_0) e^{\beta (t - t_0)} \tag{7.2}$$

Equation (7.2) is a negative exponential of time similar to equation (16) by Brutsaert (1994), (24) by Dralle *et al.* (2014), or (24) by Bartlett and Porporato (2018), among other works

6.3. Results

6.3.1. Observed data

Figure 6.2 shows the data collected in the study area between November 18, 2016, and November 29, 2018. This period comprised two very dry winters, from the day 65 to 124 for the first one, 2016-17, and the second one, 2017-18, whose drought period was cut by rain spell on February 26, 2018, day 476, that continued intermittently during the spring, greening the whole landscape.

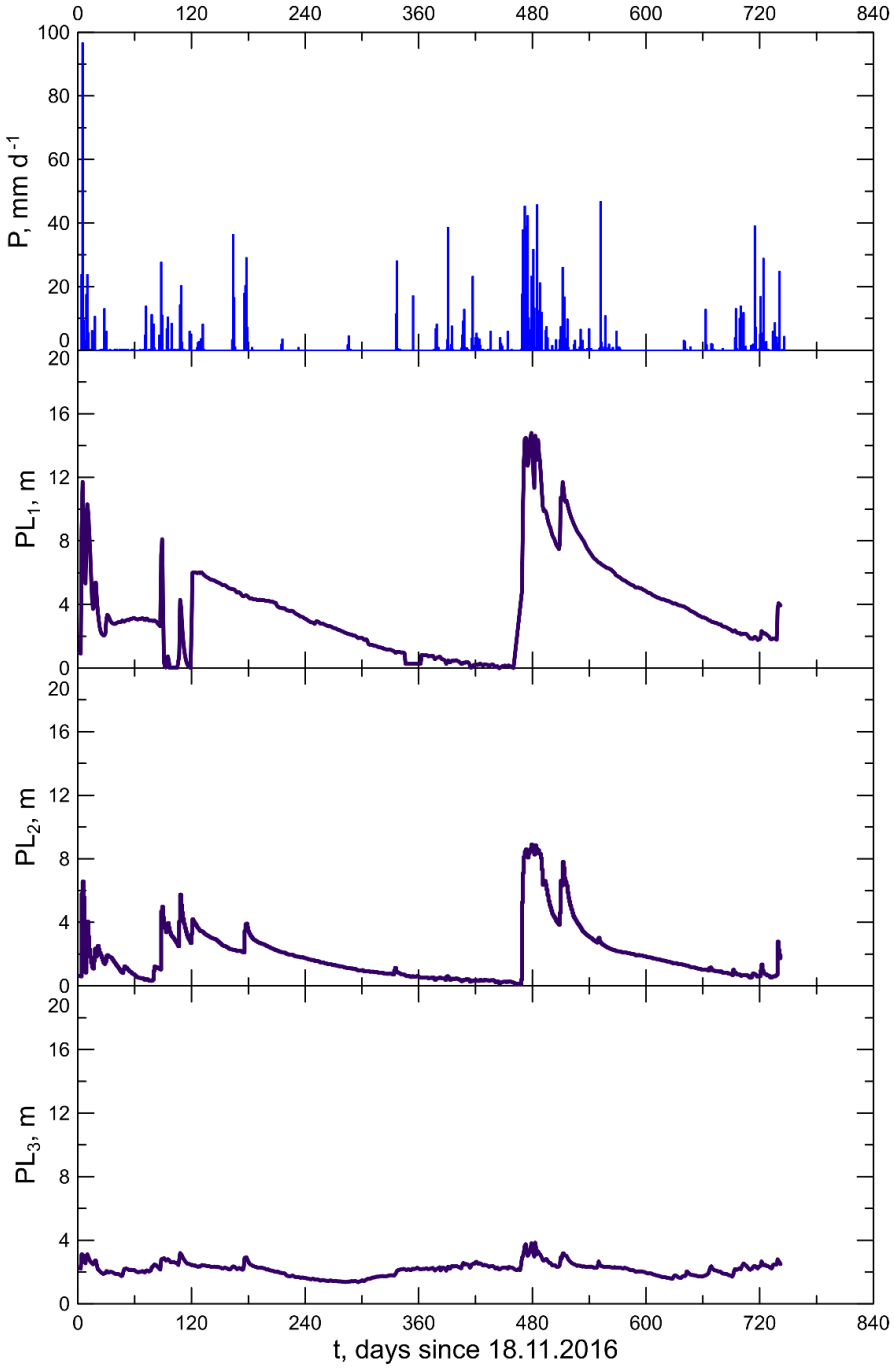

Figure 6.2.Rain pulses and evolution of piezometric levels on the north-facing hillslope.

The rain spell that started at the end of February 2018 had appreciable effects on the piezometric levels, figure 6.2, especially in the piezometers 1 and 2. The connection of Piezometer 3, located at the bottom of the valley very close to the Martín Gonzalo Creek, mitigated changes of the phreatic level.

The level drops in the piezometers 1 and 2 were very similar as figure 6.3 displays. In this figure, the level data have been shifted in time to facilitate visual comparison.

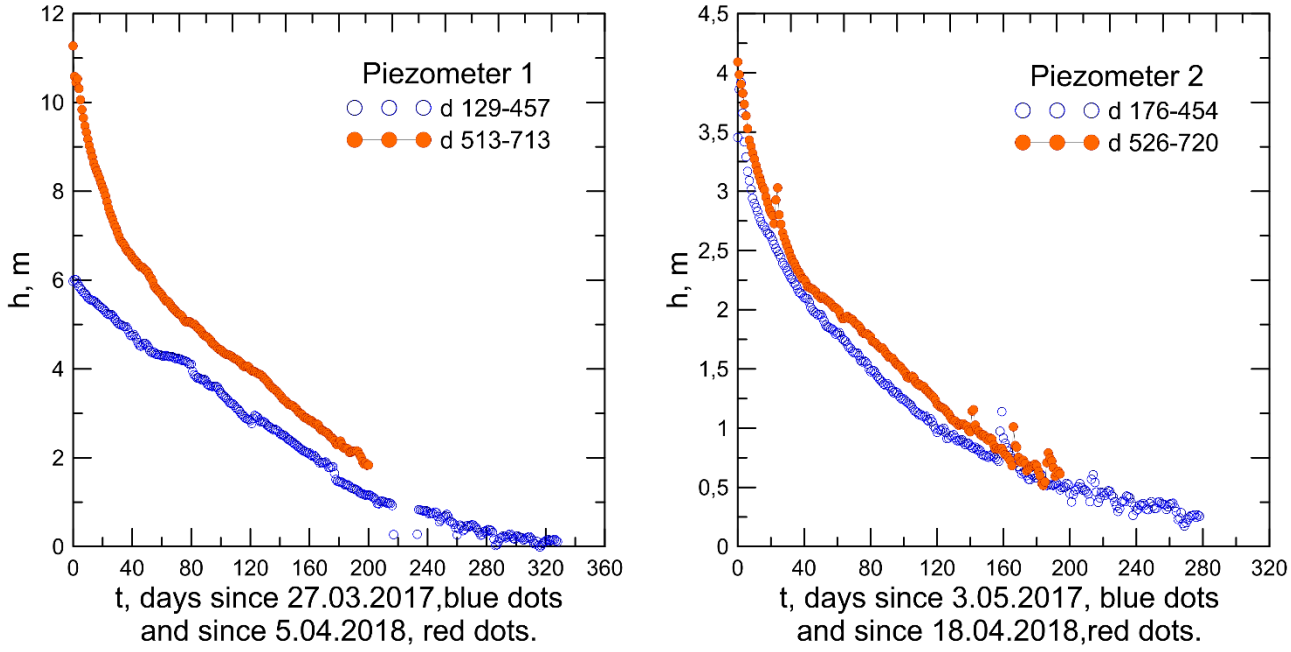

Figure 6.3. Decay of the levels in piezometers 1 (PSC1) and 2 (PSC2), during two drying periods.

6.3.2. Estimated recharge values

The WTF method developed by Heppner y Nimmo (2005) allows a more precise comparison of the behavior of the aquifer in the interval between storms than the visual inspection in figure 6.2. Figure 6.4 represents the relationship between the elevation and the decline rate of water table levels for the periods from 22.03.2017 to 16.02.2018 (days 124 to 465), and from 04.04.2018 to 17.11.2018 (days 512 to 739). The daily data were binned within the same cluster, with some exceptions caused by the amplitude of the daily time scale. A similar figure was obtained by Allocca *et al*. (2015) for the aforementioned aquifer.

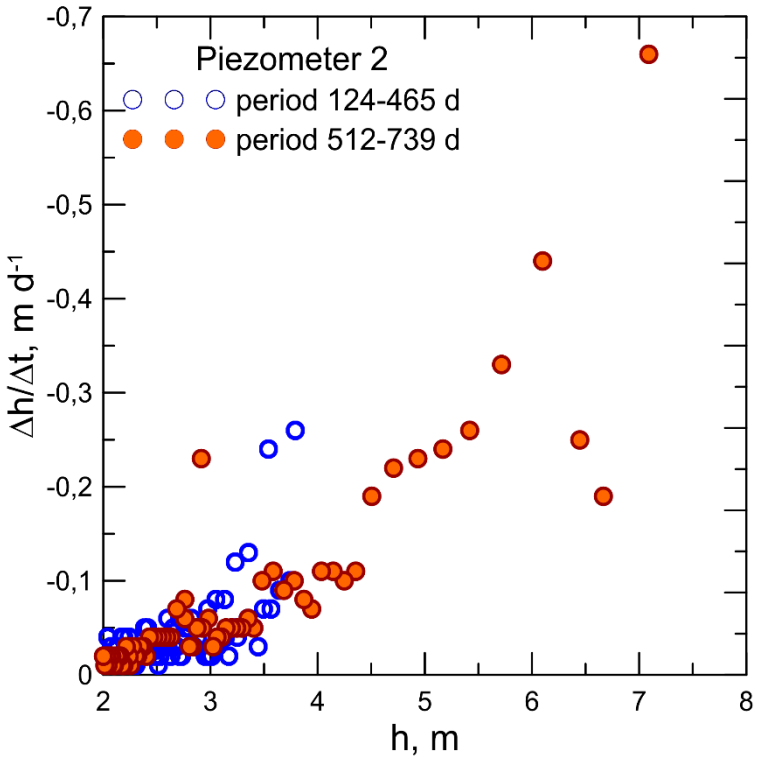

Figure 6.4. Relationships between decline rate and elevation of the water table in the Piezometer 2 for two drying periods, days 124 to 465, and days 512 to 739, measured from November 18 as in figure 6.2, using the WTF method by Heppner y Nimmo (2005).

The estimated parameter values of the MRC are gathered in Table 6.2. The most valuable information was obtained from piezometer 1 in the second low water level period, as well as from the two periods in piezometer 2. The conditions of piezometer 3 under the influence of slope and subalve flows restrict a similar interpretation.

As has been observed in other cases (*e.g.*, Krakauer & Temimi, 2011) the depletion curves, both for discharge and level analysis, are highly variable. Stoelzle et al. (2013) recommended the use of several alternative methods to study the depletion phase of aquifers and Deloitter et al. (2018) the comparison with additional piezometers.

Table 6.2. Parameters of the MRC equation

P	Period	α	β	n	r^2
	d	m d^{-1}	d^{-1}		
1	124-469	-0.0299	-0.0143	12	0.1524
	513-713	0.164	-0.0345	6	0.9386
2	124-465	0.245	-0.102	4	0.8778
	512-739	0.255	-0.0993	4	0.9924
3	108-284	0.0767	-0.046	5	0.7145
	484-628	0.102	-0.058	4	0.9087

P: piezometer; n number of level intervals.

To estimate recharge using the WTF method, the parameter values for the part of the aquifer close to each piezometer shown in Table 6.3 are assumed.

Table 6.3. Values of the parameters of the equation (7.1)

Piezometer	α, m d^{-1}	β, d^{-1}
1	0.164	-.0345
2	0.250	-.0977
3	0.0894	-.0596

Figure 6.5 compares the decline of piezometric levels with the values of the levels and the evolution of cumulative precipitation. It is important to highlight the recharge caused by the first rainfall pulses, particularly that of 21.11.2016 whose rain depth was 96.6 mm which meant an increase of almost 8 m in piezometer 1, which is close to the data collected by Gleeson et al. (2009) in an extreme episode of fast snow melting in aquifers in fractured rock formations in Canada. In the study zone, granitic rock fractures promote preferential flows as described by Nimmo et al. (2017). Although the flow is fast, a part of the percolated volume of water must be retained by the

macropores and fractures walls as well as in the rock matrix as indicated by Bailly-Compte et al. (2010) or by Rathay et al. (2018).

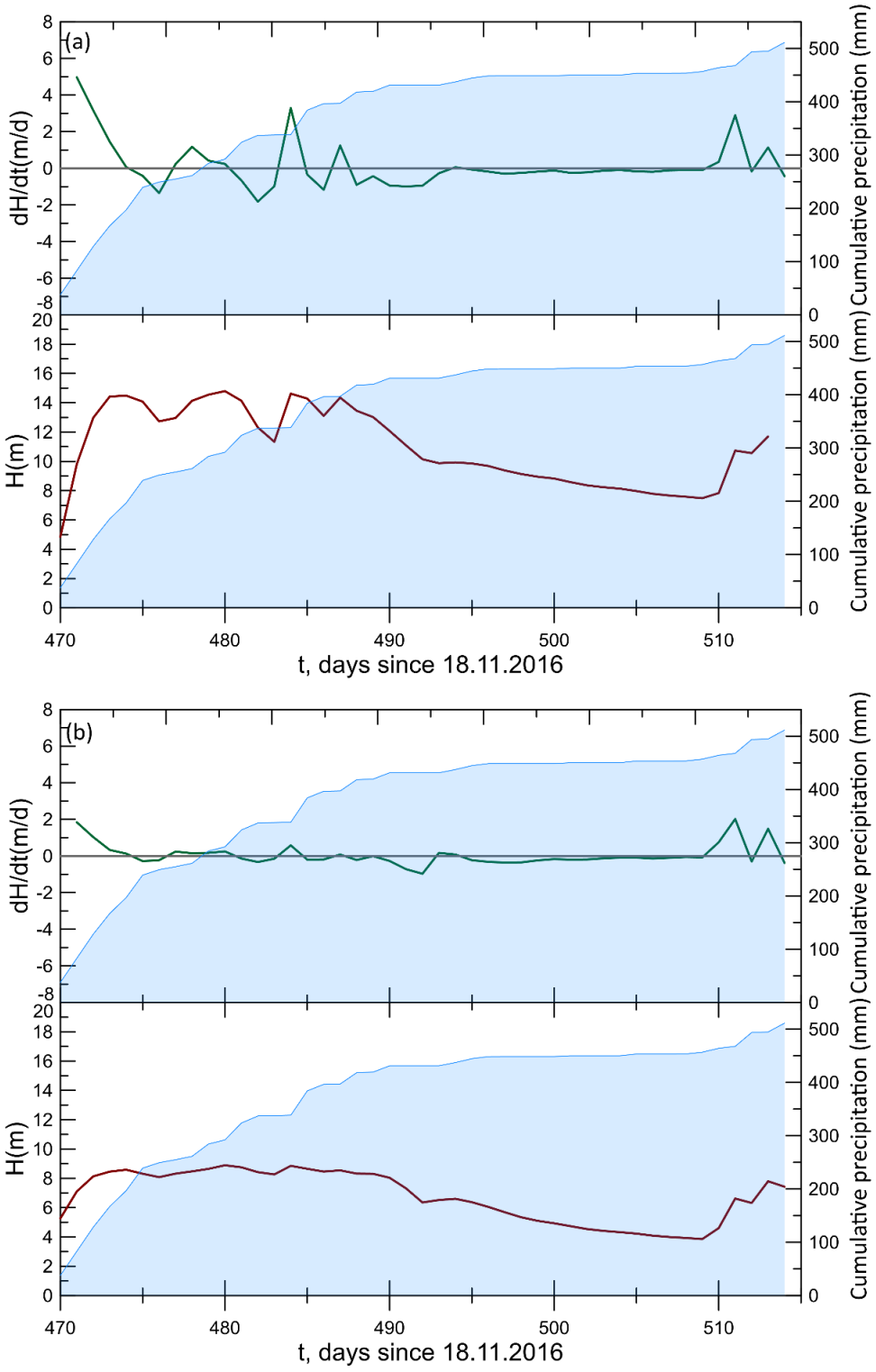

Figure 6.5. Decline (dh/dt) and piezometric levels (h) compared with the cumulative precipitation in the piezometers 1 (a) and 2 (b).

The WTF method would allow to analyze the response of the piezometric levels to the recharge, using a characteristic step-response method as suggested by Besbes and de Marsily (1984) or Kirchner (2009) among many other works. However, without the contrast of the aquifer baseflow rate into the Martín Gonzalo Creek, is not possible to perform a precise analysis.

Equation (7.0) can supply a first estimate of the specific yield of the aquifer. Figure 6.6 compares the calculated specific yield values and the recharge intensity, which could be as moisture index for the vadose zone. The relation of this figure is similar to the relation shown by Acharya et al. (2012 fig, 11), especially figure 6.6 a, although the last one corresponds to steady-state conditions, and the scarcity of data does not allow greater precision.

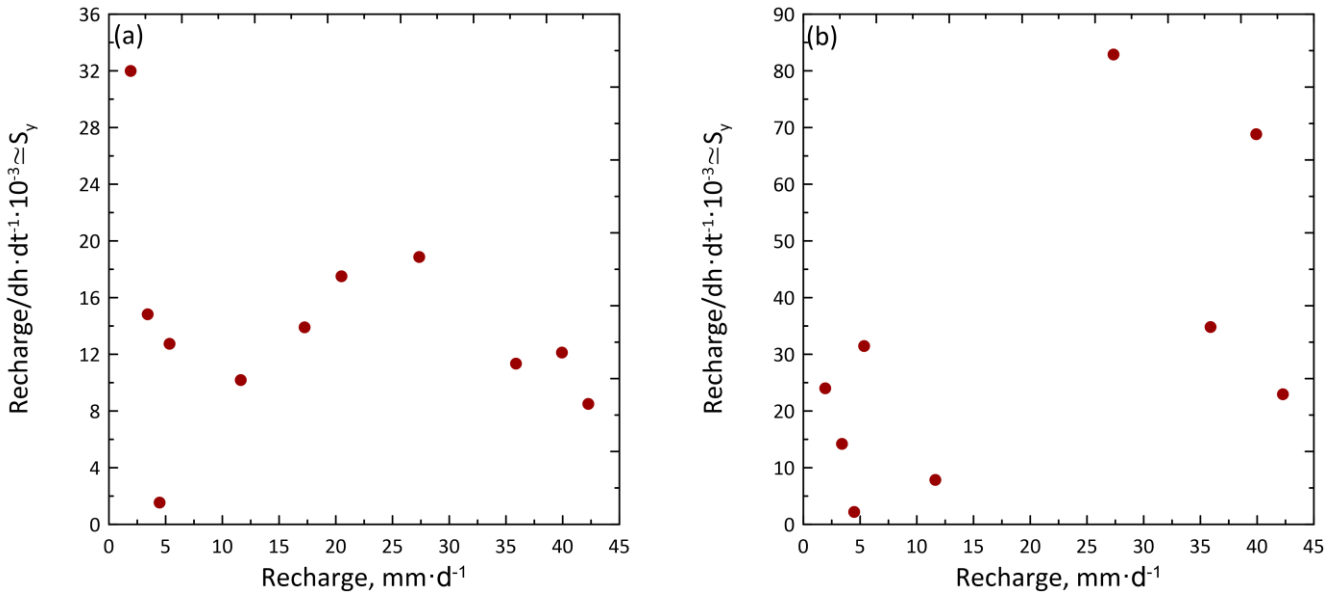

Figure 6.6. Comparison between S_y values and recharge intensity on piezometers 1(a) y 2(b).

The values of the estimated specific yield are low, but close to those collected by Healy y Cook (2002, Table 1), or to those estimated by Chinnasamy et al. (2018) in a Rajasthan roso aquifer. The contribution of the aquifer to the baseflow of the Martin Gonzalo stream can be estimated, also approximately, when in equation (6.9) the recharge value

is zero while the discharge, Q_{fb}, is not. A value of S_y=0.03 has been considered from the data of figure 6.6. The estimation appears in figure 6.7, in which fluctuations are appreciated.

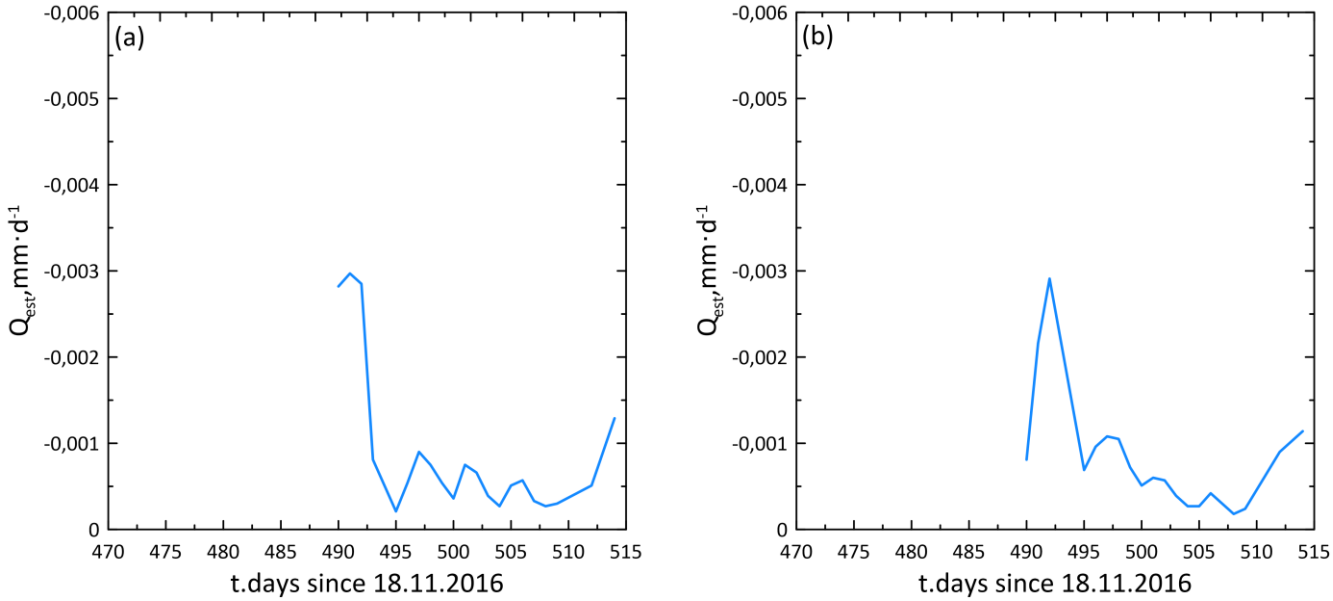

Figure 6.7. Estimation of the discharge flow, baseflow, Q_{fb} from the decline of the levels in the piezometers 1 (a) and 2 (b).

These results are a first approach to be continued the aquifer analysis, and the evaluation of the transit times of the water in it to study the processes of weathering and soil formation in the area, which depend on them (*e.g.*, Maher, 2010).

Although water flow in the hillslope aquifer is fast, rivers and streams that circulate do not usually get dry during low water level periods due to the abundance and complexity of water flow in the watershed aquifers as occurs on a regional scale (*e.g.*, Gleeson et al., 2011).

6.4. Conclusions

Aquifers formed in fractured granite rocks in Mediterranean regions under annual rainfall, around 800 mmyr^{-1}, and reduced average annual potential evapotranspiration due to height, respond quickly to rain pulses, with the fast flow on hillslopes converging

into river valleys. Fortunately for the maintenance of river circulation, the hillslope aquifers constitute only one of the many water inputs of the Sierra Morena.

Analysis of the water budget in both the soil and the underlying aquifer is to understand the behavior of the system, although detailed information is needed to evaluate different processes such as recharge through precipitation and discharge to streams and rivers with greater accuracy.

At a later stage of this work, the information needed to further refine the results noted here will be completed.

6.5. References

Acharya, S., Jawitz, J. W., & Mylavarapu, R. S. (2012). Analytical expressions for drainable and fillable porosity of phreatic aquifers under vertical fluxes from evapotranspiration and recharge. *Water Resources Research*, *48*, 1–15. https://doi.org/10.1029/2012WR012043

Alley, W. M. (1984). On the treatment of evapotranspiration , soil moisture accounting , and aquifer recharge in monthly water balance models. *Water Resources Research*, *20*(8), 1137–1149. https://doi.org/10.1029/WR020i008p01137

Allocca, V., Vita, P. De, Manna, F., & Nimmo, J. R. (2015). Groundwater recharge assessment at local and episodic scale in a soil mantled perched karst aquifer in southern Italy. *Journal of Hydrology*, *529*, 843–853. https://doi.org/10.1016/j.jhydrol.2015.08.032

Andreu, A., Graf, A., Polo, M. J., & González-Dugo, M. P. (2013). Medida de flujos de energía en superficie en un sistema adehesado y análisis de su distribución espacial con vistas a la integración con sensores remotos. In *Estudios en la Zona No Saturada. Vol XI ZNS'13: Vol. XI* (p. 256).

Bailly-Comte, V., Martin, J.B., Jourde, H., Screaton, E.J., Pistre, S., Langston, A. (2010).

Water exchange and pressure transfer between conduits and matrix and their influence on hydrodynamics of two karst aquifers with sinking streams Journal of Hydrology 386:55 66. doi:10.1016/j.jhydrol.2010.03.005

Barlett, M. S., & Porporato, A. (2018). A class of exact solutions of the Boussinesq equation for horizontal and sloping aquifers. *Water Resources Research*, 767–778. https://doi.org/10.1002/2017WR022056

Besbes, M., & de Marsily, G. (1984). From infiltration to recharge:use of parametric transfer function. *Journal of Hydrology*, *74*, 271–293. https://doi.org/10.1016/0022-1694(84)90019-2

Brantley, S. L., Eissenstat, D. M., Marshall, J. A., Godsey, S. E., Balogh-Brunstad, Z., Karwan, D. L., Papuga, S. A., Roering, J., Dawson, T. E., Evaristo, J., Chadwick, O., McDonnell, J. J., & Weathers, K. C. (2017). Reviews and syntheses: On the roles trees play in building and plumbing the critical zone. *Biogeosciences*, *14*(22), 5115–5142. https://doi.org/10.5194/bg-14-5115-2017

Brutsaert, W. (1994). The unit response of groundwater outflow from a hillslope. *Water Resources Research*, *30*(10), 2759–2763. https://doi.org/10.1029/94WR01396

Brutsaert, W. (2005). *Hydrology: an introduction*. Cambridge University Press, Cambridge.

Carracedo, M., Paquette, J. L., Alonso Olazabal, A., Santos Zalduegui, J. F., de García de Madinabeitia, S., Tiepolo, M., & Gil Ibarguchi, J. I. (2009). U-Pb dating of granodiorite and granite units of the Los Pedroches batholith. Implications for geodynamic models of the southern Central Iberian Zone (Iberian Massif). *International Journal of Earth Sciences*, *98*, 1609–1624. https://doi.org/10.1007/s00531-008-0317-0

Childs, E. C. (1960). The nonsteady state of the water table in drained land. *Journal of Geophysical Research*, *65*(2), 780–782. https://doi.org/10.1029/JZ065i002p00780

Chinnasamy, P., Maheshwari, B., Dillon, P., Purohit, R., Dashora, Y., Soni, P., & Dashora, R. (2018). Estimation of specific yield using water table fluctuations and cropped area in

a hardrock aquifer system of Rajasthan, India. *Agricultural Water Management*, *202*, 146–155. https://doi.org/10.1016/j.agwat.2018.02.016

Crosbie, R. S., Binning, P., & Kalma, J. D. (2005). A time series approach to inferring groundwater recharge using the water table fluctuation method. *Water Resources Research*, *41*, 1–9. https://doi.org/10.1029/2004WR003077

Cuthbert, M. O. (2010). An improved time series approach for estimating groundwater recharge from groundwater level fluctuations. *Water Resources Research*, *46*(August 2009), 1–11. https://doi.org/10.1029/2009WR008572

D'Odorico, P., & Rigon, R. (2003). Hillslope and channel contributions to the hydrologic response. *Water Resources Research*, *39*(5), 1–9. https://doi.org/10.1029/2002WR001708

Delottier, H., Pryet, A., Lemieux, J. M., & Dupuy, A. (2018). Estimating groundwater recharge uncertainty from joint application of an aquifer test and the water-table fluctuation method. *Hydrogeology Journal*, *26*, 2495–2505. https://doi.org/10.1007/s10040-018-1790-6

Díaz, A. (2020).Comparación de tasas de infiltración en Dehesa y vegetación natural en Sierra Morena. Universidad de Córdoba.

Dietrich, S., Carrera, J., Weinzettel, P., & Sierra, L. (2018). Estimation of specific yield and its variability by electrical resistivity tomography. *Water Resources Research*, *54*(11), 8653–8673. https://doi.org/10.1029/2018WR022938

Dralle, D. N., Boisrame, G. F. S., & Thompson, S. E. (2014). Spatially variable water table recharge and the hillslope hydrologic response: Analytical solutions to the linearized hillslope Boussinesq equation. *Water Resources Research*, *50*, 8515–8530. https://doi.org/10.1029/eo064i046p00929-04

Gleeson, T., Marklund, L., Smith, L., & Manning, A. H. (2011). Classifying the water table at regional to continental scales. *Geophysical Research Letters*, *38*(5), 1–6. https://doi.org/10.1029/2010GL046427

Gleeson, T., Novakowski, K., & Kurt Kyser, T. (2009). Extremely rapid and localized recharge to a fractured rock aquifer. *Journal of Hydrology*, *376*(3–4), 496–509. https://doi.org/10.1016/j.jhydrol.2009.07.056

Healy, R. W., & Cook, P. G. (2002). Using groundwater levels to estimate recharge. *Hydrogeology Journal*, *10*(1), 91–109. https://doi.org/10.1007/s10040-001-0178-0

Heppner, C. S., & Nimmo, J. R. (2005). A Computer Program for Predicting Recharge with a Master Recession Curve. *US Geological Survey Scientific Investigation Report*, 2005–5172.

Heppner, C. S., Nimmo, J. R., Folmar, G. J., Gburek, W. J., & Risser, D. W. (2007). Multiple-methods investigation of recharge at a humid-region fractured rock site, Pennsylvania, USA. *Hydrogeology Journal*, *15*(5), 915–927. https://doi.org/10.1007/s10040-006-0149-6

Hilberts, A. G. J., Troch, P. A., & Paniconi, C. (2005). Storage-dependent drainable porosity for complex hillslopes. *Water Resources Research*, *41*, 1–13. https://doi.org/10.1029/2004WR003725

IUSS Working Group WRB. (2014). World reference base for soil resources 2014. International soil classification system for naming soils and creating legends for soil maps. In *International soil classification system for naming soils creating legeds for soil maps* (3rd ed.). FAO, Roma.

Jarvis, N., Koestel, J., & Larsbo, M. (2016). Understanding Preferential Flow in the Vadose Zone: Recent Advances and Future Prospects. *Vadose Zone Journal*, *15*(12). https://doi.org/10.2136/vzj2016.09.0075

Kirchner, J. W. (2009). Catchments as simple dynamical systems: Catchment characterization, rainfall-runoff modeling, and doing hydrology backward. *Water Resources Research*, *45*(2), 1–34. https://doi.org/10.1029/2008WR006912

Krakauer, N. Y., & Temimi, M. (2011). Stream recession curves and storage variability in small watersheds. *Hydrology and Earth System Sciences*, *15*(7), 2377–2389.

https://doi.org/10.5194/hess-15-2377-2011

Labrecque, G., Chesnaux, R., & Boucher, M. A. (2020). Water-table fluctuation method for assessing aquifer recharge: application to Canadian aquifers and comparison with other methods. *Hydrogeology Journal*, *28*(2), 521–533. https://doi.org/10.1007/s10040-019-02073-1

Laio, F., Porporato, A., Ridolfi, L., & Rodriguez-Iturbe, I. (2001). Plants in water-controlled ecosystems: active role in hydrologic processes and response to water stress. II. Probabilistic soil moisture dynamics. *Advances in Water Resources*, *24*, 707–726. https://doi.org/10.1016/S0309-1708(01)00005-7

Maher, K. (2010). The dependence of chemical weathering rates on fl uid residence time. *Earth and Planetary Science Letters*, *294*(1–2), 101–110. https://doi.org/10.1016/j.epsl.2010.03.010

Meinzer, O. E. (1927). Plants As Indicators of Ground Water. In *US Geologycal Survey Water Supply paper* (Vol. 579). US Dept. of Interior.

Miguez-Macho, G., Li, H., & Fan, Y. (2008). Simulated water table and soil moisture climatology over North America. *Bulletin of the American Meteorological Society*, *89*(5), 663–672. https://doi.org/10.1175/BAMS-89-5-663

Milly, P. C. D. (1994). Climate,soil water storage, and the average annual water balance. *Water Resources Research*, *30*(7), 2143–2156. https://doi.org/10.1029/94WR00586

Neuman, S. P. (1987). *On methods of determining specific yield* Ground Water 25: 679–684. https://doi.org/10.1111/j.1745-6584.1987.tb02208.x

Nimmo, J. R., Creasey, K. M., Perkins, K. S., & Mirus, B. B. (2017). Preferential flow, diffuse flow, and perching in an interbedded fractured-rock unsaturated zone. *Hydrogeology Journal*, *25*(2), 421–444. https://doi.org/10.1007/s10040-016-1496-6

Nimmo, J. R., Horowitz, C., & Mitchell, L. (2015). Discrete-storm water-table fluctuation method to estimate episodic recharge. *Groundwater*, *53*(2), 282–292.

https://doi.org/10.1111/gwat.12177

Pauwels, V. R. N., & Uijlenhoet, R. (2018). Confirmation of a Short-Time Expression for the Hydrograph Rising Limb of an Initially Dry Aquifer Using Laboratory Hillslope Outflow Experiments. *Water Resources Research*, *54*(12), 10,350-10,361. https://doi.org/10.1029/2018WR023580

Peel, M. C., Finlayson, B. L., & McMahon, T. A. (2007). Updated world map of the Köppen-Geiger climate classification. *Hydrology and Earth System Sciences*, *11*, 1633–1644. https://doi.org/10.5194/hess-11-1633-2007

Rathay, S.Y., Allen, D.M., Kirste, S. (2018). Response of a fracured bedrock aquifer to recharge from heavy rainfall. Journal of Hydrology 561:1048-1062. https://doi.org/10.1016/j.jhydrol.2017.07.04.

Rempe, D. M., & Dietrich, W. E. (2018). Direct observations of rock moisture, a hidden component of the hydrologic cycle. *Proceedings of the National Academy of Sciences*, *115*(11), 2664–2669. https://doi.org/10.1073/pnas.1800141115

Román-Sánchez, A., Vanwalleghem, T., Peña, A., Laguna, A., & Giráldez, J. V. (2018). Controls on soil carbon storage from topography and vegetation in a rocky, semi-arid landscapes. *Geoderma*, *311*, 159–166. https://doi.org/10.1016/j.geoderma.2016.10.013

Sala, O.E., Lauenroth, W.K., & Parton, W.J. (1992). Long-term soil water dynamics in the shortgrass steppe. Ecology 73:1175-1181. https://doi.org/10.2307/1940667

Schenk, H. J., & Jackson, R. B. (2005). Mapping the global distribution of deep roots in relation to climate and soil characteristics. *Geoderma*, *126*, 129–140. https://doi.org/10.1016/j.geoderma.2004.11.018

Sclaepfer, D.R., Lauenroth, W.K., Bradford, J.B. (2012). Ecohydrological niche of sagebrush ecosystems. Ecohydrology 5:453-466. doi:10.1002/eco.238.

Soil Survey Staff. (1999). Soil Taxonomy: A basic system of soil classification for making

and interpreting soil surveys. In *USDA Agr. Hbk.* (2º, Issue 436). USDA,NRS,Washington. https://doi.org/10.1007/BF01574372

Steenhuis, T. S., & Van der Molen, W. H. (1986). The Thornthwaite-Mather procedure as a simple engineering method to predict recharge. *Journal of Hydrology*, *84*, 221–229. https://doi.org/10.1016/0022-1694(86)90124-1

Stoelzle, M., Stahl, K., & Weiler, M. (2013). Are streamflow recession characteristics really characteristic? *Hydrology and Earth System Sciences*, *17*(2), 817–828. https://doi.org/10.5194/hess-17-817-2013

Weeks, E. P. (2002). The Lisse effect revisited. In *Ground Water* (Vol. 40, Issue 6, pp. 652–656). https://doi.org/10.1111/j.1745-6584.2002.tb02552.x

White, W.N. (1932). A method of estimating ground-water supplies based on discharge by plants and evaporation from soil: Results of investigations in Escalante Valley, Utah. U.S. Geol. Surv. Water-Supply pap. 659-A, U.S. Government Printing Office, Washington, D.C.

Chapter 7

Could temperature indicate the evolution of soil moisture?

COULD TEMPERATURE INDICATE THE EVOLUTION OF SOIL MOISTURE?

ABSTRACT

The use of heat as a hydrogeological tracer in phreatic aquifers is widely accepted. Nevertheless, heat has not been frequently used as a tracer of soil water except for a few cases. In this report, an analysis of the simultaneous evolution of soil moisture and temperature has been made to explore the feasibility of the use of heat as a tracer of the water recharge in the profiles of several soils formed on decaying granites in a watershed of the Sierra Morena near the village of Cardeña in southern Spain.

Some solutions of the heat convection-diffusion equation under steady-state conditions have been applied to the estimation of the apparent thermal diffusivity of the soil and the average water recharge.

The results show that the estimation of the apparent thermal diffusivity gives reasonable results whereas the estimation of the average water recharge yields greater values than what was expected.

Furthermore refined treatments are required to get more accurate estimations of the average soil water recharge.

7.1. Introduction

The net radiation incident on the soil surface induces a heat flow on it, mainly carried by conduction by the direct contact between particles. This process is characterized by two characteristic soil parameters, the capacity to transfer heat, the thermal conductivity, λ, ($Wm^{-1}K^{-1}$), which depends on the geometrical disposition of the particles and their respective contributions, as initially proposed by de Vries (1963), (see also Tarnawski and Leong 2016), and the volumetric heat capacity of the soil, C_s, ($Jm^{-3}K^{-1}$), which represents the specific energy required to increase the temperature, T, (C), per unit of volume. The equation that describes the temporal evolution of the soil profile temperature, at time t, and depth z, Eq. 7.1, is a

typical diffusion equation, in which it is commonly admitted that the thermal conductivity does not vary in the process of heat conduction. Both the thermal conductivity and the heat capacity are combined in the thermal diffusivity, with the adjective apparent, due to its integrating character of the edaphic conditions, κ (m^2s^{-1}).

$$\frac{\partial T}{\partial t} = \frac{\lambda}{C_s}\frac{\partial^2 T}{\partial z^2} \equiv \kappa \frac{\partial^2 T}{\partial z^2} \tag{7.1}$$

When rainfall water infiltrates the soil, its temperature is usually different from that of the soil solution, inducing a heat flow with the subsequent change in the thermal profile. The energy input is represented in equation (7.2) by the density of water flux, q, the heat capacity of water, C_w, as well as by variation of thermal diffusivity to temperature, $\partial\kappa/\partial T$, combined in a parameter, W (ms^{-1}), called apparent heat convection parameter.

$$W = \frac{C_w}{C_s} q - \frac{\partial \kappa}{\partial z} \tag{7.2}$$

With this convective flow, equation (7.1) becomes

$$\frac{\partial T}{\partial t} = \kappa \frac{\partial^2 T}{\partial z^2} - W \frac{\partial T}{\partial z} \tag{7.3}$$

Figure 7.1 shows the temperature evolution in one of the measurement profiles that will be described in the Material and methods section, comparing the soil and air data, from February 28 to March 13, 2018, when, after a prolonged autumn and winter drought, a rain spell of several days occurred. The soil thermal changes with rain are evident in figure 7.1.

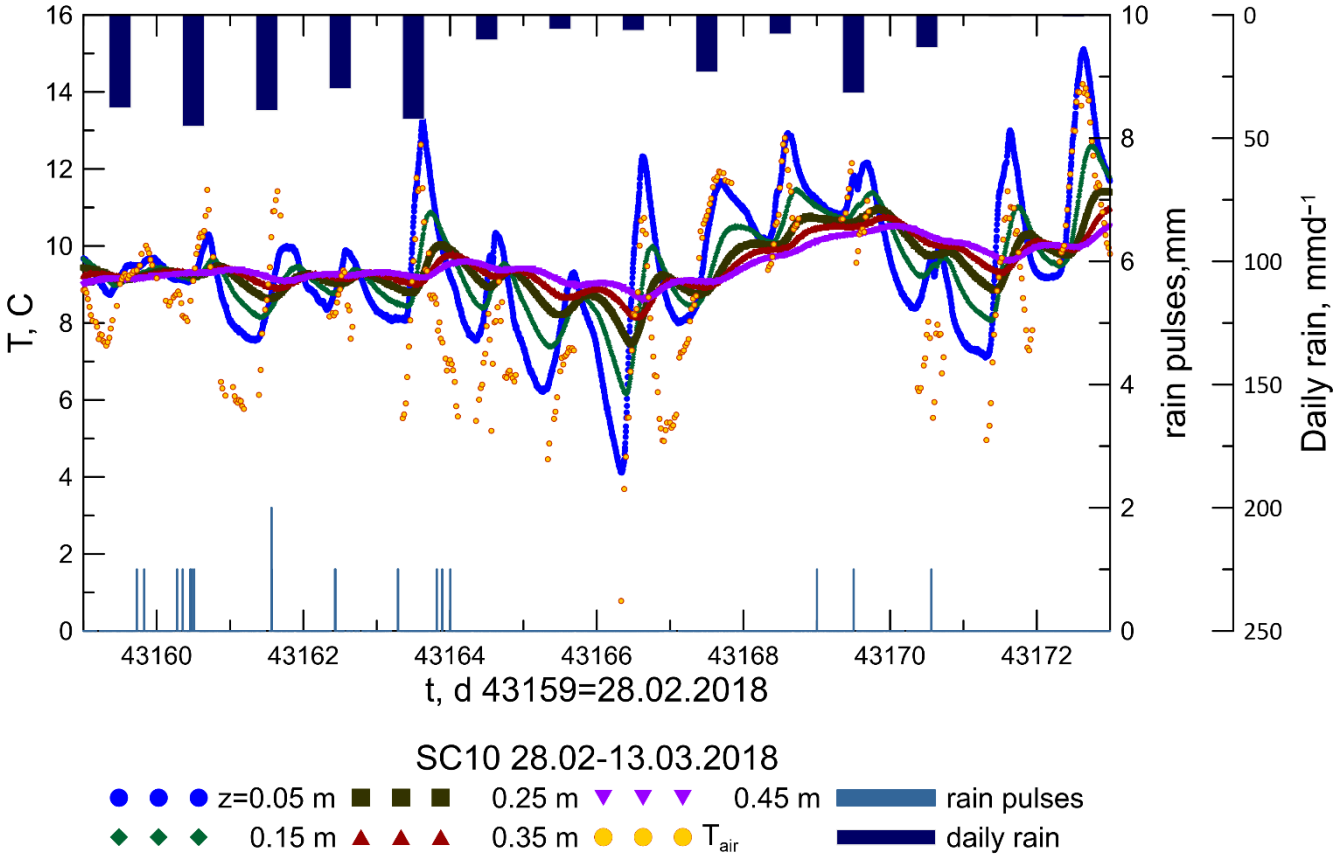

Figure 7.1. Precipitation and temperature evolution at the surface and different depths in the SC10 soil profile.

Petroleum geophysicists had observed in the 1930s that the flow of water and other fluids modified the thermal gradients in the Earth's crust as indicated by Bredehoeft and Papadopoulos (1965). Almost simultaneously, but apparently in an independent form, Stallman (1965) and Suzuki (1960) proposed the analysis of soil temperature to estimate the vertical flow of water in the soil, applying an apposite solution to the heat conduction-convection equation that was in the book of Carslaw and Jaeger (1959 § 15.2.III). In his work Stallman (1965) suggested that the detection limit of this method was about 3 mm d^{-1}. Is it possible to use it on shallow measurements of soil temperature measured in the field?

In this work, some observations from a field trial are analyzed with the solution of the heat conduction-convection equation to estimate the value of its parameters and to check the recharge or discharge rates on them.

7.2. Material and methods

7.2.1. Characteristics of the field trial

Between June and July 2016, in a private farm, Santa Clotilde, an oak woodland savannah or 'dehesa' located in Cardeña, southern Spain, latitude 38.20° N, longitude 4.17° W, and elevation 700 m a.s.l., a capacitance sensor network measuring moisture, temperature, and the electric conductivity of soil solution, CS655 (Campbell Scientific), was installed and started recording on 24.11.2016. The sensors were located at different depths (0.05, 0.15, 0.25, 0.35, and 0.45m) along two convergent slopes, north-south, in seven locations SC-10 to SC-4. Measurements were recorded half-hourly. Solar panels with a maximum power of 15 W at 12 V provide the required energy for maintenance and data recording.

Climatic data, daily precipitation, and air temperature were recorded by an automated weather station installed by the Andalusian Institute of Agriculture Research and Training (IFAPA) in an area close to the study site. Additional rainfall information was supplied by rain gauges installed near the soil pits, every 10-min.

7.2.2. Soil heat conduction-convection equation

Although in some cases the recharge has been assumed to vary temporally sinusoidally (e.g. Wang et al., 2012), the available precipitation data recommended the use of daily pulses. A sinusoidal variation of temperature at the soil surface described as a Fourier series with several harmonic terms with a mean value T_0, an amplitude An, and a phase angle ϕ_n for each harmonic n is admitted.

$$T(0,t) = T_0 + \sum_{n=1}^{nh} A_n \cos(n\omega t + \varphi_n) \quad (7.4)$$

The solution of the heat conduction-convection equation subject to condition (7.4) was presented by Carslaw and Jaeger (1959, 15.2.14)

$$T(z,t) = T_0 + \sum_{n=1}^{nh} \Xi_n(z)\, cos[\Omega_n(z,t)] \tag{7.5}$$

with

$$\Xi_n(z) = A_n exp\left[\frac{Wz}{2\kappa}(1-\alpha)\right]$$
$$\Omega_n(z,t) = n\omega t + \varphi_n - \frac{W\beta_n z}{2\kappa} \tag{7.6}$$

The parameters α_n and β_n are

$$\alpha_n = 2^{-1/2}\left\{\left[1 + \left(\frac{4\kappa n\omega}{W^2}\right)^2\right]^{1/2} + 1\right\}^{1/2} \tag{7.7}$$
$$\beta_n = (\alpha_n^2 - 1)^{1/2}$$

The value of both parameters, the apparent thermal diffusivity,κ, and the apparent heat convection parameter, W, were estimated by minimizing the sum of the square of the differences between measured and calculated temperatures for the level immediately below the surface. This solution has been used in other hydrological problems such as the attenuation of water flow fluctuations in soil (Bakker & Nieber, 2009).

However, in many cases, a single harmonic may be sufficient to adjust the temperature evolution at the soil surface. Thus, the estimation of the parameter values, W and κ is simplified as advanced by Gao et al. (2003) and Gao (2005) although their solutions are incomplete misprint. This method was first proposed by Suzuki (1960) for the estimation of the water percolation rate in a paddy field and extended later with greater detail by Stallman (1965) for the assessment of the seepage rate from water channels and the return flow from irrigated areas. In this method, the semi-amplitudes, A_1, and A_2, and the phase angles, Φ_1 and Φ_2, observed in the evolution of daily soil temperatures at the respective depths z_1 and z_2 were related to the parameters of the conductive, κ, and convective heat flow, W. Therefore, from the semi-amplitudes

$$A_1 = \Xi_1(z_1) \quad A_2 = \Xi_1(z_2) \tag{7.8}$$

and from the phase angles

$$\Phi_1 = \Omega_1(z_1, 0) \quad \Phi_2 = \Omega_2(z_2, 0) \tag{7.9}$$

The logarithm of the respective ratio can be written as ζ

$$\zeta = \frac{\ln(A_1/A_2)}{z_1 - z_2} = \frac{W}{2\kappa}(1 - \alpha) \tag{7.10}$$

and the gradient of the phase angle, parameter η

$$\eta = \frac{\Phi_1 - \Phi_2}{z_1 - z_2} = \frac{W}{2\kappa}\beta \tag{7.11}$$

Equations 7.10 and 7.11 are a system of equations whose unknowns, the values of the parameter, κ, and W can be found.

However, as Carslaw and Jaeger (1959) warned, these solutions are valid when a steady-state regime has been reached. Wiltshire (1982, 1983) explored in detail the more general solution of heat conduction in the soil. Philip (1973) explained the possible errors due to the assumption of a constant apparent thermal diffusivity value especially in dry soils or arid regions.

In the case of rainless, the apparent thermal diffusivity may be estimated by one of the methods suggests by Horton et al. (1983), such as the amplitude difference method, which was successfully used by Verhoef et al. (1996) in their field campaign. The amplitude difference method is based on a solution to the diffusive heat flow equation without convection, Carslaw, and Jaeger (1959, § 2.6.18)

$$T(z,t) = T_0 + \sum_{n=1}^{nh} A_n exp\left[\frac{z}{z_{an}}\right] \cos\left[n\omega t + \varphi_n - \frac{z}{z_{an}}\right] \tag{7.12}$$

In which the depth of damping, z_{an}, is

$$z_{an} = \left(\frac{2\kappa}{n\omega}\right)^{1/2} \tag{7.13}$$

In the case of a single harmonic an expression for estimating the value of the apparent thermal diffusivity is (Horton et al., 1983)

$$\kappa = \frac{\omega}{2}\left[\frac{z_2 - z_1}{\ln(A_1/A_2)}\right]^2 \tag{7.14}$$

7.3. Results

The daily average temperature of the air showed two distinct drops that were detected in the mean soil temperatures, as shown in Fig.7.2.

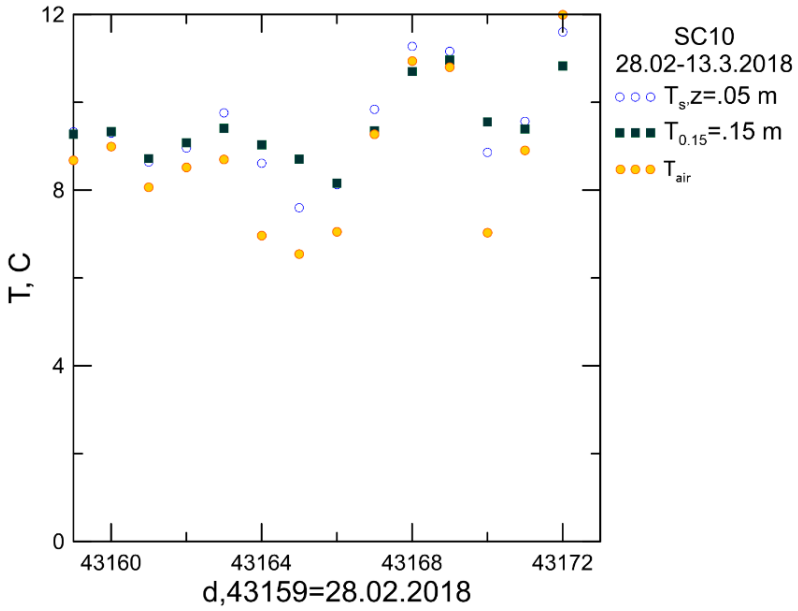

Figure 7.2. Mean temperatures of air and upper soil horizons at SC10.

Soil temperature is very dependent on external weather conditions, as illustrated below.

The effect of the sudden drop of the air temperature was detected in the soil profiles at SC10 location, although not in soil moisture, at least on March 5,6, 11, and 12, 2018, as is shown in Fig. 7.3.

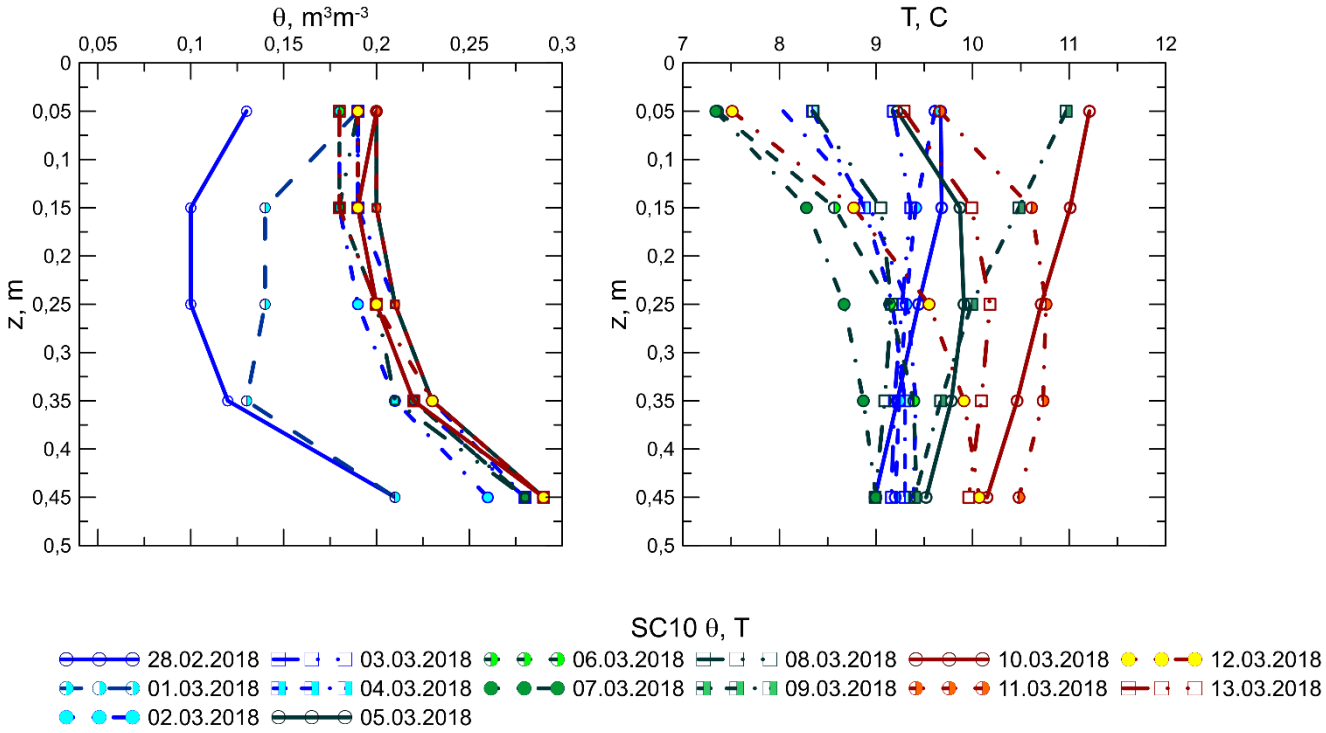

Figure 7.3. SC10 soil moisture and temperature profiles measured at midnight.

The temperature of the closest point to the surface, 0.05 m depth, was adopted as the surface temperature, given its proximity to the atmosphere. The estimated values of the parameters are shown in table 7.1 from the half-hourly measured temperature at the depth of 0.15 m. The estimated value of the parameters W and κ shown in Table 7.2 were obtained with the measured data of February 28, 2018, whose profile was selected from those plotted in Fig. 7.1 and 7.3. Figure 7.4 permits a comparison of the goodness of fit. The surface temperature fit with 4 harmonics allows a better approximation to the measured temperature, but with a higher computational effort, without a remarkable difference.

Table 7.1. Average temperature, T_0, semiamplitudes, A_i, and phase angle ϕ_i, of the daily soil temperature measured at 0.15 m depth, site SC10, day 28.02.2018.

Harmonics, i	T_0, C	Ai, C	ϕ_i
	9.33		
1		.387	.721
2		.148	-1.16
3		.039	1.59
4		.006	2.31

Table 7.2. Fourier series fit parameters to surface soil temperature, site SC10, day 28.02.2018

Harmonics	W, md^{-1}	κ, m^2d^{-1}	e_{NS}
1	.160	.099	.758
4	.275	.065	.844

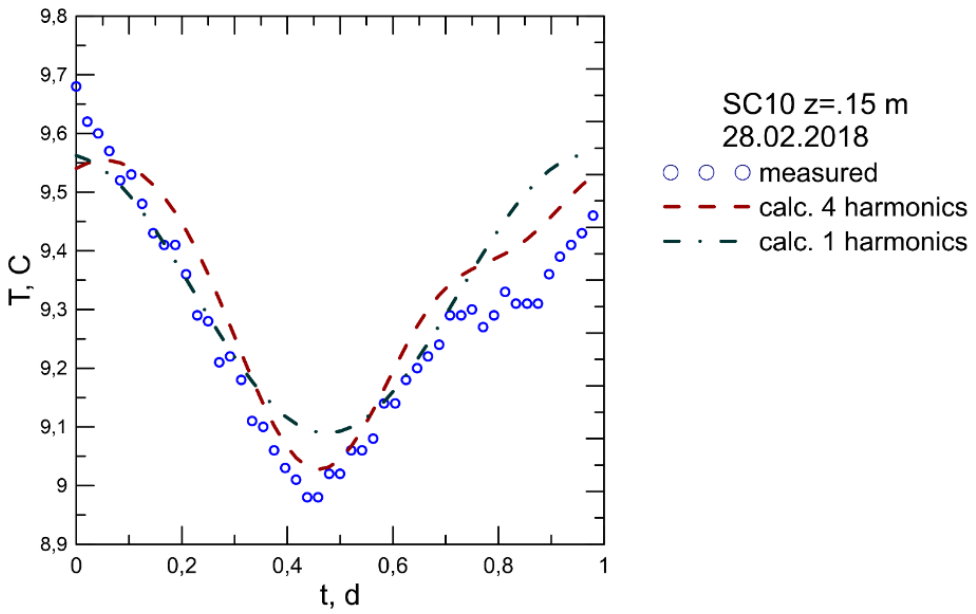

Figure 7.4. Comparison of temperatures measured at 0.15 m depth at site SC10 on February 28, 2018, with the values obtained with the solution of the convective and diffusive heat flow equation from the one- and four-harmonic surface temperature fit.

The values of the convection coefficient *W*, given in Table 7.2 are high because, considering a volumetric heat capacity for water C_w=4.18 MJ $m^{-3}K^{-1}$, and for soil C_s=2.0 MJ $m^{-3}K^{-1}$, and,

assuming a depth uniform apparent thermal diffusivity, the value of the estimated soil water recharge is about q=76 mm d^{-1} using a single harmonic and q=130 mm d^{-1} with the four harmonics, which are higher than the registered precipitation. Precipitation can indeed vary locally and that water flow can be concentrated in soil macropores, but even so, these results are excessive. Interestingly Hu et al. (2016) obtained results of the same order, 206 mm d^{-1}, but, although their goodness of the fit analysis was apparently satisfactory they did not present the measured water recharge rate.

7.3.1. Evolution of thermal apparent diffusivity estimated from soil temperature data measured at location SC10

Using the diffusivity expression, we have obtained the data shown in Fig. 7.5:

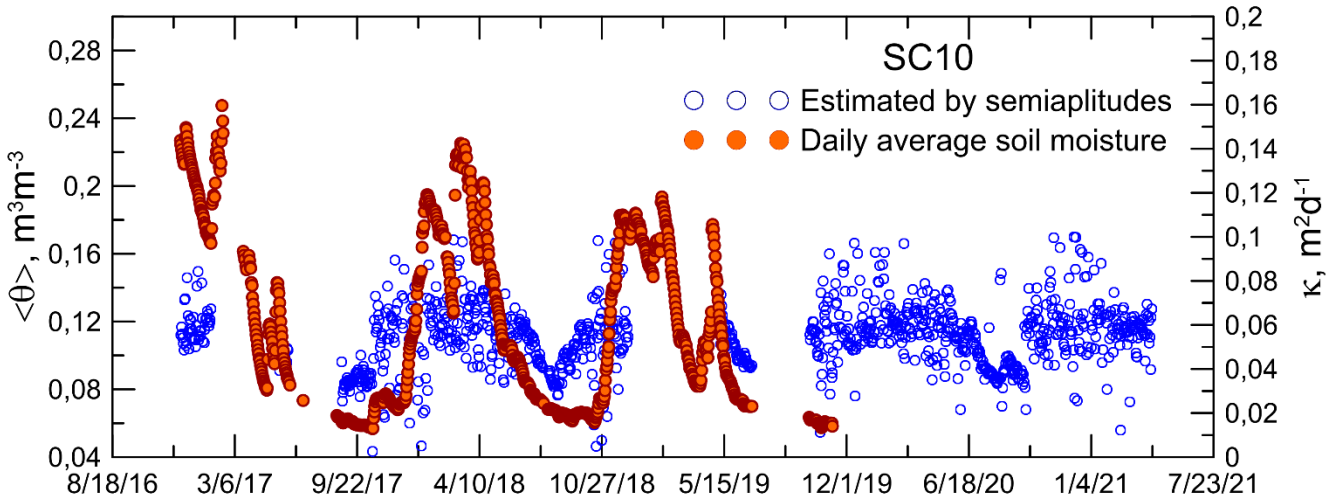

Figure 7.5. Evolution of the estimated apparent thermal diffusivity in the surface 0.15 m of the soil at site SC10, and of the mean soil moisture in the profile.

The apparent thermal diffusivity fluctuates with soil moisture as already indicated by de Vries (1963). If both magnitudes are compared as shown in Fig.7.6, a relationship very similar to that obtained by Jackson and Kirkham (1958) was found.

These results seem to confirm that the estimates of the apparent thermal diffusivity of the soil deduced from the in situ temperature measurements are reasonable, which also implies the goodness of the data obtained by the sensors.

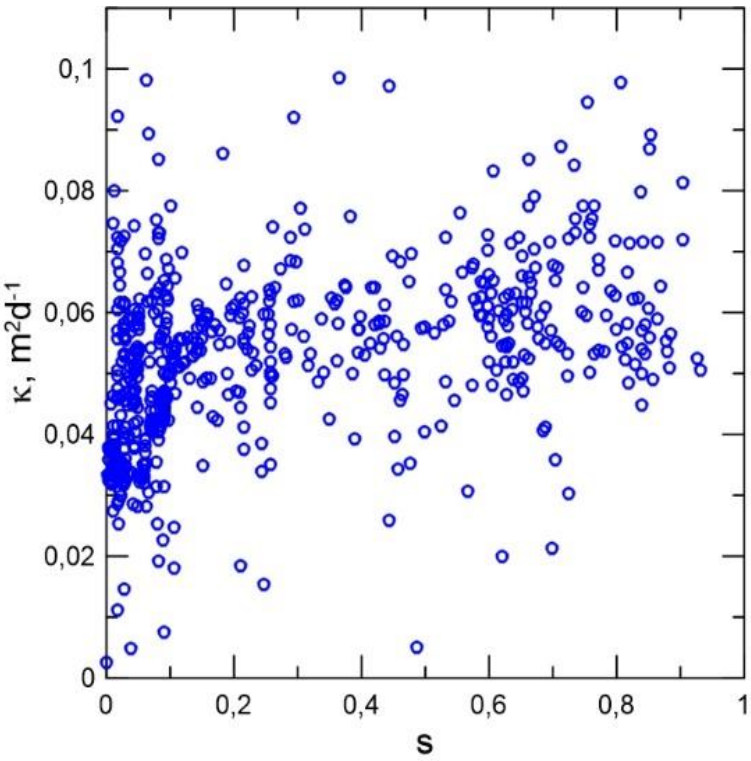

Figure 7.6. Relation between the estimated apparent thermal diffusivity in the surface 0.15 m with the effective saturation ratio.

7.4. Conclusions

Although the estimation of the apparent heat convection parameter with the solution of the heat conduction-convection equation in the soil assuming steady-state conditions is overestimated, both this solution and that of heat transport by conduction allow the evaluation of the apparent thermal diffusivity of the soil from the temperature data measured by the sensors in the field.

The estimation of the soil water recharge with thermal measurements requires a more detailed analysis.

The apparent thermal diffusivity data showed the influence of soil moisture is reasonably considered.

7.5. References

Bakker, M., & Nieber, J. L. (2009). Damping of sinusoidal surface flux fluctuations with soil depth. *Vadose Zone Journal*, *8*(1), 119–126. https://doi.org/10.2136/vzj2008.0084

Bredehoeft, J. D., & Papadopulos, I. S. (1965). Rates of vertical groundwater movement estimated from the Earth's thermal profile. *Water Resources Research*, *1*(2), 234–236. https://doi.org/10.1029/WR001i002p00325

Carslaw, H. S., & Jaeger, J. C. (1959). *Conduction of heat in solids* (2º ed.). Clarendon Press, Oxford.

Churchill, R. V., Brown, J. W., & Verhey, R. F. (1974). *Complex variables and applications* (3ª ed.). McGraw-Hill, New York.

de Vries, D. A. (1963). Thermal properties of soils. In W. R. van Dijk (Ed.), *Physics of the plant environment* (pp. 210–235). North Holland, Amsterdam.

Gao, Z., Fan, X., & Bian, L. (2003). An analytical solution to one-dimensional thermal conduction-convection in soil. *Soil Science*, *168*, 99–107. https://doi.org/10.1097/00010694-200302000-00004

Gao, Z. (2005). Determination of soil heat flux in a Tibetan short-grass prairie, *Boundary-Layer Meteorology* 114: 165-178. https://doi.org/10.1007/s10546-004-8661-5

Horton, R., & Wierenga, P. J. (1983). Estimating the soil heat flux from observations of soil temperature near the surface.*Soil Science Society of America Journal* 47: 14-20 https://doi.org/10.2136/sssaj1983.03615995004700010003x

Horton, R., Wierenga, P. J., & Nielsen, D. R. (1983). Evaluation of methods for determining the apparent thermal diffusivity of soil near the surface. *Soil Science Society of America Journal*, *47*(1), 25–32. https://doi.org/10.2136/sssaj1983.03615995004700010005x

Hu, G., Zhao, L., Wu, X., Li, R., Wu, T., Xie, C., Qiao, Y., Shi, J., Li, W., & Cheng, G. (2016). New Fourier-series-based analytical solution to the conduction-convection equation to calculate

soil temperature, determine soil thermal properties, or estimate water flux. *International Journal of Heat and Mass Transfer*, *95*, 815–823. https://doi.org/10.1016/j.ijheatmasstransfer.2015.11.078

Jackson, R. D., & Kirkham, D. (1958). Method of measurement of the real thermal diffusivity of moist soil. *Soil Science Society of America Journal*, *22*(6), 479–482. https://doi.org/10.2136/sssaj1958.03615995002200060001x

Philip, J. R. (1973). Periodic nonlinear diffusion: An integral relation and its physical consequences. *Australian Journal of Physics*, *26*(4), 513. https://doi.org/10.1071/ph730513

Stallman, R. W. (1965). Steady one-dimensional fluid flow in a semi-infinite porous medium with sinusoidal surface temperature. *Journal of Geophysical Research*, *70*(12), 2821–2827. https://doi.org/10.1029/jz070i012p02821

Suzuki, S. (1960). Percolation measurements based on heat flow through soft with special reference to paddy fields. *Journal of Geophysical Research*, *65*(9), 2883–2885. https://doi.org/10.1029/JZ065i009p02883

Tarnawski, V.R., Leong, W.H. (2016). Advanced geometric mean model for predicting thermal conductivity of unsaturated soils. *International Journal of Thermophysics*, 37, 18 https://doi.org/10.1007/s10765-015-2024-y

Verhoef, A., Van Den Hurk, B. J. J. M., Jacobs, A. F. G., & Heusinkveld, B. G. (1996). Thermal soil properties for vineyard (EFEDA-I) and savanna (HAPEX-sahel) sites. *Agricultural and Forest Meteorology*, *78*(1–2), 1–18. https://doi.org/10.1016/0168-1923(95)02254-6

Wang, L., Gao, Z., Horton, R., Lenschow, D. H., Meng, K., & Jaynes, D. B. (2012). An analytical solution to the one-dimensional heat conduction–convection equation in soil. *Soil Science Society of America Journal*. https://doi.org/10.2136/sssaj2012.0023N

Wiltshire, R. J. (1982). Solutions of the heat conduction equation in a non-uniform soil. *Earth Surface Processes and Landforms*, *7*, 241–252. https://doi.org/10.1002/esp.3290070303

Wiltshire, R. J. (1983). Periodic heat conduction in a non-uniform soil. *Earth Surface Processes and Landforms*, *8*, 547–555. https://doi.org/10.1002/esp.3290080606

Chapter 8

Conclusions and Future Research

8.1. Conclusions and Future Research

The interaction between soil, plant and water with the atmosphere and underground stores is essential to sustain life on the planet. This dissertation is dedicated to a small area where by a concurrence of different factors the granite rocks are weathered at an appreciable rate. Under the current evolution of erosive processes, we need to understand better the mechanisms of soil formation. The dissertation considers a reduced aspect: the role of water on soil evolution. Hydrological flow in the soil is an important agent in soil formation. This interaction plays a decisive role in weathering, physical and chemical, of the parental material, and together with erosion and deposition processes modify slopes. The information contained in this Thesis summarizes a long period of field measurements in an interesting zone not only for the physical processes involved but for the socioeconomic relevance for the Mediterranean environments. Krueger et al. (2021) pointed out that the use of soil moisture-based tools improves grassland biomass production estimates incorporating it into mechanistic models that are usually precipitation-based.

In chapter 2, a detailed soil moisture analysis unravels the control exerted by the slope aspect on hydrologic flows. The water holding capacity is expanding on the noth-facing slope (NFS) due to the deep layer of highly weathered material extending beneath the soil, as opposed to the south-facing slope (SFS) where the soil is underlied by bedrock directly. This allows for more vegetation on the NFS compared to the SFS. On the latter, soil moisture, and Normalized Difference Vegetation Index (NDVI) has a strong correlation while on the NFS the correlation is weak with soil moisture and good with the water table, indicating that vegetation uptakes water from different water pools on the NFS, rock moisture and saturated zone.

In chapter 3, the 1-D model SoilGen was applied to the simulation of the pedogenesis and the measured chemical weathering status over a 20000-year period. The variability of the index Chemical depletion fraction (CDF) values is apparenty better explained by hydrological variables, i.e. soil water recharge and discharge, than by the topography. Despite the complexity of the catena and the hydrological conditions, a good correspondence was obtained between modelled and measured CDF. For the profile average chemical weathering, maximum values were observed for intermediate precipitation values, around 800 mm. The results showed a marked depth gradient for rainfall under 800 mm for the CDF, but it showed a uniform depth distribution for precipitation above 800 mm.

In chapter 4, the analysis of temporal stability (TS) of soil moisture shows that the monitoring locations situated on the NFS generally show higher temporal stability of the 5 different depths at which soil moisture measurements are taken. On the contrary, the points located in the valley show lower TS. The applied Principal Component Analysis (PCA) showed two independent Principal components (PCs) describe 97.5 % of the full soil moisture dataset's variance. The dominant pattern PC_1, which explains 92.5 % of the variance, might be identified with climate. While PC_2, which explains 5.1 % might be identified with topography.

In chapter 5, water flow in these soils is very fast during both, infiltration and evaporation processes. The topsoil does not exert much control over the water cycle, although the vegetation role is not neglectable due to surface shading, uptake homogenizing, and development of small pores in the soil profile. The influence of the slope aspect on the hydrological processes induces important modifications, not only in the soil but also in the vegetation that grows on them, in their formation, and the subsurface flow. The evolution of the soil moisture profiles revealed the importance of the downslope subsurface flow of water.

In chapter 6 it is shown that the aquifers formed in fractured granite rocks in Mediterranean regions respond quickly to rain pulses, with the fast flow on hillslopes converging into river valleys. Analysis of the water budget in both the soil and the underlying aquifer is to understand the behavior of the system, although detailed information is needed to evaluate different processes such as recharge through precipitation and discharge to streams and rivers with greater accuracy.

In chapter 7, the influence of soil moisture in the apparent thermal diffusivity (κ) data has been explored. Although the estimation of the apparent heat convection parameter (W) with the solution of the heat conduction-convection equation in the soil assuming steady-state conditions is overestimated, both this solution and that of heat transport by conduction allow the evaluation of κ of the soil from the soil temperature data measured by the sensors in the field. The estimation of the soil water recharge with thermal measurements requires a more detailed analysis.

As a result of this thesis, some research lines emerge as a priority for the further research effort. A better description of the weathering front, or boundary between fresh and weathered bedrock, is needed given the evident irregularity of the rocks distribution and the surface relief. This information is required to improve our knowledge of the soil and landscape evolution (Phillips et al., 2019). In the field, soil profile description has been considered down to approximately 1-meter depth and in the up to 18 m boreholes, taken to install the piezometric wells, the soil was not distinguished from the saprolite. The direct examination of weathering profiles or cores might be complemented with geophysical methods such as electrical resistance tomography and seismic methods that can identify deeper boundaries with intact bedrock (Olesen et al., 2013).

The second line of future research would be the measurement of actual evapotranspiration because it considers the effect of the slope aspect on vegetation attributes. Any option to measure evapotranspiration had been considered very complicated at this scale and this terrain. However, Heusinkveld et al. (2006) developed simple, portable, and affordable microlysimeters to measure dew formation and evaporation in both flat and slope areas in the Negev Desert (Israel). Based on their design Uclés et al. (2013) designed their low-cost microlysimeters, which were installed in a steppe semiarid Mediterranean ecosystem, with different cover types to measure non-rainfall atmospheric water input, an important water source in this and the previous one study environments.

Last but not least, a third line of research should focus on the evaluation of the overland and groundwater flow. Since the 2000s, there has been growing interest to document groundwater and surface water interactions to protect both resources, from a multidisciplinary perspective (Woessner, 2000). The available measuring methods of the interaction are numerous: direct measurements of water flux, heat tracer methods, methods based on Darcy's Law, and mass balance approaches (Kalbus et al., 2006). However, because this interaction encompasses several scientific disciplines, the characterization, quantifying, and modelling of groundwater-water surface interactions are still challenging (Lewandowski et al., 2020).

8.2. References

Heunsinkveld, B. G., Berkowicz, S. M., Jacobs, A. F. G., Holtslag, A. A. ., & Hillen, W. C. A. M. (2006). An Automated Microlysimeter to Study Dew Formation and Evaporation in Arid and Semiarid Regions. *American Meteorological Society*, 825–832.

Kalbus, E., Reinstorf, F., & Schirmer, M. (2006). Measuring methods for groundwater – surface water interactions : a review. *Hydorlogy and Earth System Sciences*, *10*, 873–887.

Krueger, E. S., Ochsner, T. E., Levi, M. R., Basara, J. B., Snitker, G. J., & Wyatt, B. M. (2021). Grassland productivity estimates informed by soil moisture measurements: Statistical and mechanistic approaches. *Agronomy Journal*, *113*(4), 3498–3517. https://doi.org/10.1002/agj2.20709

Lewandowski, J., Meinikmann, K., & Krause, S. (2020). Groundwater – Surface Water Interactions : Recent Advances and Interdisciplinary Challenges. *Water*, *12*, 1–7.

Olesen, O., Kierulf, H. P., Brönner, M., Dalsegg, E., Fredin, O., & Solbakk, T. (2013). Deep weathering , neotectonics and strandflat formation in Nordland , northern Norway. *Norwegian Journal of Geology*, *93*, 189–213.

Phillips, J. D., Pawlik, Ł., & Pavel, Š. (2019). Weathering fronts. *Earth System Science Data*, *198*. https://doi.org/10.1016/j.earscirev.2019.102925

Uclés, O., Villagarcía, L., Cantón, Y., & Domingo, F. (2013). Agricultural and Forest Meteorology Microlysimeter station for long term non-rainfall water input and evaporation studies. *Agricultural and Forest Meteorology*, *182–183*, 13–20. https://doi.org/10.1016/j.agrformet.2013.07.017

Woessner, W. W. (2000). Stream and Fluvial Plain Groun Water Interactions: Rescaling Hydrogeologic Thought. *Ground Water*, *38*(3), 423–429.

Appendices

Peer-reviewed publications and conference publications

JOURNAL PUBLICATIONS

(J1) García-Gamero, V., Peña, A., Laguna, A. M., Giráldez, J. V., y Vanwalleghem, T. 2021. Factors controlling the asymmetry of soil moisture and vegetation dynamics in a hilly Mediterranean catchment. Journal of Hydrology, 598, 126207. https://doi.org/10.1016/j.jhydrol.2021.126207

(J2) García-Gamero, V., Vanwalleghem, T., Peña, A., Román-Sánchez, A. and Finke, P.A.: Modelling the effect of catena position and hydrology on soil chemical weathering, SOIL Discuss. [Preprint], https://doi.org/10.5194/soil-2021-78, in review, 2021.

CONFERENCE PUBLICATIONS

(C1) García, V., Román-Sánchez, A., Sáenz de Rodrigáñez, M., Peña, A., Laguna, A.M, Vanwalleghem, T., and Giráldez, J.V. Caracterización de los procesos hidrológicos en una ladera formada por granitos parcialmente descompuestos. Estudios en la Zona No Saturada 2017. Vol. XIII: 39-47. I.S.B.N.: 978-84-947468-9-5

(C2) García, V., Giráldez, J.V., peña, A. Avances sobre la hidrología y descomposición de algunos granitos de Sierra Morena. VI Congreso Científico de Investigadores en Formación de la Universidad de Córdoba. I.S.B.N.: 978-84-9927-239-9

(C3) García, V., Román-Sánchez, A., Sáenz de Rodrigáñez, M., Peña, A., Laguna, A.M., Vanwalleghem, T. and Giráldez, J.V. Characterization of hydrological processes in a partially decomposed granite hillslope in the Mediterranean region. 20th EGU General Assembly, EGU2018, Proceedings from the conference held 4-13 April 2018 in Vienna, Austria, p.15822

(C4) García-Gamero, V., Román-Sánchez, A., Peña, A., Laguna, A.M., Vanwalleghem, T., Giráldez, J.V. and Finke, P.A. How soil forms in a Mediterranean granitic region: a

progress report. 21st EGU General Assembly, EGU2019, Proceedings from the conference held 7-12 April 2019 in Vienna, Austria, id.10025

(C5) García-Gamero, V., Peña, A., Laguna, A.M., Vanwalleghem, T. and Giráldez, J.V. Evolución temporal del nivel piezométrico en un acuífero somero en terrenos graníticos. Estudios en la Zona No Saturada 2019. Vol. XIV:123-129. I.S.B.N.: 978-84-948550-8-5

(C6) García-Gamero, V., Giráldez, J.V., Peña, A., Laguna, A.M., Vanwalleghem, T., Martínez-García, G. and Vanderlinden. Estudios de la estabilidad de la humedad del suelo en una cuenca Mediterránea sobre material granítico. Estudios en la Zona No Saturada 2021.https://www.udc.es/gl/zns21/.

(C7) García-Gamero, V., Peña, A., Laguna, A.M., Giráldez, J.V. and Vanwalleghem T.Efectos hidrológicos de la orientación de las laderas en una cuenca Mediterránea. Estudios en la Zona No Saturada 2021. https://www.udc.es/gl/zns21/

(C8) García-Gamero, V., Laguna, A.M., Peña, A., Vanwalleghem, T., González, M.P. and Giráldez, J.V. ¿Puede la temperatura indicar la evolución de la humedad del suelo? Estudios en la Zona No Saturada 2021. https://www.udc.es/gl/zns21/